Nonlinear Optical Properties of Sn(IV) phthalocyanines: Experimental and Theoretical Approach

A thesis submitted in fulfilment of the requirements for the degree of

MASTERS OF SCIENCE

at

RHODES UNIVERSITY

by

Marcel Severiano Louzada

August 2016

Dedicated to

My late friend

Kira

You have always been with me.

Acknowledgments

First and formost, I would like to thank my supervisor, Dr Samson Khene, for putting up with me and prodding me when necessary, and for giving insight and advice when I would listen. I also thank the various faculty members of my Department for the help they have given along the way, Dr Mack for always being a reliable source of knowledge and Dr Lobb, for patiently explaining my computational failings.

I also want to thank the people who put up with me daily, my lab mates Zainab, Asanda and Grace. My friends from the Keg, Colin, Zane, Justin, Martijn, Ivan and Pj. You broke many hours of solitude with your comradery, and I am grateful.

To my friends and coffee companions Roxann and Jessica, thank you for dragging me from the lab, I know I can have been that good company, but you kept doing it and it meant the world to me.

Thank you as well to the technical staff at the department for always resolving my issues, and never asking what I was doing with all that acid.

I would like to thank the National Research Foundation for funding this study.

But most of all I want to thank Cai, you never had to do a thing you did, but you helped me anyway.

Abstract

This work presents the nonlinear properties of six Sn(IV) Phthalocyanines. Three of the phthalocyanines are linked by an alkylthiol substituent and the rest are linked with a phenoxy substituent. For all six compounds non-linear optic analysis was carried out in four solvents: chloroform, toluene, dichloromethane, and tetrahydrofuran, and their differences were recorded. Calculation of the linear, singlet excited, triplet excited and two photon absorption cross-sections were also carried out and the results compared. To form a comparison the first order hyperpolarizabilities, DFT calculations were also performed and the results compared to see if the behaviour between the two properties can be predicted using DFT.

Table of Contents

List of Symbols

$(\sigma)_{e0}$	-	Total excited state cross-section
$(\sigma)_{s0}$	-	Linear ground state absorption cross-section
N_{s0}	-	Population of the grounds state
N_e	-	Population of the excited state
σ_{npa}	-	n-Photon absorption cross-section
I	-	Incident light intensity
$\vec{P}$	-	Polarization of a material
$\vec{E}$	-	Electric field component vector
χ	-	Electrical susceptibility
$\vec{u}$	-	Dipole moment
β_I	-	Intensity dependent nonlinear absorption coefficient
α	-	Linear absorption coefficient
α_n	-	n-Photon absorption coefficient
T_n	-	Transmittance
z_s	-	Z-Scan position
L_{eff}	-	Effective propagation length in the material
$\omega(z_s)$	-	Beam width in the sample plane at point zs
z_0	-	Focal position
z_r	-	Rayleigh range
λ	-	Wavelength
Q_0	-	Maximum value for q0 (zs)
$q_0(z_s)$	-	Nonlinearity of transmittance
P_0	-	Peak laser power
ε_0	-	Permittivity of free space
c	-	Speed of light in a vacuum
N_A	-	Avagadros number
f	-	Lorentz local field factor
α_2	-	Molecular coefficient for TPA
N	-	Concentration
β_{The}	-	Theoretical two photon absorption cross-secction
h	-	Plank's constant
v	-	Frequency of light
n	-	Refractive index
μ_{gi}	-	Oscillator strength between the ground state and intermediate state
μ_{if}	-	Oscillator strength between the intermediate and final state.

E_{gi}	-	Energy difference between the ground and intermediate state
$T_{OA(nPA)}$	-	Transmittance due to n-photon absorption
σ_T	-	First triplet excited state cross-section
σ_S	-	First singlet excited state cross-section
T_1	-	First triplet state
S_1	-	First singlet excited state
T_n	-	nth triplet excited state
τ_{ISC}	-	intersystem crossing time
τ_{ISCg}	-	Triplet lifetime
S_n	-	nth Singlet excited state
S_0	-	Ground state
τ_{10}	-	Fluorescence decay time
σ_{ij}	-	Cross-section for absorption between states i and j
N_x	-	Population of state x
β	-	First hyperpolarizability
γ	-	Second hyperpolarizability
M_L	-	Orbital angular momentum
β_{HRS}	-	First hyperpolarizability, calculated via Hyper Rayleigh Scattering
Vr	-	Solution volume

List of Abbreviations

B3LYP	Becke, three-parameter, Lee-Yang-Parr
CCSD	Connected single and double couple cluster
DBN	1,5-diazabicyclo[4.3.0]non-5-ene
DBU	1,8-diazabicylo[5.4.0]undec-7-ene
DFT	Density Functional Theorem
ESA	Excited State Absorption
HF	Hartree-Fock
IEFPCM	Integral equation formalism variant of the Polarizable Continuum Mode
ISC	Intersystem crossing
LANL2DZ	Los Alamos National Laboratory 2-double-zeta
MCD	Magnetic Circular Dichroism
Mo(s)	Molecular orbital(s)
MP	Møller–Plesset
MPA	Multiple photon absorption
MPc(s)	metal phthalocyanine(s)
NLA	Nonlinear absorption
NLO	Nonlinear optics
OL	Optical limiting
OPLs	Optical power limiters
Pc(s)	Phthalocynine(s)
RF	Reaction field
RSA	Reverse saturable absorption
SA	Saturable absorption
SnPc(s)	Tin(IV) phthalocyanine(s)
TCSPC	Time Correlated Single Photon Count
TPA	Two photon absorption

List of Figures

Table of Schemes

List of Tables

Chapter 1. Introduction

1.1 Metal Phthalocyanines

Phthalocynines (Pcs) are blue macrocyclic compounds, known for their distinct blue-green colour and their unique spectroscopic properties. Discovered in 1927[1], Pcs have since found use in dyes[1,2], catalysis[3–5], optical based electronics[6,7], electro sensing,[8] photovoltaic cells[9–12], medicine[13–15] and non-linear optic devices. These applications all stem from their Pi electron configuration of the Pcs.

1.2.1 Synthesis of Phthalocyanines

Scheme 1.1 shows the different methods of synthesising MPcs that have been found. As well as the aforementioned methods, the use of o-cyanobenzamide (3) (Scheme 1.1), phthalic anhydride (Scheme 1.2) phthalimide (6), 1,3-diminoisoindoline (5), phthalic acid (7) and phthalonitrile (8) were used to synthesise Pcs. Phthalonitriles are the most widely used precursors due to their ease of use and relatively mild reaction conditions.

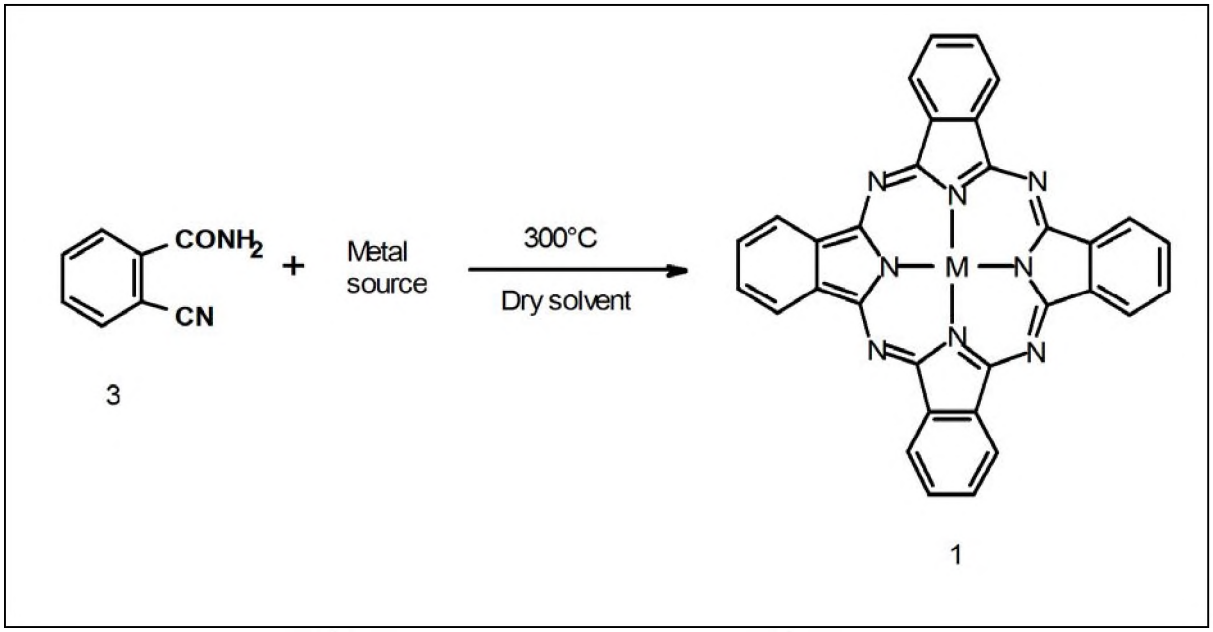

Scheme 1.1: Synthesis of MPc from o-cyanobenzamide (3).

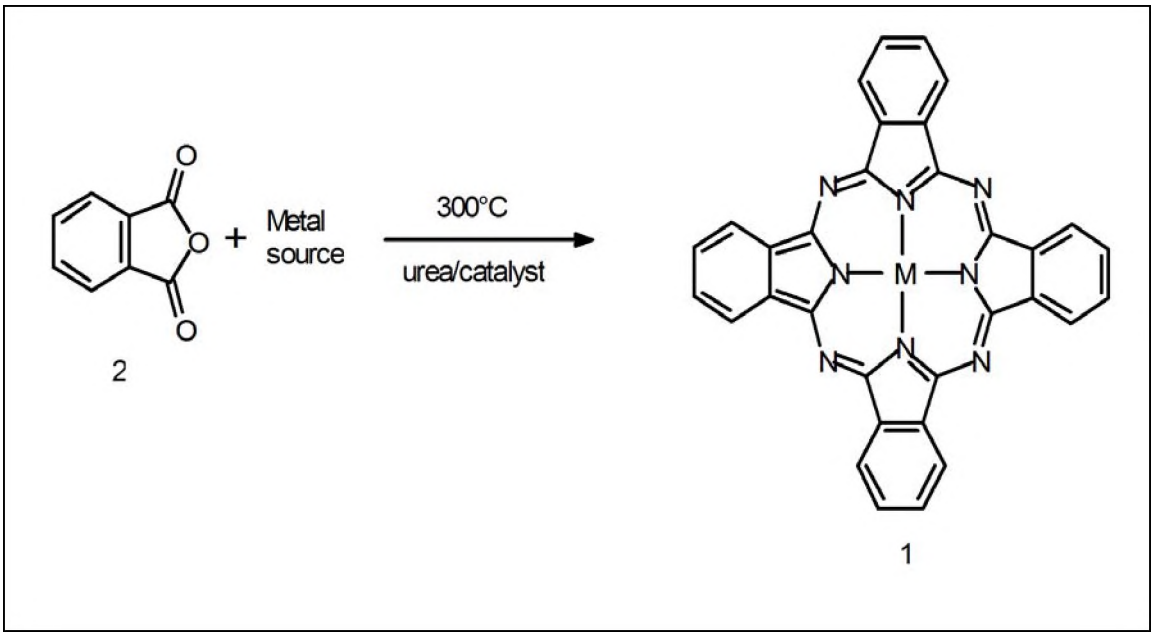

Scheme 1.2: Synthesis of MPc from phthalic anhydride (2).

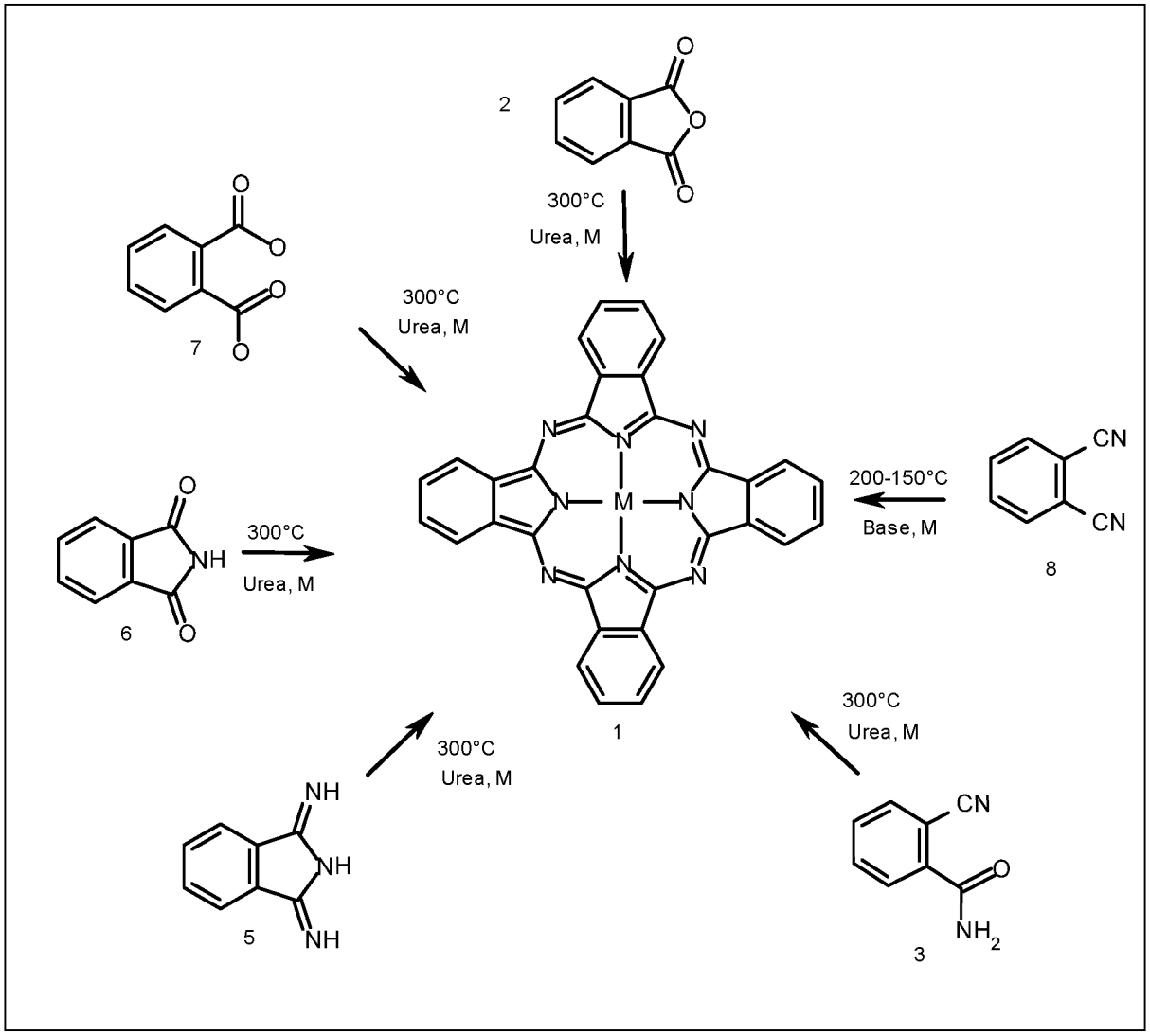

Scheme 1.3: Possible synthesis pathways for a MPc.

Depending on the MPc's desired structure, level of symmetry, type of substituents and the choice of central metal, the procedure to create one MPc can differ drastically from another. Things to consider when varying the substituents of a Pc are availability, cost and the safety factors of the required precursors for the synthesis as well as the ease of synthesis, as industrial applications of Pcs which are difficult to synthesise are few.

The presence of a basic solvent environment enhances the reactivity of the starting material and hence increases the product yield. This is normally done by the addition of small amounts of bases such as 1,8-diazabicylo[5.4.0]undec-7-ene (DBU), 1,5-

diazabicyclo[4.3.0]non-5-ene (DBN) to the reaction. Lithium can be used as a reaction centre for the Pc cyclisation, and is used to allow subsequent insertion of a larger metal atom into the Pc's central cavity.

The solvent used for the reaction should have high boiling point (between 100 to 300 °C). Solvents such as pentanol and octanol are used, as well as quinolone, tri-chlorobenzene and even toluene in some cases[16].

Un-metalated Pcs (MPcs without a central metal atom) are formed by reacting the MPcs with sulphuric acid as shown in Scheme 1.4. This would leave the central cavity protonated with two H atoms. The metal salt is removed as a by-product.

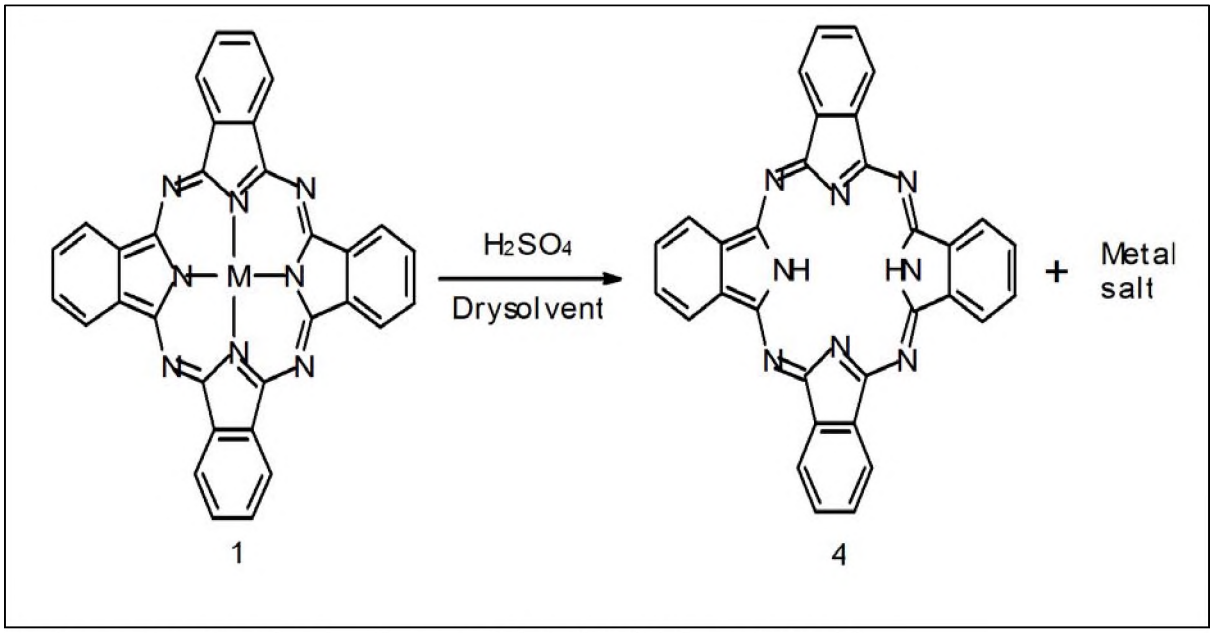

Scheme 1.4: Synthesis of un-metalated Pc(4) from MPc (1).

1.2.2 Metal Phthalocyanine substituents

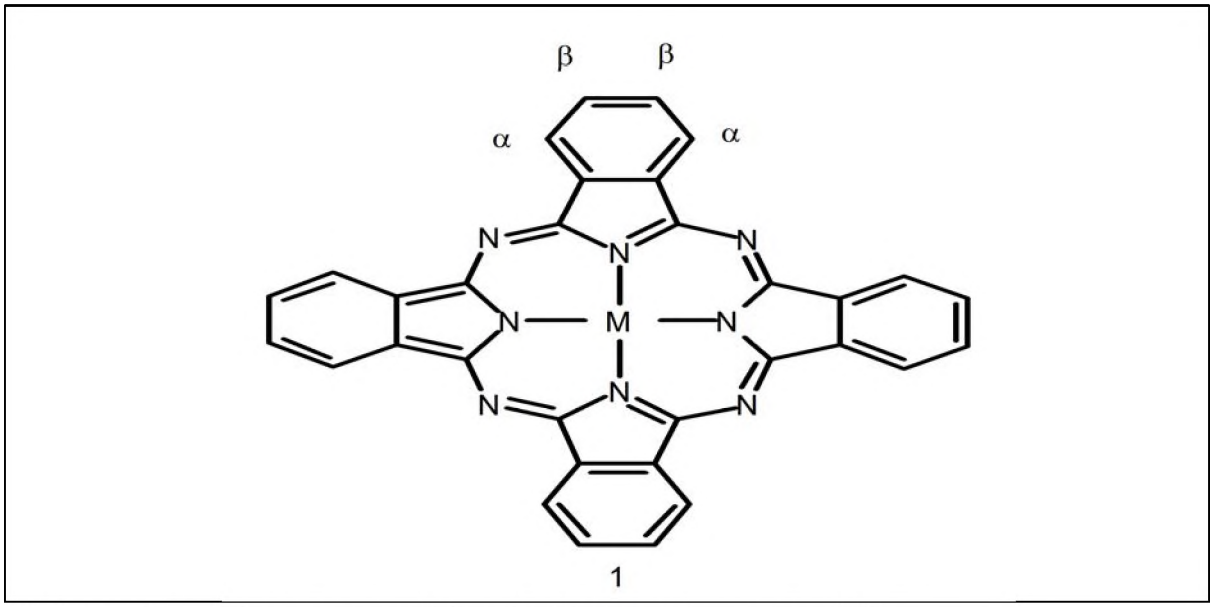

Scheme 1.5: The four possible substitution sites for an MPc.

The hydrogens on the peripheral benzo rings of the MPcs can be substituted and modified with other functional groups in order to change the physical properties of the parent MPc, as an example an unsubstituted CuPc is hardly soluble, but introduction of solphonyl groups to the benxo rings results in a highly soluble solvent dye. As shown in **Scheme 1.5**, the Pcs' four peripheral rings contain two sets of carbons at mirror positions. These are dubbed α for the non-peripheral locations, and β for the peripheral locations. Usuallly modification of these positions is done on the precursors to the Pc. The degree of modification is often sterically limited, with substitution by large groups more difficult to effect [17].

Assuming only one starting reagent, i.e. possessing only one substituent at either the α or β -position, the Pc will consist of a mixture of 4 isomers with each substituted at one of the two possible positions[18]. The four isomers possess C_{4h}, D_{2h}, C_{2v}, and C_s symmetries (**Scheme 1.6**), though the difference in the isomers is small enough that the mixture of the four isomers are used experimentally in most cases.

Pc substituents are generally classified by their mesomeric and inductive effects[19]. Most substituents possessing both properties but being distinguished on their more

prominent nature. Inductive effects are electrostatic in nature and affect the rest of the molecule, meaning that the energy gaps between molecular orbitals (MOs) remain the same as any inductive effect will shift the MOs a either up or down uniformly[20]. Mesomeric effects differ in that they are based on structural resonance[21] and will only affect certain regions of a substituted Pc. As a result, certain MOs are shifted differently and this will present itself as a shift in the absorbance spectra of different substituents. The shifts themselves depend on degree of electron withdrawing or donating of the substituents. More withdrawing groups leading to blue shifting of the spectra and more donating causing red shifting of the spectra[22]. Thus, shifts due to mesomeric effects are based on structural resonance, differences in these effects can are observed when the substituent is placed at the different substitution sites. α substitutions yield far larger shifts than the β substitutions as the MOs responsible for the majority of visible spectra lie on the α carbon(a_{2u},a_{1u})[23,24].

This work will use two different substituents, a thiol and a phenoxy substituent, substituted respectively. To synthesize 6 Mpcs 3 different substitution positions of the Pc, α, β and ββ (both β positions substituted) will be used.

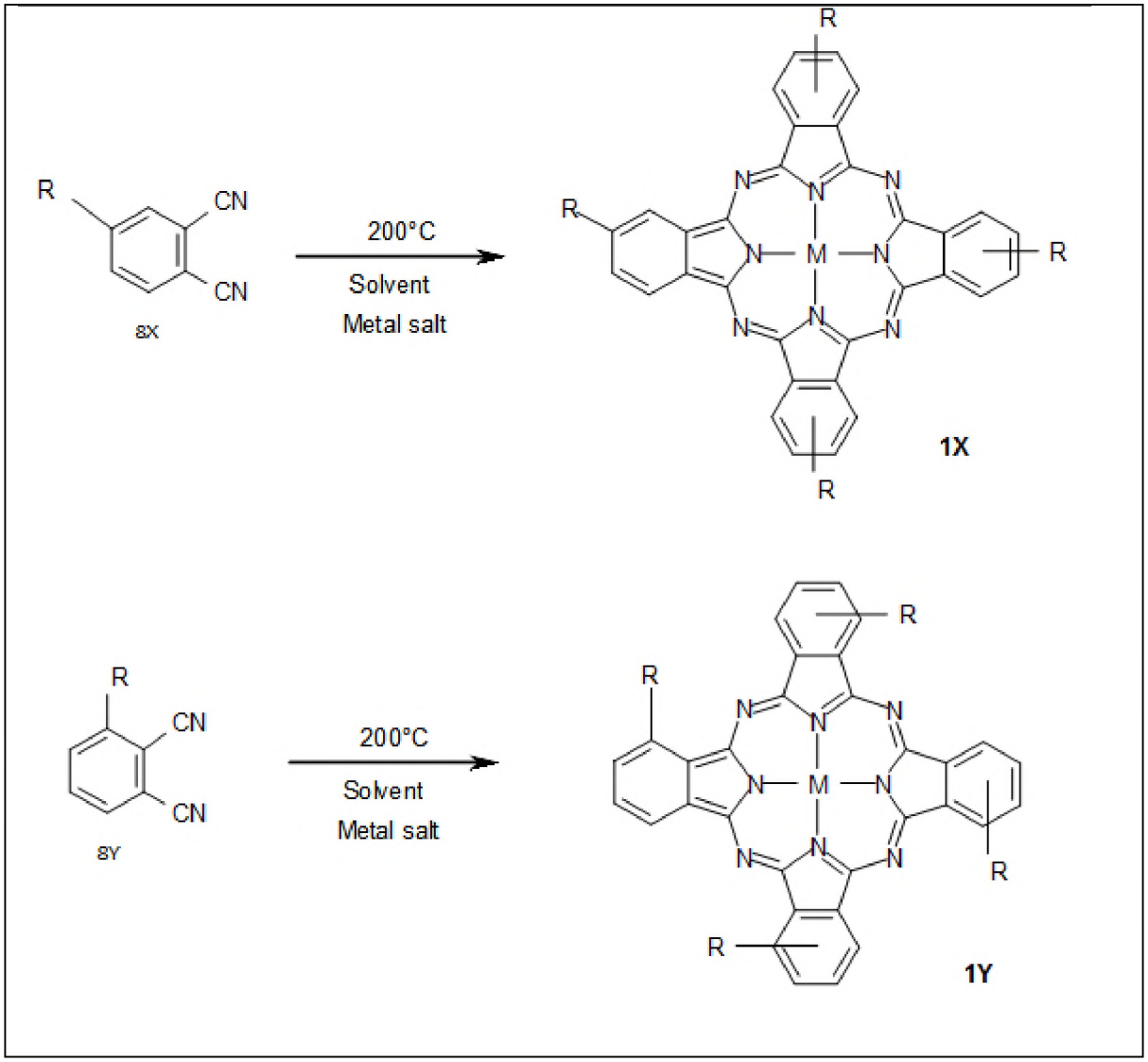

Scheme 1.6: Possible isomers of mono substituted Phthalonitriles when making MPc (1X,1Y).

1.2.4 Central metal of an MPc

The central cavity of unmetalated Pcs (called free base Pcs) contains two hydrogens. However, this cavity can also be filled by metals. The Pc's cavity carries a charge state of -2, allowing it to easily coordinate to any metal cation small enough to fit in it, and in some cases even those that are slightly bigger. More than seventy metals can form stable complexes with Pcs and each of these will change the electronic nature of the Pc ligand accordingly. Metalation normally occurs insitu, that is during the formation

of the Pcs macrocycle. However, it is also possible to insert a metal ion into the cavity of synthesised free base Pc. This is done simply with the use of a suitable solvent and heat.

Different metal centers bring with them different effects on the Pc macro cycle as a whole, since the metal is right in the middle of the π electron cloud it will certainly change the properties of it. Different metals will interact in different ways with the macrocycle, and those which are more electronegative can shift the absorption spectra to higher energies, while electropositive metals can shift it to the lower energies. Axially coordinated ligands for M(III) and M(IV) central metals can also attenuate the π electron cloud, as well as introduce other physical properties to the Pc[25].

In this work Tin(IV)Cl_2 was used as a central metal complex, as there have been extensive work on similar MPcs[26–29]. Tin(IV) centred Pcs have not been studied as extensively as other elements from its period, and the axial ligands of Cl were used because they formed naturally when creating a Pc using the most readily available Tin salts.

1.2.5 Phthalocyanine absorption spectra

Pcs are known for their distinct blue-green colour, characterised by two absorption bands in the visible region of the spectrum at 350 nm and spanning from 600 nm to 800 nm, respectively depending on the Pc. The origin of these bands was explained by Gouterman for pophyrins[24]. They are due to their four frontier molecular orbitals, given the designation of a_{1u}, a_{2u} and e_g from their point group symmetry. This explanation is called the Gouterman's four orbital model and is shown in Scheme 1.7, and shows that the transitions from the occupied orbitals (a_{1u} or a_{2u}) to the unoccupied orbitals (the degenerate e_g) can have change in the angular momentum quantum number , Δm_l of ± 1 or ± 9.

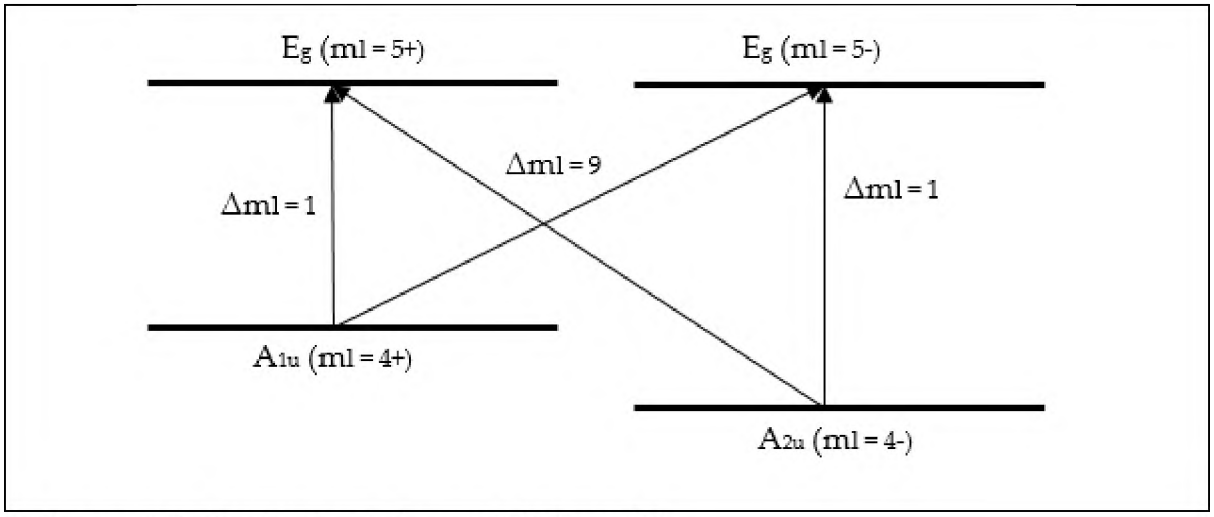

Scheme 1.7: Gouterman's four orbital model.

The transitions resulting in a change of ± 9 m_l are considered forbidden, as the accepted transition selection rule is a change in m_l of ± 1 or 0. and its strength is much lower in other (non-tetra aza) porphyrins. The absorption intensity in Pcs is due to the symmetry being broken by replacement of the four central carbons with nitrogens. This breaks the pseudo parity of the two independent Q transitions and allows them to be observed[30] (i.e. they no longer cancel each other out).

Metalated Pcs possess D_{4h} planar symmetry, so the e_g orbitals are degenerate. However, the unmetalated Pcs possess a D_{2h} symmetry, which manifests as a shift in one of the e_g orbitals (now called b_g with the change in point group) and thus a shift in energies of all transitions to that orbital[31]. This is the cause of the splitting in the MPc when compared with the umetalated acid conjugate absorption spectra as shown in Figure 1.1

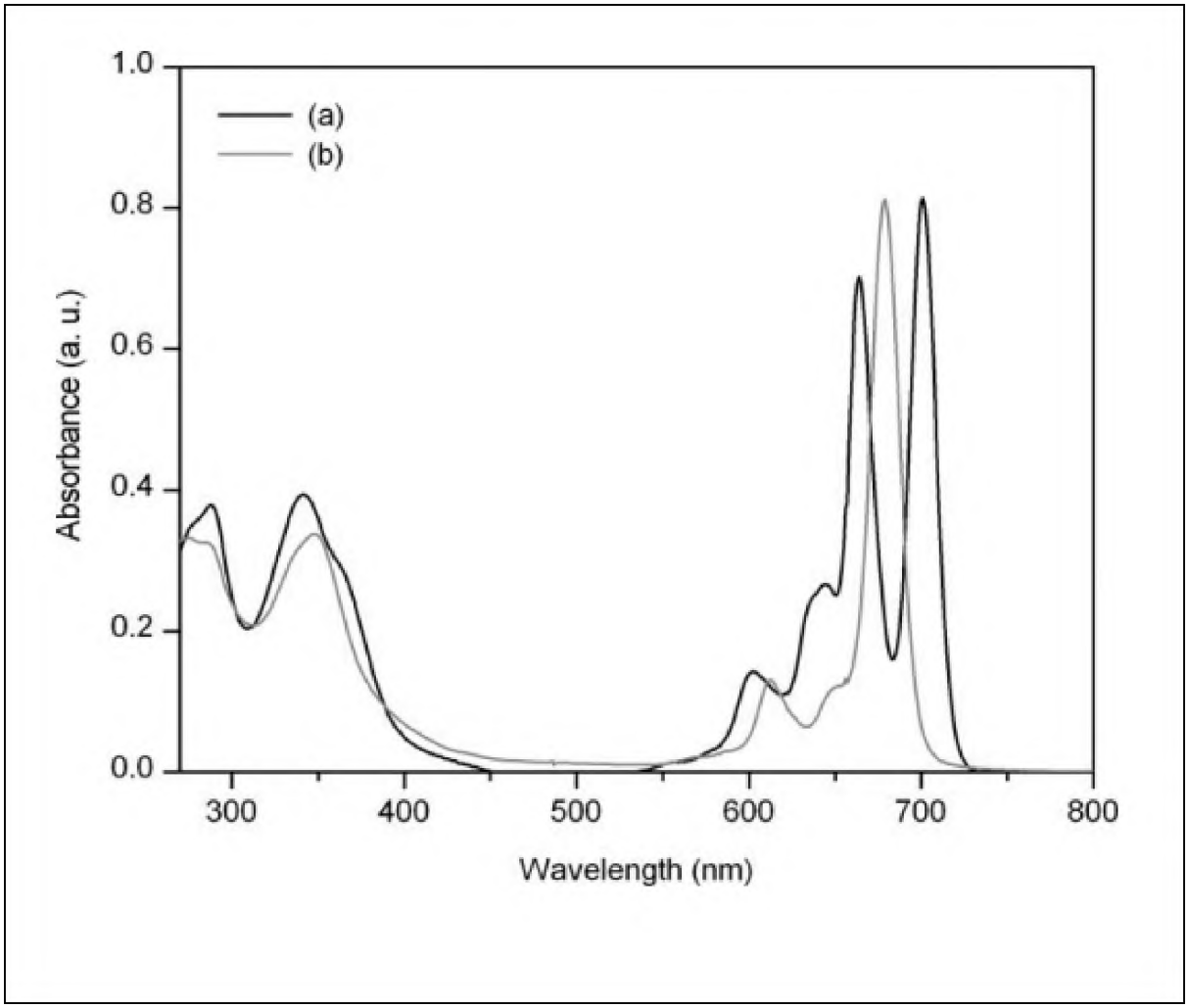

Figure 1.1: Absorption spectra of an unmetalated Pc (a) and a MPc (b) [32].

Gouterman's four orbital model was later adapted in order to account for all the transitions, including some observer in the sub 300 nm region. This resulted in the current model used to describe Pc absorption bands. Among the absorption peaks are the high energy B bands[31], these are due to transitions from lower lying orbitals shown in Scheme 1.8.

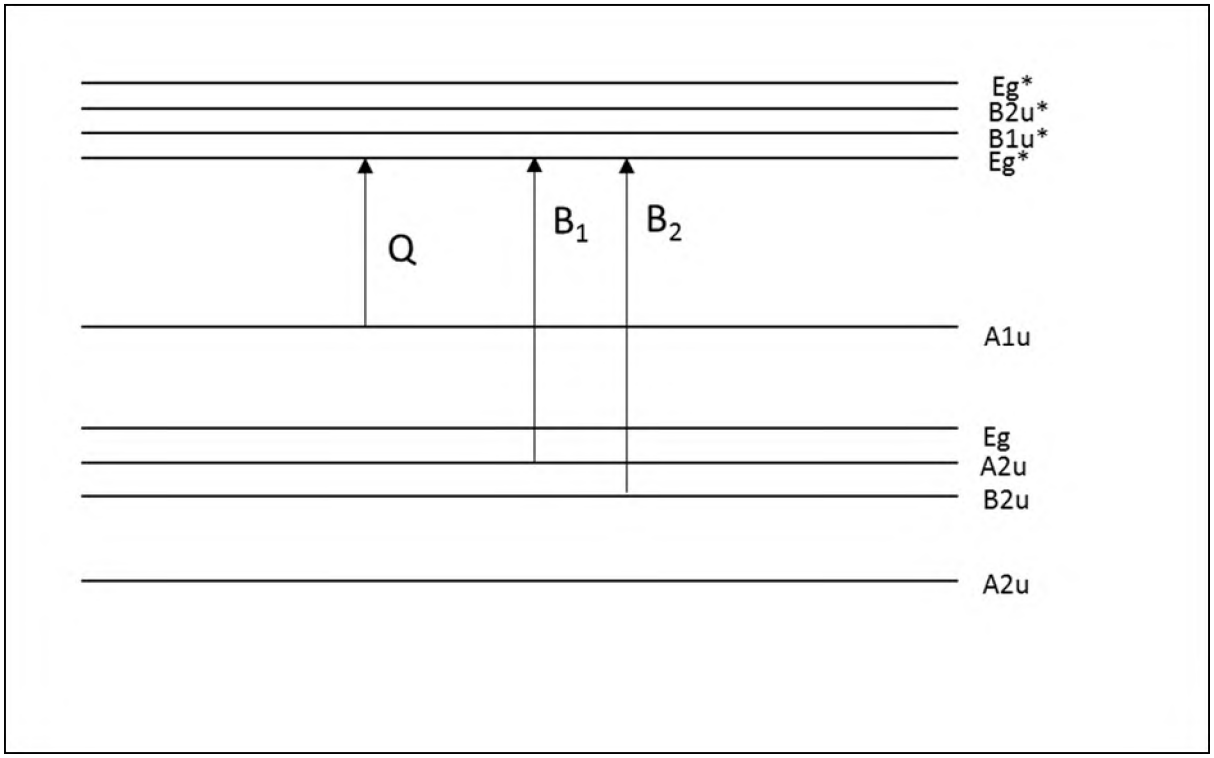

Scheme 1.8: Transitions responsible for absorption bands in MPc.

1.3 Non Linear Optics

1.3.1 Optical limiting materials

Non-linear optics (NLO) is a field studying the non-linear aspects of materials' optical responses. The field is large and has many branches that are worthy of study. One such branch is optical power limiting (OPL) and deals with the difference between the incident light and transmitted light in a material. NLO Interest has arisen in this field as it offers a means of controlling intensity levels of light through a non-mechanical means[33]. The intensity is controlled by the nature of electron interaction with light and the reaction times are relatively instantaneous when compared to even the fastest mechanical response as shown in Figure 1.2. Reporting of the NLO properties of a material is done by either the intensity dependent non-linear absorption parameter (β_I) or by the associated imaginary third order susceptibility ($Im[\chi^{(3)}]$)[27].

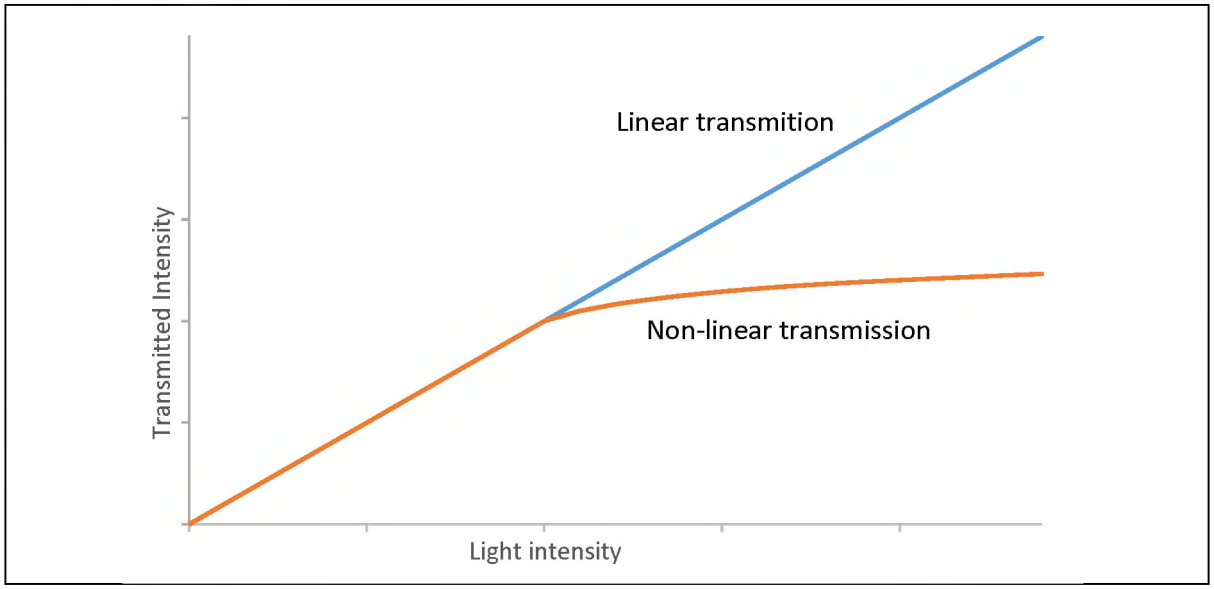

Figure 1.2: Graph of light transmitted in an Optical limiter.

As light absorption is the primary concern with limiting, it becomes obvious that dyes are ready candidates for optical power limiters (OL). The problem of using a dye is that their natural absorption can inhibit their application as an OL. Pcs can be used as optical limiters since a number of their properties facilitate their use- namely their chemical stability, non-toxicity, and very specific absorption and transparency regions[33].

Pcs have found use as OL due to their versatility and tenability, properties which most other inorganic OPL do not possess. The exact type of Pc use in OL can vary, though heavy metal centred Pcs are preferred, normally with axial ligands, shown in Figure 1.3, to reduce aggregation[34]. Pcs also possess large and more dispersed electron systems, hence systems with large π conjugation.[35] Thus their behaviour in NLO can be modified by the addition of suitable substituents, changing how the extended molecular electron cloud is effected by external electromagnetic fields. Normally a mixture of electron withdrawing and donating groups will be used[36] as this creates a push-pull system. In this work, an electron-withdrawing centre and electron-donating periphery are used to create this push-pull system.

The use of group 14 metals listed in Table 1.1 like Tin(IV) the metal used in this study, is not prevalent as only few reported cases of fair to good OL response is found in

literature, since in most case heavy transition metals are preferred due to their low lying d orbitals[35].

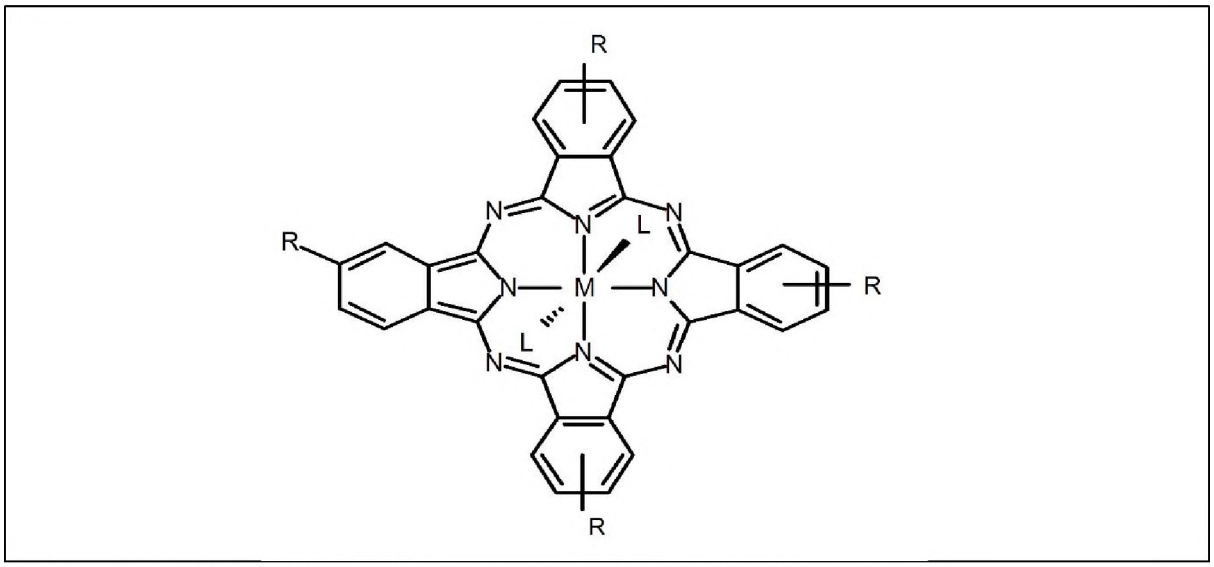

Figure 1.3: MPc with a M(IV) possessing two axial ligands .

Pc Ana.	Metal (M)	Substituent (R)	Ligand (L)	Solvent/ film	Im[$\chi^{(3)}$] (esu)	β_I (cmW^{-1})	Method	Ref.
Nc	Sn(IV)	(OC_4H_9)	$OSi(C_2H_5)_3$	film	2.07E-12	1.48E-08	THG*	29
Nc	Si(IV)	($SC_{10}H_{21}$)	$OSi(C_2H_5)_3$	film	56.0E-12	4.01E-07	THG	29
Pc	Ge(IV)	(t-Bu)	(OH)	film	10.5E-12	7.52E-08	THG	29
Pc	Pd	NA	NA	$CHCl_3$	6.5E-12	4.66E-08	Z-scan	29
Pc	Si	NA	NA	$CHCl_3$	2E-9	1.43E-05	Z-scan	29
Pc	Sn(IV)	Oxyether-4benzaldehyde	Cl	THF	2.93E-12	2.10E-08	Z-scan	36
Pc	Ge(IV)	Oxyether-4benzaldehyde	Cl	THF	4.05E-12	2.90E-08	Z-scan	36

Pc	Sn(IV)	Oxyether-4nitrobenzene	Cl	DMF	4.05E-12	2.90E-08	Z-scan	[36]
Pc	Sn(IV)	Nitro	ether-3,5 methyl benzene	THF	1.26E-12	9.03E-09	Z-scan	[36]
Pc	Sn(IV)	F	Cl	THF	5.58E-12	4.00E-08	Z-scan	[36]
Pc	Sn(IV)	Cl	F	CLN	2.09E-12	1.50E-08	Z-scan	[36]
Pc	Ge(IV)	Cl	ether-3,5 methyl benzene	$CHCl_3$	3.21E-13	2.30E-09	Z-scan	[36]
Pc	H_2	2(Oxyether-hetptane)	N.A.	film	4.86E-11	3.48E-07	Z-scan	[37]
Pc	Zn(II)	2(Oxyether-hetptane)	N.A.	film	11.3E-11	8.10E-07	Z-scan	[37]
Pc	Ga(III)	t-butyl	Cl	Toluene	1.2E-11	8.60E-08	Z-scan	[38]
Pc	Ga(III)	t-butyl	(*p*-TMP)	Toluene	1.1E-11	7.88E-08	Z-scan	[38]
Pc	In(III)	t-butyl	Cl	Toluene	1.6E-11	1.15E-07	Z-scan	[38]
Pc	In(III)	2(hexane)	Cl	Toluene	1.2E-11	8.60E-08	Z-scan	[38]

Table 1.1: NLO Parameters of Pcs in literature. **Nc = naphthalocyanine, Esu = 1.395556e-8 m^2/V^2. THG = Third harmonic generation.**

1.3.2.1 Deriving Non-linear Properties

Having stated that Pcs exhibit NLO behaviour it becomes prudent to then define what is regarded as a good measure of NLO and what measurements and analysis must be taken in order to determine this. Reverse saturable absorption (RSA) occurs when the effective excited state cross-section (σ_E) of a material exceeds the effective ground state cross-section (σ). The cross-section of a molecule refers to the effective area that will absorb radiation/light and is measured in units of area. In the case of NLO materials, the material will possess two or more cross-sections, with the additional cross-sections being due to the excited states of the material in question. Under normal irradiance levels these cross-sections do not contribute to the absorption spectra as the excited states themselves are not populated. However once their population values pass a threshold (determined by the ratio of the size of the excited state cross-section to the ground state cross-section, (σ/σ_E) non-linear absorption will observed. In the case of optical limiters, the σ_E have larger cross-sections than the ground state and this process is called RSA[39]. In the case where the excited states have smaller cross-section than the ground state it is referred to as saturable absorption (SA).

Furthermore, the extent of absorption can depend on multiple photon absorption (MPA) which scales with light intensity, giving another NL absorption parameter. The total change in intensity of light passing through the material (that is lost to absorption) can be integrated form the following equation[40]

$$\frac{dI}{dz'} = -\alpha I = -[\sigma_{s0}N_{s0} + \sigma_{e1}N_e]I - \beta_n N_{s0} I^n \qquad (1.1)$$

Here α is the total absorption coefficient for the material. This value includes the contribution of the linear ground state absorption cross-section ((σ_{s0}) and excited state

absorption cross-section (σ_e) multiplied by population of the grounds state (N_{s0}) and excited state (N_e), respectively. The final term is the absorption due to MPA, represented as the population of the ground state multiplied by the n-Photon absorption cross-section (σ_{npa}) in units of Goeppert-Mayer (GM) with 1 GM=10^{-50}cm^4 s photon^{-1}, and increases with integer powers of incident intensity(I^n).

Thus, a well performing OPL material can be screened through by a comparison of the cross-sections of its excited state to the grounds state cross-section. It has been widely accepted that the ratio (σ_e/σ_{s0}) is an indicator of nonlinear absorption strength of a material[33]. However the difference (σ_e - σ_{s0}) has been put forward as a far better means of indicating the strength of nonlinear absorption[41] as it take account of the absolute absorption ability differnce. In this work both approaches will be used to quantify the strength of nonlinear absorption of SnPcs. Further, the degrees of MPA experienced will contribute, in some cases significantly, to the total non-linear absorption and so must be considered as well, albeit separately.

1.3.2.2 Naming of the nonlinear absorption coefficient (β)

The fundamental approach to the interaction of light with a material is to view the light as an electromagnetic wave and its effects on the material then can be viewed as a polarization by an electric field of the material given by:

$$\vec{P} = \chi\vec{E} \tag{1.2}$$

Here $\vec{P}$ is the polarization field of the material, $\vec{E}$ is the electric field component vector and χ is the electrical susceptibility. This can be expanded as a Taylor series to become

$$\vec{P} = \chi^1\vec{E} + \chi^2\vec{E}^2 + \chi^3\vec{E}^3 + \cdots \quad (1.3)$$

With this expansion we isolate individual components of the polarization field, namely the tensors χ^1,χ^2,χ^3*etc.* referring to the linear electric susceptibility, second-order nonlinear susceptibility, third-order nonlinear susceptibility and so on.

The linear component χ^1, is straightforward and can be examined using normal optical measurement.

The second-order term describes the first type of nonlinear properties, such as optical rectification, second harmonic generation, hyper-Rayleigh scattering and sum-frequency generation[42–44]. These methods can all be used to find the second-order susceptibility for a range of compounds. However for centrosymmetric compounds the second term is zero, due to the χ^2 tensor reducing to a case of $\chi^2 = -\chi^2$ under time inversion and thus having only one solution ($\chi^2 = 0$).

The third term, γ, is then the dominant term in centrosymmetric compounds and it gives rise to its own set of phenomena such as third-harmonic generation, self-phase modulation, self-focusing, four-wave mixing, and phase conjugation.[45–47] Furthermore it is a complex term having both an imaginary and real component

$$\chi^3 = \chi^3_{Re} + \chi^3_{Im} \quad (1.4)$$

Each component describes different behaviors, the real component describes refractive processes and the imaginary describes nonlinear absorption (NLA) and optical power limiters (OPLs) [48].

For molecules in a small electric field caused by plane polarized light the polarization of the molecule can be discribed by an induced dipole characterized as:

$$\vec{u} = \alpha_p \vec{E} + \beta \vec{E}^2 + \gamma \vec{E}^3 + \cdots \tag{1.5}$$

Here the α_p is the linear polarizability (the subscript 'p' is to differentiate this symbol from the other α used in this work). The second and third terms, β and γ, are the first and second hyperpolarizabilities of the molecule. The first hyperpolarizability(β) is the sum of its dipolar ($\beta_{j=1}$) and octupolar ($\beta_{j=3}$) components. While the second hyperpolarizability (γ) (like its corresponding susceptibility) will be split into its real ($Re[\gamma]$) and imaginary($Im[\gamma]$) components. As these are just the molecular specific values, they describe the same phenomena as they did in bulk, but with a concentration dependence.

Measurements for OPL are often done by intensity comparisons for incident light and the amount that is absorbed by the sample:

$$\frac{dI}{dz'} = -\alpha I \tag{1.6}$$

$$\Delta\alpha = \beta_I I \tag{1.7}$$

Here α is the total absorption coefficient of the material due to all effects. When looking for nonlinear components the degree of variation from linear absorption is used.

Here β_I is the intensity dependent NLA coefficient and is normally acquired via fittings of OL data. In the same way that the linear absorption coefficient is related to the effective linear cross-section σ_{s0}, the NLA coefficient is related to processes that absorb light where the relationship between absorption and intensity is nonlinear.

With increases in β_I corresponding to increases in the performance of the material as an optical limiter. Two of these processes are RSA and SA, which correspond to the absorption of light by the excited states of a molecule, where the excited states cross-section (σ_E) can be either smaller than (SA), or larger than (RSA) the ground state as mentioned earlier. Another process that will contribute to β_I is multiphoton absorption, here the coefficient relates the NLA to the multiphoton absorption cross-section (β_{nPA}, but in this work $\sigma_{0n}^{(2)}$ is used). Furthermore the coefficient that relates the absorption to the multiphoton absorption cross-section is sometimes, confusingly, also called β_{nPA}.

All β's have been properly described and classified with subscripts. However, in practice this leads to a large amount of confusion.

1.3.3 Models for Non-linear absorption

1.3.3.1 Intensity Dependent Nonlinear Absorption

A fitting of a Z-scan measurements must be done in order to retrieve nonlinear optical information from the data. This is done in several ways, some which we apply in this thesis.

The first[49] is a general NLA fit, which gives a NLA coefficient based on the extent of nonlinearity the material shows. In this case the parameters of the laser beam are important, and the benefits of NLA fit is that the parameters values are also determined. The equation below describes the Z-scan transmittance profile.

$$T_n(z_s) = \frac{1}{Aq_0(z_s)} \int_{-\infty}^{\infty} \ln[1 + q_0(z_s) f(\tau)]\, d\tau \tag{1.8}$$

Here the transmittance (T_n) is written as a function of the position (z_s), and A is the normalization constant:

$$A = \int_{-\infty}^{\infty} f(\tau)\, d\tau$$

Where $f(\tau)$ is a function describing the temporal profile of the laser pulse. $q_0(z_s)$ is a parameter describing the degree of nonlinearity, given for a circular beam as

$$q_0(z_s) = \frac{2\beta_I P_0 L_{eff}}{\pi\omega^2(z_s)} \tag{1.9}$$

Where β_I is the non-linear absorption coefficient, P_0 is the peak power of the laser pulse, L_{eff} is the effective propagation length in the material, and $\omega(z_s)$ is the beam width in the sample plane at point z_s, given by

$$\omega(z_s) = \omega_0 \sqrt{1 + \frac{z_s - z_0}{z_r}} \tag{1.10}$$

Here ω_0 is the beam width at the focal point, z_s the position of the sample in the beam profile,z_0 the position of the focal point and z_r the Rayleigh range given by

$$z_r = \frac{\pi\omega_0^2}{\lambda} \tag{1.11}$$

Here λ is the wavelength of the laser. Now with the terms defined it becomes apparent that in order to obtain the NLA coefficient, a numerical fitting of $q_0(z_s)$ must be done. This can be a difficult task as q_0 has to be evaluated at all values of z_s, however, these values were calculated for each fit, depending on the nature of the beam pulse[50].

$$q_0(z_s) = \begin{cases} a_0 + a_1 T_n(z_s) + a_2 T_n^2(z_s) + a_3 T_n^3(z_s), & T_n(z_s) \leq 0.75 \\ c_0 + c_1 [T_n(z_s)]^{c_2}, & T_n(z_s) \geq 0.75 \end{cases} \quad (1.12)$$

Here the *a* and *c* terms are parameters dependent on the temporal profile of the beam used, either Gaussian or hyperbolic secant (Sech):

Coefficients	Gaussian pulses	Sech pulses
a_0	15.66	17.26
a_1	-37.45	-41.47
a_2	30.76	34.18
a_3	-8.97	-9.97
c_0	-2.301	-2.328
c_1	2.156	2.180
c_2	-1.563	-1.645

Table 1.2: Coefficients for Gaussian and Sech laser pulses

With parameters defined and a substitution of **Equation 1.9** into **1.10** the definition of $q_0(z_s)$ can be written as

$$q_0(z_s) = \frac{Q_0}{1 + (\frac{z_s - z_0}{z_r})^2} \tag{1.13}$$

With

$$Q_0 = \frac{2\beta_I P_0 L_{eff}}{\lambda z_r} \tag{1.14}$$

With Q_0 being the maximum value for $q_0(z_s)$ at $q_0(z_0)$ and is a single value. Thus we can derive the value of the NLA coefficient (β_I).

$$\beta_I = \frac{Q_0 \lambda z_r}{2P_0 L_{eff}} \tag{1.15}$$

This NLA coefficient can then be used to determine the imaginary third order susceptibility

$$Im[\chi^3] = \frac{2n\varepsilon_0 c\lambda\beta_I}{2\pi} \tag{1.16}$$

Here n is the refractive index of the solvent, ε_0 is the permittivity of free space, c the speed of light in a vacuum, λ the wavelength of the light used and β_I is as described above.

With the susceptibility defined it then becomes possible to define the second order-hyperpolarizability (γ), or at least the imaginary component of it as the imaginary third order susceptibility is described as

$$Im[\gamma] = \frac{Im[\chi^3]}{fNN_A} \tag{1.17}$$

Here f is the Lorentz local field factor, N the concentration and N_A is Avogadro's number.

1.3.3.2 Multi Photon Absorption

MPA occurs with the simultaneous absorption of 2 or more photons, allowing the absorption in regions where there is little or no single photon absorption. As these transitions depend on the absorption of multiple photons the probability scales with the product of the power of the exciting beam (E). Hence two photon absorption (TPA) scales with E^2 and three photon absorption with E^3 and so on. This property allows materials that exhibit MPA to also possess NLO properties, as their absorption will scale nonlinearly with increasing light intensity[45]. MPA is prevalent in almost every material that exhibits one photon absorption, hence any material with high linear absorption coefficient (such as dyes) will tend to have high MPA[51]. Studies of MPA are mostly limited to TPA and 3PA since the probability of absorption decreases with each additional photon, whereby it is used as a means to access higher level orbitals without the use of high energy excitation wavelengths[51]. Like certain cases of single photon absorption, MPA depends on the size of electron dispersion with larger delocalisation giving rise to larger MPA cross-section areas and thus a higher chance of absorption per molecule[52]. Furthermore TPA obeys the transition rules opposite to one photon absorption in centro-symmetric molecules, if a transition from a gerade (g) to ungerade (u) state are permissible in one photon then this will not be the case in TPA[53]. TPA states are (nearly) simultaneous transmissions from an occupied state to a higher state, in this transition the first molecule will excite the electron up to a

nonstationary state, which is a superposition of the g and u states. This state lasts only as long as the effect of the field of the first photon is felt by the molecule, whereby it can be excited up to the last state by the second photon[53].

$$\frac{\partial I}{\partial z} = -N\alpha_2 I^2 \tag{1.18}$$

Equation 1.18 describes the change in intensity of light passing through a medium due to two photon absorption, where N is the concentration of TPA active centres in the beam path, α_2 the molecular coefficient for TPA and I is the intensity of the light.

Now, for a two photon transition in plane polarised light, the TPA cross-section can be written as[53]:

$$\beta_{The} = \frac{2\pi h v^2 L^4}{\varepsilon_0 n^2 c^2}\left(\frac{1}{\Gamma}\right) S_{ig} \tag{1.19}$$

$L = \frac{(n^2+2)}{3}$ where n is the refractive index of the medium in which the measurement takes place. h is Plank's constant, v the frequency of light, c the speed of light and ε_0 the permeability of free space. The term Γ refers to the half width at half maximum of the TPA band, and has units of energy. The TPA cross-section is written as β_{The} due to the difficulty in deriving all the terms for **Equation 1.19** experimentally, hence it is calculated using theoretical modelling.

$$S_{ig} = \left[\sum_i \frac{\langle \boldsymbol{\mu}_{gi}\boldsymbol{\mu}_{if}\rangle}{(E_{gi} - h\nu)}\right]^2 \tag{1.20}$$

Here the vectors $\boldsymbol{\mu}_{gi}$ and $\boldsymbol{\mu}_{if}$ refer to the amplitude of the oscillator strength between the ground state and intermediate state, and the intermediate and final state respectively, and E_{gi} is the energy difference between the ground and intermediate state (In order to get an average of the two vectors' projection in the direction of the optical field.). This can be a complicated derivation as the vectors span all orientations of the molecule, but is simplified by only examining the solution where the two vectors lie parallel to each other, as the exciting photons must have the same directional components[54].

$$S_{ig} = \frac{1}{5}\left[\left(\frac{\Delta\mu_{gf}\mu_{gf}}{h\nu}\right)^2 + \sum_{i\neq f,g}\left(\frac{\mu_{gi}^2\mu_{if}^2}{\left(E_{gi}-h\nu\right)^2}\right)\right] \tag{1.21}$$

Equation 1.21 comprises of two terms, the D term on the left and the T term on the right. The D term is called the "dipolar" term and the T term the "two-photon". For centrosymmetric molecules (like Pcs) there is no natural dipole, so S_{ig} can be simplified to just the T term.[53] So

$$S_{ig} = \frac{1}{5}\sum_{i\neq f,g}\left(\frac{\mu_{gi}^2\mu_{if}^2}{\left(E_{gi}-h\nu\right)^2}\right) \tag{1.22}$$

With this simplified equation, **Equation 1.19** and **1.22** can be recombined to yield

$$\beta_{The} \approx C\frac{\mu_{gi}^2\mu_{if}^2}{\left(\left(E_{gi}/h\nu\right)-1\right)^2\Gamma} \tag{1.23}$$

Here all the previous constants are grouped under the new constant *C*. With the equation simplified, the dependence on the difference between the ground state and the intermediate virtual state (E_{gi}) can be noticed. For a one photon transition this difference is the total transition, $E_{gi} = hv$ and the equation reduces down to a one photon transition.

$$T_{OA(nPA)} = \frac{1}{\left[1 + (n-1)a_n L \left(\frac{I_{00}}{1+(\frac{z_s}{z_r})^2}\right)^{n-1}\right]^{\frac{1}{n-1}}} \tag{1.24}$$

This equation describes the Transmission (T_{OA}) of a material that undergoes *n*-photon absorption. Here α_n is the *n*-photon absorption coefficient, *L* the effective path length and I_{00} the input irradiance.

A fitting can be made for any *n*, though the true value of *n* will give a better fit. For higher *n* the shape of the absorbance profile will narrow, giving sharper fits for high *n* and broader fits for low *n*. The reason for this is apparent on inspection of the equation[55].

Substituting *n*=2 into **equation 1.24**,

$$T_{OA(2PA)} = \frac{1}{\left[1 + a_2 L \left(\frac{I_{00}}{1+(\frac{z_s}{z_r})^2}\right)\right]} \tag{1.25}$$

A much simpler equation is obtained. Here a_2 is the TPA coefficient. This coefficient can then be related to the molecule specific TPA cross-section σ_{TPA} using the equation

$$\sigma_{TPA} = \frac{\alpha_2}{N} \tag{1.26}$$

Here the TPA cross-section(σ_{TPA}) is related to its coefficient (α_2) via the concentration (N) in which the sample was analysed.

1.3.3.3 The Multi orbital model

Excitation of an electron in a linear case will be from an occupied orbital to an unoccupied orbital. However, excitation to a non-existent virtual orbital can occur. Once excited, the electron will take some small amount of time to fall back down. However, in the case of RSA these excited electrons are further excited and this excitation will lead to an increase in overall absorption.[56]

Base excitation is the excitation that first moves an electron to the excited state. In most cases this is done by the linear absorption of a single photon. This absorption is constant for all intensity of light and does not scale, measured using the extinction coefficient (ε) or the ground state cross-section (σ_g). Another type of excitation arises from an occupied state to an excited one and is referred to as MPA; in this case the absorption does scale with the square of light intensity.

Once the electrons are excited it is possible for them to absorb another photon. The probability of this occurring is controlled by the cross-section of the state in question. If the effective excited state cross-section of the material as a whole is larger than the ground state cross-section, RSA is said to occur. As there is an infinite amount of virtual excited states, the models that look at this behaviour are reduced to only the most active states.[56]

1.3.3.3.1 The Three Orbital Model (Scheme 1.9)

The three orbital model is used when the primary cross-section responsible for excited state absorption (ESA) is the first singlet excited state (S_1). In this situation ground excitation leads to the population of the S_1 state, from where ESA occurs. If the S_1 cross-section(σ_g) is larger than the ground state cross-section, then RSA will occur. This model can be used when the excitation pulse is shorter than the inter system crossing (ISC) time of the material, or when σ_T is much smaller than σ_S so that a population in the triplet state has no effect on the total ESA.

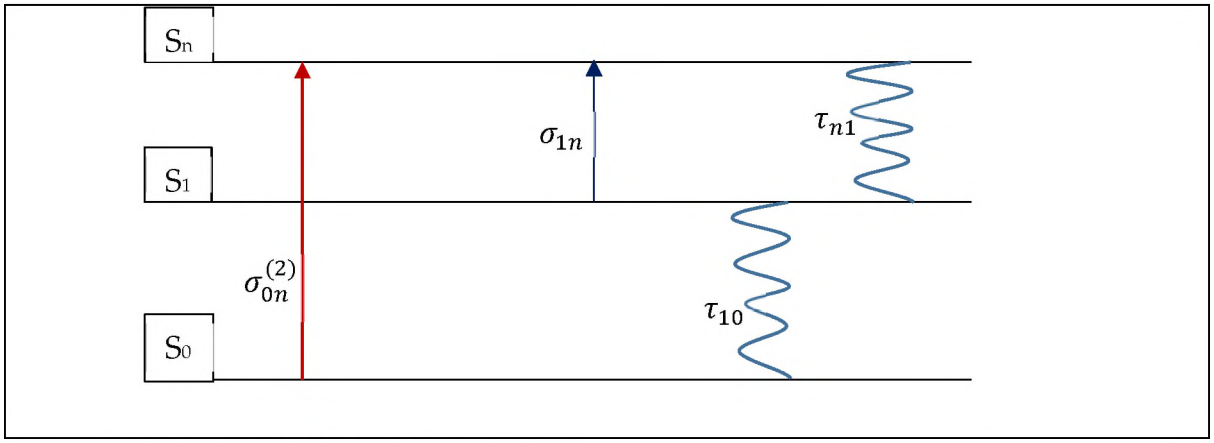

Scheme 1.9: The Three orbital model.

1.3.3.3.2 The Four Orbital Model (Scheme 1.10)

The four orbital model makes use of the first triplet state (T_1) as the primary cross-section responsible for ESA. Ground state absorption (via any process) populate the first singlet excited state (S_1). However, in this model σ_1 is vanishingly small. This leaves the excited electron in S_1 only two options- fluorescence decay or (ISC), moving from the S_1 to the T_1 state. Here the electron can be excited further (T_1 ->T_n)[57]. As the decay time shortens for higher excited states, this electron can instantly return to the T_1 state after absorption of a photon due to 'Kashas Rule'[58]. This model depends heavily on the ISC time (τ_{ISC}) as well as the triplet lifetime (τ_{ISCg}) as very short decays can inhibit the ESA in this state. Unless a probe is being used, this system is very dependent on the pulse duration (of the pump), if the pump's duration is shorter than the τ_{ISC} then no measurements can properly be done on the ESA of the T_1 state[59].

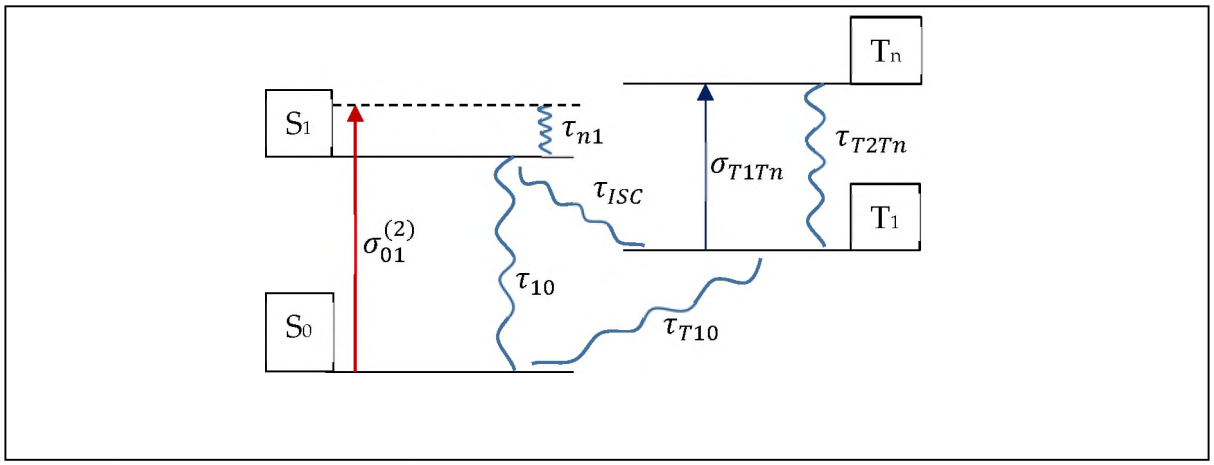

Scheme 1.10: The Four orbital model.

1.3.3.3.3 The Five Orbital Model (Scheme 1.11)

Should the situation occur whereby neither the first singlet excited state S_1 nor the first triplet excited state T_1 can be ignored, due to experimental setup or material nature, it becomes necessary to enlarge the amount of states considered in the model. The five orbitals considered then become the ground state (S_0), the first and N^{th} excited state (S_1 and S_n respectively. As the exact value of N depends on the material and the means of excitation) and the first and N^{th} triplet excited state, T_1 and T_n respectively, (as the exact value of N depends on the material and the means of excitation). Similar to simpler models, the excitation can occur via linear or non-linear processes and then ESA will occur[60]. In this situation the excited state cross-section is composed of the σ_T and the σ_S.

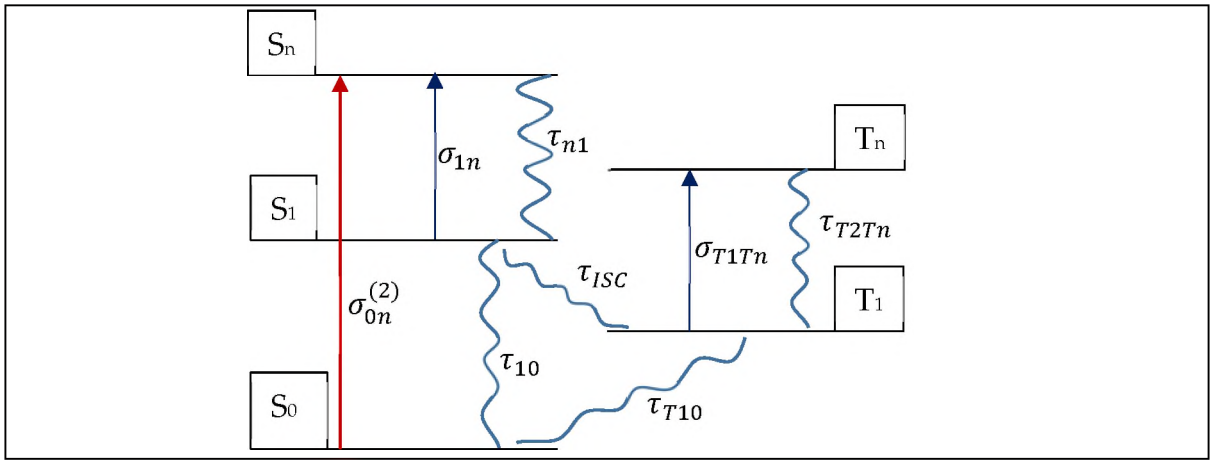

Scheme 1.11: The Five orbital model.

1.3.4 Computational methods

The inputs required are a set of experimental data, that are for the same Pc in the same solvent. This set of data should ideally be of a varied power. Multiple data sets of the same Pc/solvent at different and known powers are essential, with greater data sets giving greater accuracy. Next approximations of the three cross-sections are made, these are initial guesses made based on similar Pcs reported in literature or already calculated. Next the parameters of the sample must be set: the concentration of the sample (implied is the sample length but this will remain unchanged for all samples), the fluorescence (τ_{10}) and phosphorescence ($\tau_{ISCg} = \tau_{30}$) decay times and the ISC time (τ_{13}). Any of these values can be floated however accuracy will be affected and additional data sets should be used to improve the fit and floating more than one will lead to too many degrees of freedom to form a reliable fit.

Initially an absorption curve is formed by using these parameters to generate an initial approximation. However, the dynamics of the sample is not a single value fit. This is due to the sample not being a monolayer of NLO material, but a cell cuvette of length L. If the material in question is a NLA then the degree of absorption is not

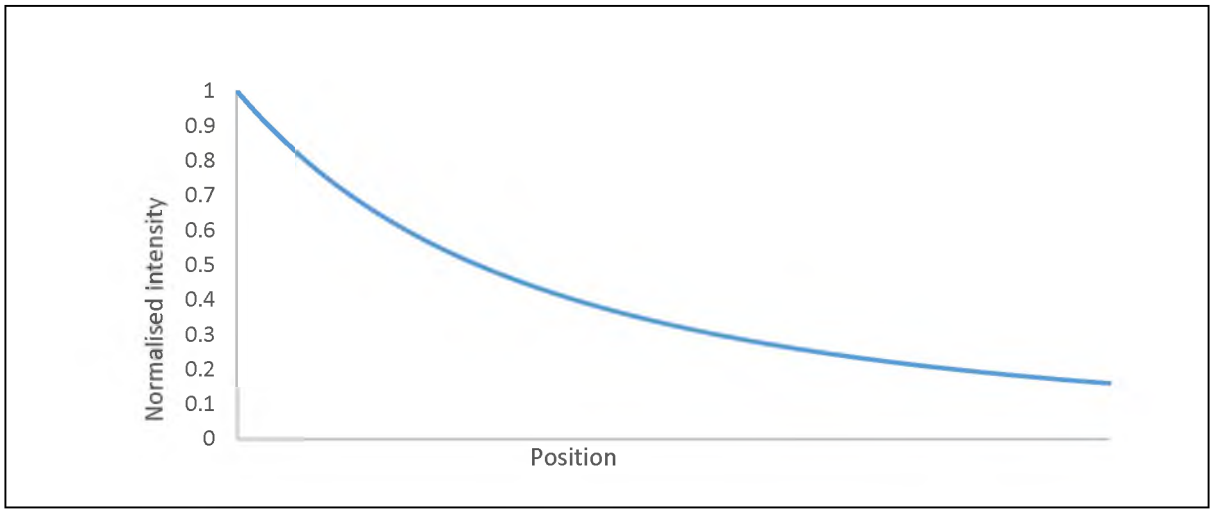

Figure 1.4: Normalised intensity as it moves through a nonlinear absorber.

linear, depending on the intensity of the light. This means that light is absorbed mostly in the first few units of the cell and decays down as light progresses through the total length of the cell, this is illustrated in Figure1.4

This implies that any theoretical fitting of the sample must account for the decrease in intensity over the length of the sample.

The absorption however is also a function of time. Initially the system obeys (approximate) linear absorption rules, but once the intensity per unit area starts to rise the probability of TPA begins to increase. This TPA is the first NLA that is observed at a 532 nm wavelength for Pcs and, for very short laser pulses(<1 ps), is the only NLA effect that will be observed[59]. For longer pulses (>1 ns) however, other effects will begin to take place.

The pulse itself is Gaussian in nature (a Gaussian pulse is shown in Figure 1.5), implying that the incident knee of the Gaussian curve will be almost unaffected by the NLA properties of the material, as the intensity here is low. As the Gaussian pulse progresses more and more NLO processes become active and stay active until there is no more exciting light. Thus, the tailing knee of the Gaussian curve is absorbed more than the incident knee.

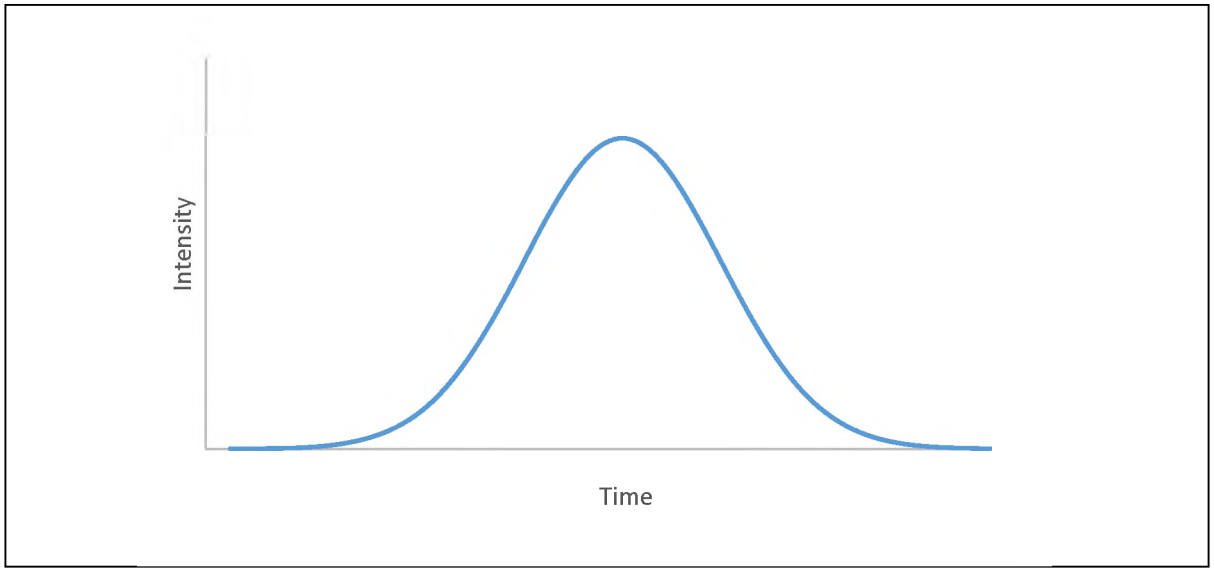

Figure 1.5: Graph of a Gaussian pulse's temporal profile

Initially all molecules in the sample are in the ground state, with the excited states all being empty. Once the laser pulse begins to pass through the sample excitation will begin to occur. Initially this is done by TPA in Pcs, as at this wavelength (532 nm) Pc

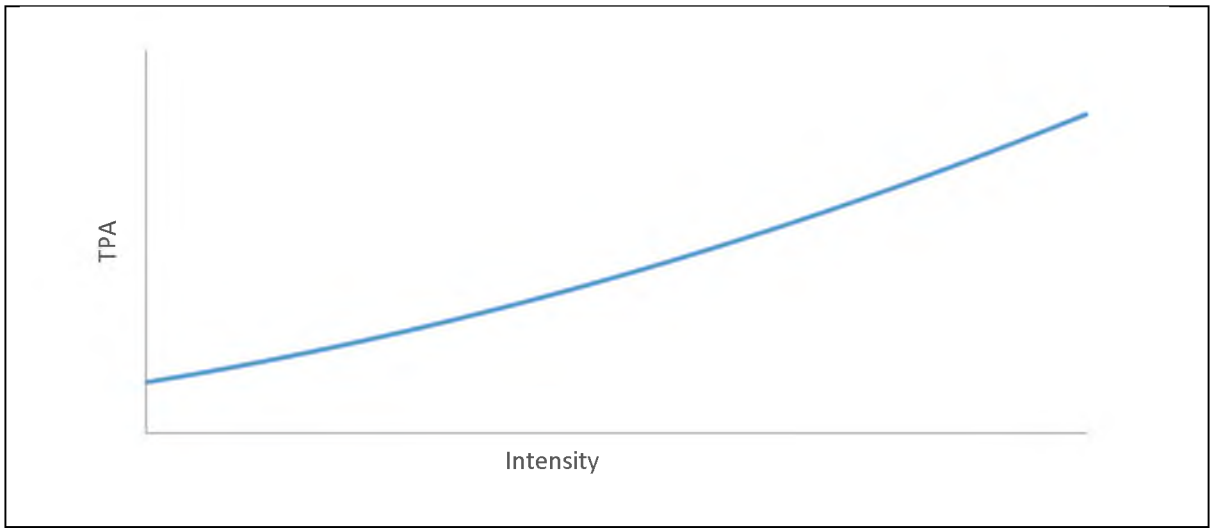

Figure 1.6: Degree of nonlinear absorption vs Intensity

are virtually optically transparent[28]. This initial absorption will only start to take place at higher light intensities, not having a 'threshold' but scaling into the nonlinear absorption ,shown in Figure 1.6, with an exponential relationship[61].

This response demonstrates the usefulness of TPA in optical limiting, being highly selective for higher light intensities, and ignoring low intensity. However, after TPA, electrons do not decay down to ground state, first settling in the first few excited states. Once in these states the electrons acquire the ability to absorb further photons via ESA. This changes the light absorption profile of the sample, Figure 1.7, going from the exponential relation of TPA to a higher exponential relation due to the new ESA processes.

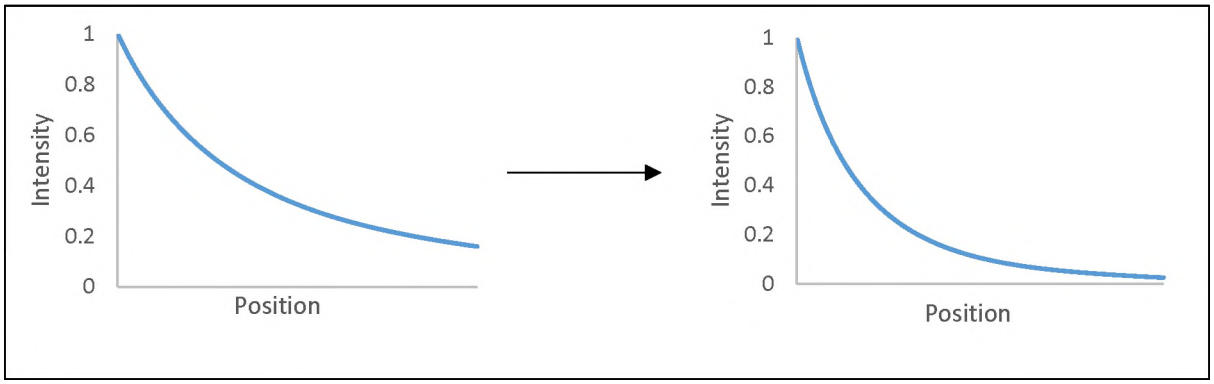

Figure 1.7: Change in the degree of absorption vs length travelled in a nonlinear absorbing material when more than one factors become active.

Thus the total absorption of each unit length of the sample, and the absorption of each subsequent unit length must be calculated independently.

If the laser is operated at a sufficiently low power, then the change in population of molecules in the ground state can be ignored as there will not be enough power to excite them all. This simplifies population calculations as well as minimizes the effect of ground state depletion. This does not mean that calculation of S_0 should be ignored, but this condition will simplify the initial measurements. As the linear absorption is minimal, the only process that decreases the S_0 population is TPA, and the processes that increase it are the fluorescence and phosphorescence decays.

The ESA can then be thought of to be caused by the TPA transitions that decay down into the excited states (for the molecules used here at least). These transitions can be

thought to transition straight from the S_0 to the S_1 state as the decays from the higher excited states to the lower excited states are close to instantaneously due to Kasha's rule[58]. The ESA, which comprise of excitations from both T_1 an S_1, are then calculated as a product of the population of the respective states and their cross-sections. The populations of the excited states also depend on the position of the molecules in the sample cell, with those closer to the zero-point experiencing higher light intensities, and thus higher TPA, and thus greater excited state population.

The equations that describe the change of populations of each of the states can be shown as[62]

$$\frac{dN_{S_0}}{dt} = -\frac{I^2\sigma^{(2)}_{s_{01}}N_{S_0}}{2(\hbar\omega)^2} + \frac{N_{S_1}}{\tau_{10}} + \frac{N_{T_1}}{\tau_{30}} \tag{1.27}$$

$$\frac{dN_{S_1}}{dt} = \frac{I^2\sigma^{(2)}_{s_{01}}N_{S_0}}{2(\hbar\omega)^2} - \frac{N_{S_1}}{\tau_{10}} + \frac{N_{S_n}}{\tau_{21}} - \frac{\sigma_{12}IN_{S_1}}{\hbar\omega} - \frac{N_{S_1}}{\tau_{13}} \tag{1.28}$$

$$\frac{dN_{T_1}}{dt} = \frac{\sigma_{34}IN_{T_1}}{\hbar\omega} - \frac{N_{T_n}}{\tau_{43}} + \frac{N_{S_1}}{\tau_{13}} - \frac{N_{T_1}}{\tau_{30}} \tag{1.29}$$

$$\frac{dN_{T_n}}{dt} = \frac{\sigma_{34}IN_{T_1}}{\hbar\omega} - \frac{N_{T_n}}{\tau_{43}} \tag{1.30}$$

$$\frac{dN_{S_n}}{dt} = \frac{\sigma_{12}IN_{S_1}}{\hbar\omega} - \frac{N_{S_n}}{\tau_{21}} \tag{1.31}$$

Where I is the intensity of light at that unit length, and N_x is the population of state x, σ_{ij} is the cross section for absorption between states i and j.

1.4 Theoretical calculations

1.4.1 Solvents

Most photophysical studies are done in solvents. As such, taking baseline readings on the solvent in use before taking measurements is an important part in isolating the correct values in question. However, NLO properties are a little more involved, as solvents interactions are similar to the sample interaction with external electromagnetic fields. According to the reaction field (RF) theory put forward by Barker and Watts[63], the polarizing effect of the solvent field is similar to the field induced from the stimulating light. However, while the exciting field created by the excitation source radiation is homogenous, the polarizing effect of the solvent acts only the regions of the molecule where the solvent coordinates to.

Pcs are known to be relatively insoluble[64]. The peripheral substituents on MPcs are the primary regions for solvent interaction and must be added to a basic Pc in order to solvate it. This creates a situation whereby the solvent will create a slight polarisation on the Pc through the substituents[65]. The above effects can be seen to significantly influence the effects of NLO behavior. NLO behavior can be described by **Equation 1.2,** which indicates that a simple base level reading of the solvent system before a measurement will be insufficient to accurately determine the full effects of the solvent.

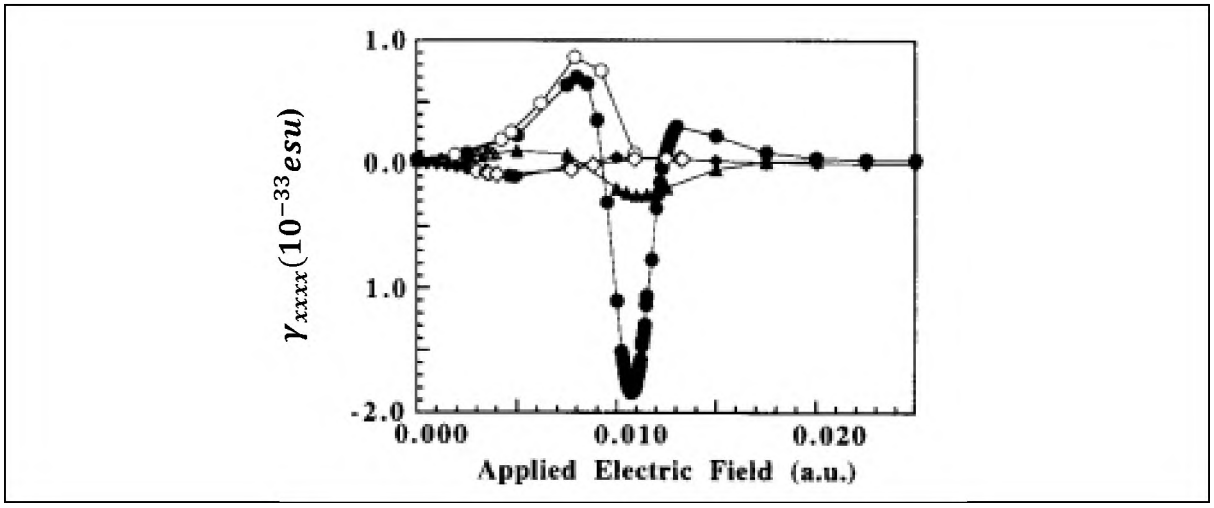

Figure 1.8: Effects of Applied electric field on the third order polarizability(γ)[66].

Figure 1.8 shows the effects of the existing polarizing field on a few molecules, and shows how solvents can affect the third order polarizability (γ)[66].

Unsubstituted Pcs are known to be very insoluble in most solvents, and only slightly soluble in others[18,67,68]. This implies that most solvents have very little coordination with the basic Pc ring, and the Pc is best solvated when it has substituents around its periphery ring[18]. Thus the polarizing effects of solvents on the Pc can be thought of to be localized around the substituents.

1.4.2 Computational simulations

The fastest means of determining the effects of solvation on a molecule's NLO parameters would then be to run computational simulations on the molecule in one or more solvents and see if any observable trends, shown in Figure 1.8, arise. This is done via a variety of methods outlined in **1.5.4,** but the common problem in this approach is that of computation time[69,70]. For large molecules like Pcs that take some time using Density Functional Theorem (DFT), or even with some semi-empirical methods, its becomes computationally prohibitive to calculate their higher order NLO parameters with reliable accuracy[70]. However, it has been shown that it is possible to calculate lower order NLO parameters using acceptably accurate methods[74], and so it might be possible then to find and observe the behavior of the lower NLO parameters as they change through different media and make any possible comparisons with the higher order NLO parameters.

1.5 Interments and methods

1.5.1 Time Correlated Single Photon Count

A Time Correlated Single Photon Count (TCSPC) is done by stimulating a sample with a suitable excitation source (normally a laser) and then observing the fluorescence emission. Specifically, the excitation source emits a very short (ps range) pulse that excites the samples and primes the emission detector. Once primed the emission detector (that is perpendicular to the excitation pathway (**Scheme 1.12**) starts to record the emission of photons from the sample as the sample decays back down from the excited state to the ground state. The emission bands for most materials will decay

sharply after excitation, and a time to amplitude converter is used to match up the time of excitation to the beginning of the decay curve.

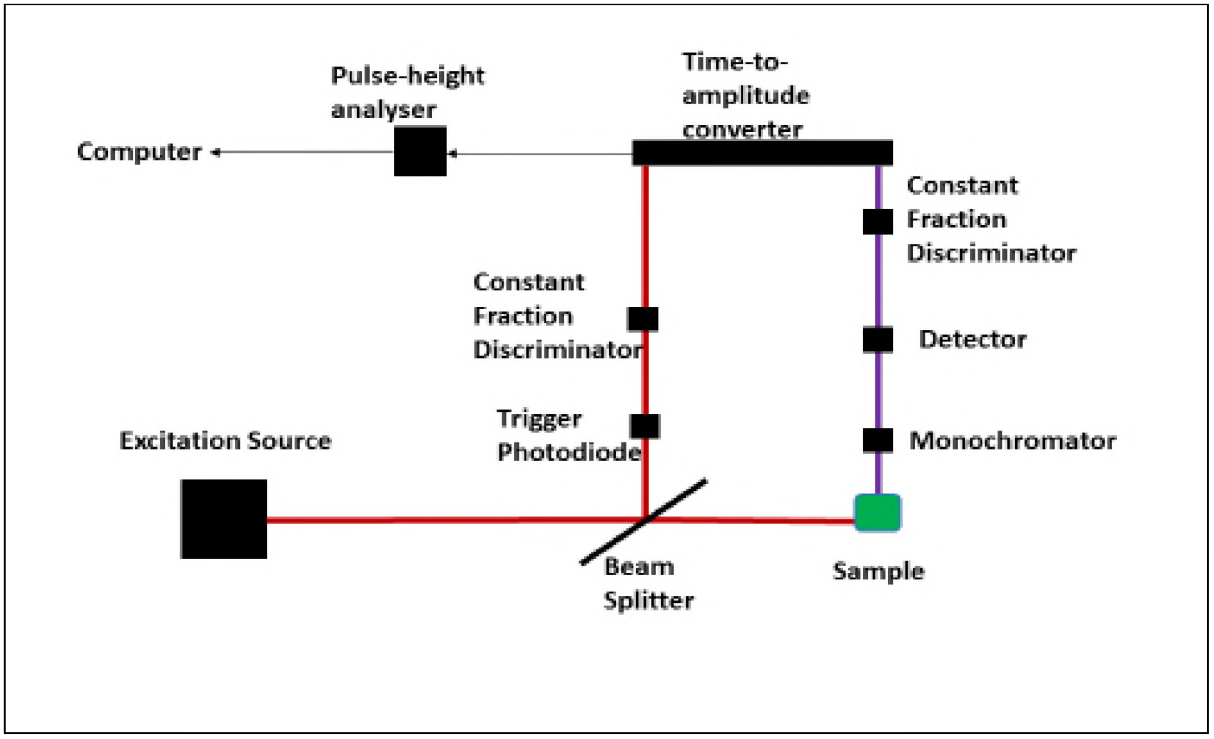

Scheme 1.12: Setup of a Time Correlated Single Photon Count.

The data from the photodiode and emission detector are combined to give a decay profile for the sample, displayed in Figure 1.9 **.** This data can be analysed to give the life time of the excited state of a molecule. Furthermore, if horizontal and vertical polarisers are in place the decay curve of the two different polarisations of light can be used to give the molecules' rotational information.

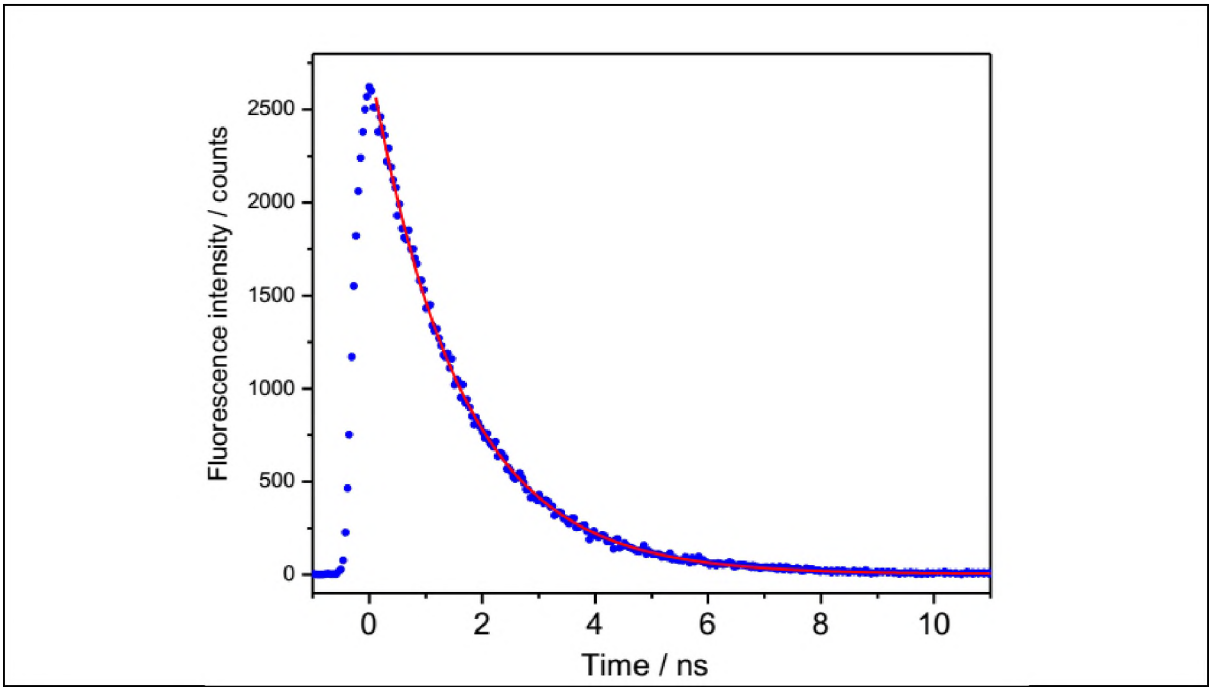

Figure 1.9: A decay curve from a Time Correlated Single Photon Count [71].

In this study the fluorescence lifetimes of the six Pcs in question were analysed in the four solvents of choice using a 670 nm laser. These lifetimes were then used later in calculating the NLO parameters.

1.5.2 Z-Scan

Z-Scan is a process of determining the second hyperpolarizability of a sample by moving it along a focused beam line, as an illustration in Scheme 3.2. The result of this set up is that the fluence at the sample position changes but the irradiance does not. Observing the decrease (or increase) in the total light being received in the detector in comparison to a reference detector allows the determination of the imaginary component of the second hyperpolarizability Im[χ^3]. If an aperture is placed in front of the final detector then the real component of the second hyperpolarizability Re[χ^3] can be determined as well, as this component is dependent on refraction.[72,73]

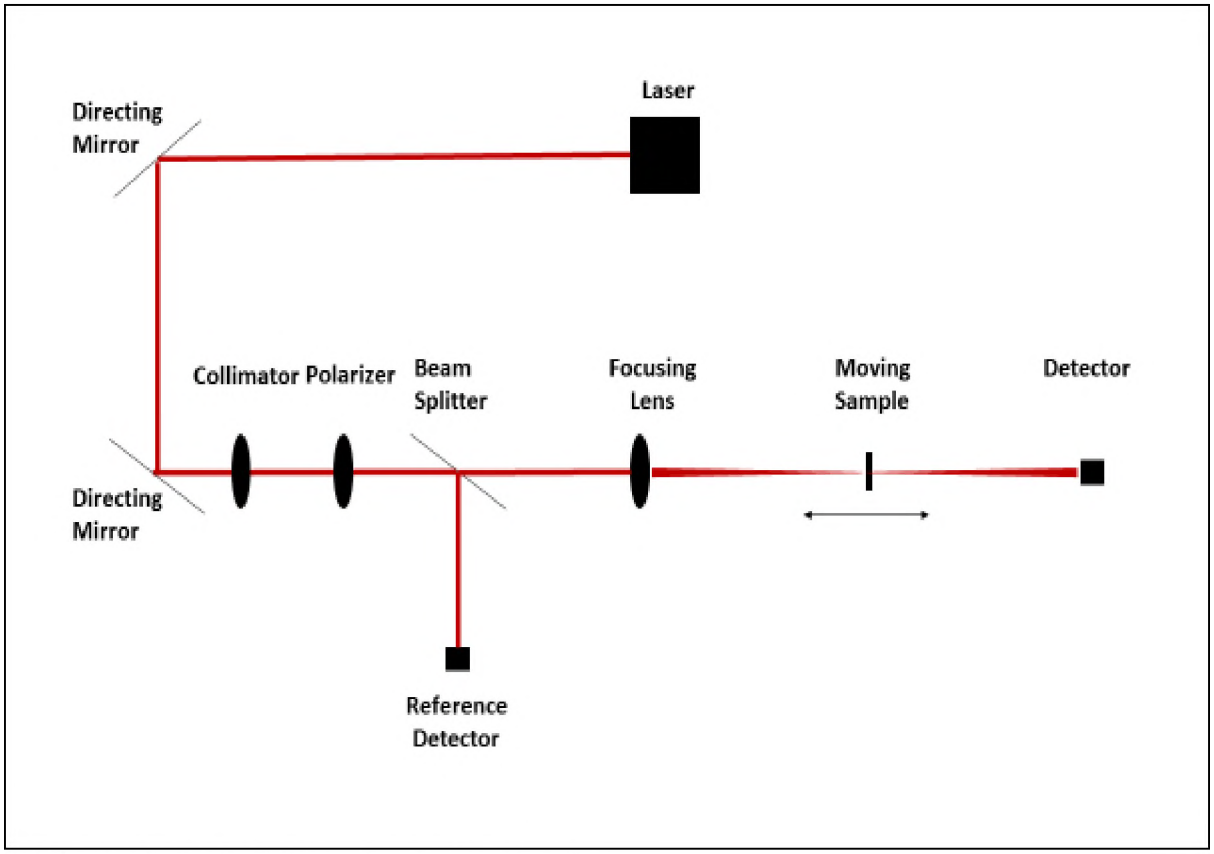

Scheme 1.13: **A Z-Scan (open aperture).**

The data acquired from an open aperture Z-Scan will always give the relative change in absorbance shown in Figure 1.10, however it is important to note that this is for a particular wavelength and results can vary between different types (and thus different wavelengths) of lasers.

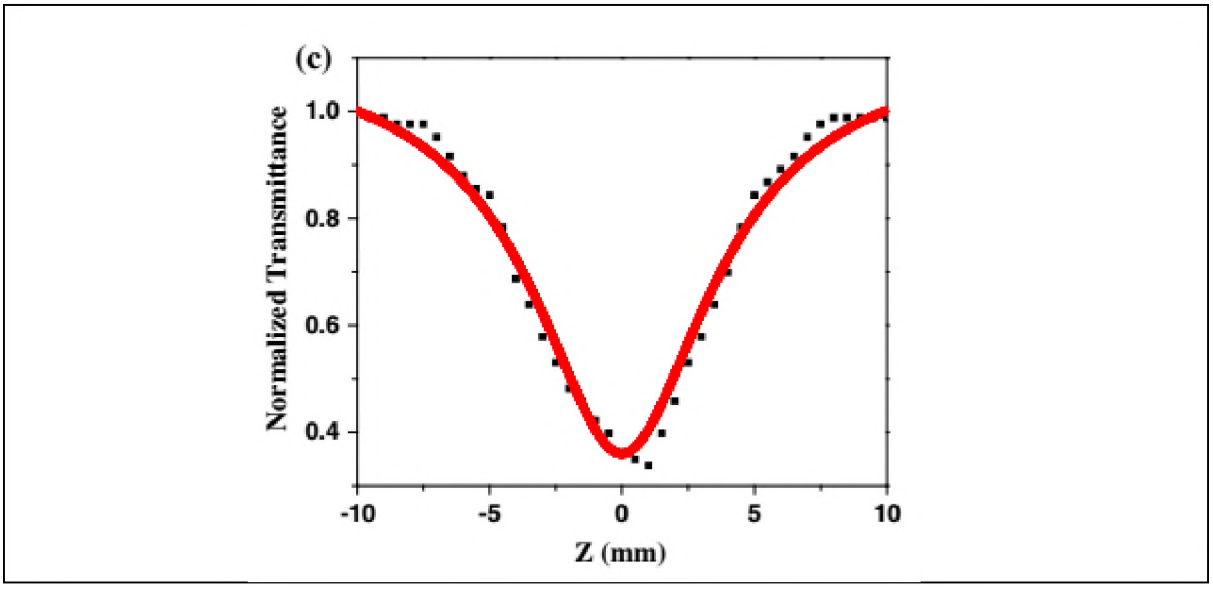

Figure 1.10: A Z-Scan for a reverse saturable absorbing material[74].

1.5.3 Magnetic Circular Dichroism

Magnetic Circular Dichroism (MCD) is a method very similar to UV/vis spectroscopy in its approach. However, MCD can also detect the differences in the way a molecule, such as a Pc shown in Figure 1.10, polarises light. This makes MCD very useful in characterising Pcs as both the B and the Q bands are MCD active and this can be easily shown using the MCD spectra[75].

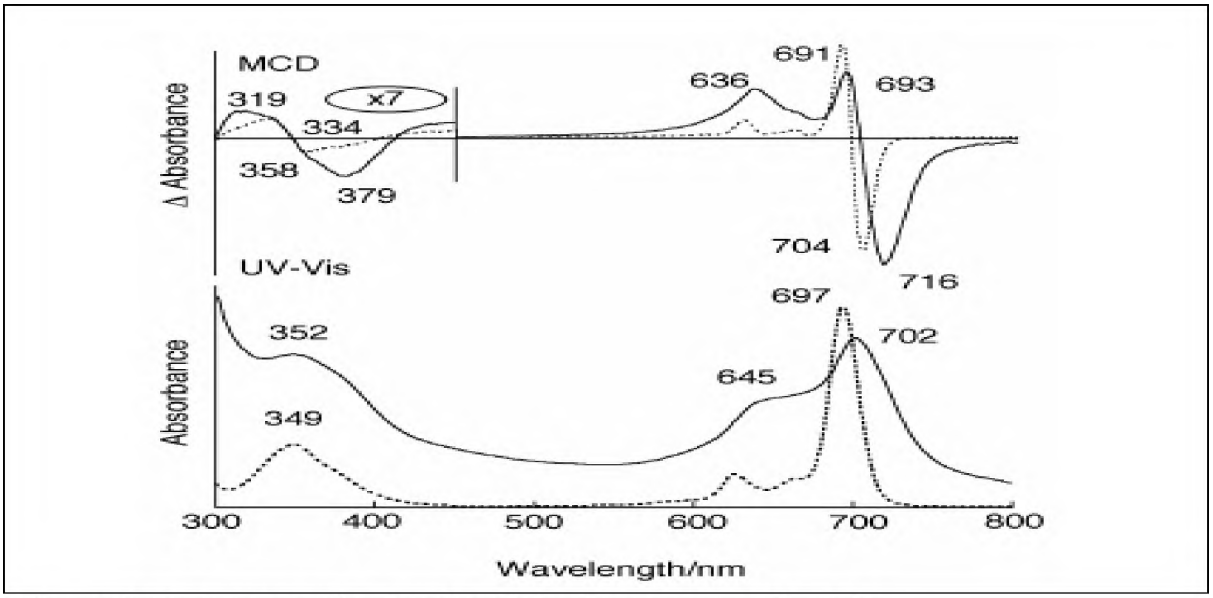

Figure 1.11: A Magnetic circular dichroism spectra of a Pc[76].

MCD works by having a polarised light, normally emitted from a Xenon lamp and monochromated, is passes through a sample in a magnetic field. The magnetic field is of the order of 1 Telsa to properly distinguish between the difference in the asymmetrical absorbance of a molecule. A full set of data requires two runs, with the magnet in opposite orientations for each, to acquire a full spectrum of data, as seen in Figure 1.11.

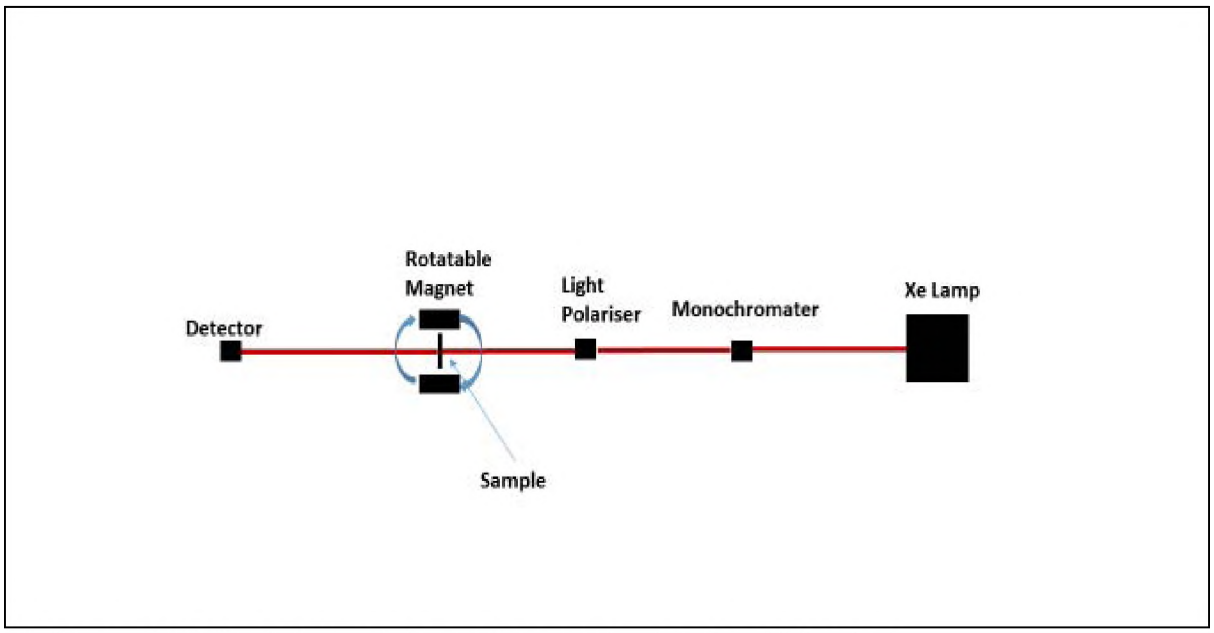

Scheme 1.14: Basic layout for an Magnetic circular dichroism.

1.5.4 Molecular Modelling

All calculations were done using the Gaussian09[77] computation package. Geometric optimizations were done using the Becke, three-parameter, Lee-Yang-Parr (B3LYP) functional and the Los Alamos National Laboratory 2-double-zeta (LANL2DZ) basis set. The absorption and polarisation properties were calculated with the same configuration, with the integral equation formalism variant of the Polarizable Continuum Mode (IEFPCM) to account for solvent contributions. Calculations were done on the molecule without any addition or simplification of their structures. This

allowed for any effects due to the IEFPCM to take place on the full potential area of the molecule.

1.5.4 Constraints

Due to the large average molecular structure of Pcs the use of very resolved basis sets and highly accurate functionals for calculating the properties of Pcs is resources restricted.

1.5.4.1 Metal

The central metal is often the largest challenge in acquiring a good optimisation for a Pc[78]. This is due to most central metal candidates having some d electrons and some full p shells. To fully analyse a MPc, it is often prudent to allocate a second basis set, generally far less accurate than the one used to describe the main ring of the Pc, to the metal[79]. Basis sets that normally use a pseudo potential of the atom in question give the system a general idea of the metal's electron behaviour and allow calculation of the electron of the metal on the Pc's electron structure as a whole.[80]

1.5.4.2 Periphery

The periphery substituents on the Pc cause the bulk of the issues due to steric hindrance. Depending on the type of substituent, these contributions can become significant to the accuracy and time of the model uses. In most cases, the substituents can be pruned at a certain length, as the contribution to the Pc's electron structure due to a $C_{10}H_{21}$ (R group) will be almost identical to the contributions due to a C_3H_7 (R group). For the optimisations done here, no structural approximations were made, in case solvent effects changed with the change of area available for interaction. (Though in the single case run as a test the differences were found to be negligibly small). Further complications arise from the nature of substituents as they are not necessarily

from the first row p atoms. Such is the case for the thioether used for half of the Pcs in this thesis. These atoms cannot simply be pruned from the model as their contributions are not as simple as a methyl chain. The two options then available are to find a basis set that accurately accounts for their contributions and provides reliable values for the main Pc ring, or to lump these atoms with the metal in a second, less accurate basis set. As the substituents often do not absorb light directly (and not in the analysis window around 532 nm), and only affect the main Pc ring by stabilising or destabilising the A_{2u} orbitals relative to the A_{1u}, it is often prudent to use the second option and analyse these atoms using the additional basis set[80].

1.5.4.3 Analysis

Modern consideration of the theoretical transition for a Pc are based on the work of Gouterman[24], whereby the inner ring of a Pc is equated to $C_{16}H_{16}^{2-}$ cyclic polyene, which has the same number (18) of π electrons distributed along the ring. The molecular orbitals of this system can then be arranged according to their increasing orbital angular momentum $M_L = 0, \pm1, \pm2, \pm3, \pm4, \pm5, \pm6, \pm7$. Gouterman calculated that the frontier orbital of the Pc were then the ±4 and ±5 orbitals so that the absorption transitions were the ±4 to the $\pm$ 5 MOs. These adequately described the absorption bands in the 300 to 400 nm range with $(-4 \rightarrow -5)$ and $(+4 \rightarrow +5)$ transitions, however in Pc the dominant absorption region is in the 650 to 800 nm range and has no classical analogue. Gouterman put forward the concept of a pair of forbidden transitions from $(-4 \rightarrow +5)$ and $(+4 \rightarrow -5)$ that possess a ΔM_L of ±9 so as to adequately describe these bands. The forbidden nature of these transitions was due to the fact the photons can only transfer an angular momentum of $M_L = \pm1$. These bands then became known as the Q bands after the Japanese word for 9, ku. Michl[81] further showed that MOs can be further grouped based on their node symmetry, with MOs having nodes on the xy plane of the molecular ring being a or $-a$ and those MO not having nodes in the xy plane assigned the terms s and $-s$. These assignments allowed

a better understanding of the transitions between ground and excited states by showing where and how additions and replacements in the ring can alter the MO. In the case of Pcs, this showed that the primary effects of the addition of the aza-nitrogens were to stabilize the s MO, allowing greater separation of the two types of orbitals. This then allowed the assignment of the Q band to the $a \rightarrow -a$and $a \rightarrow -s$ transitions.

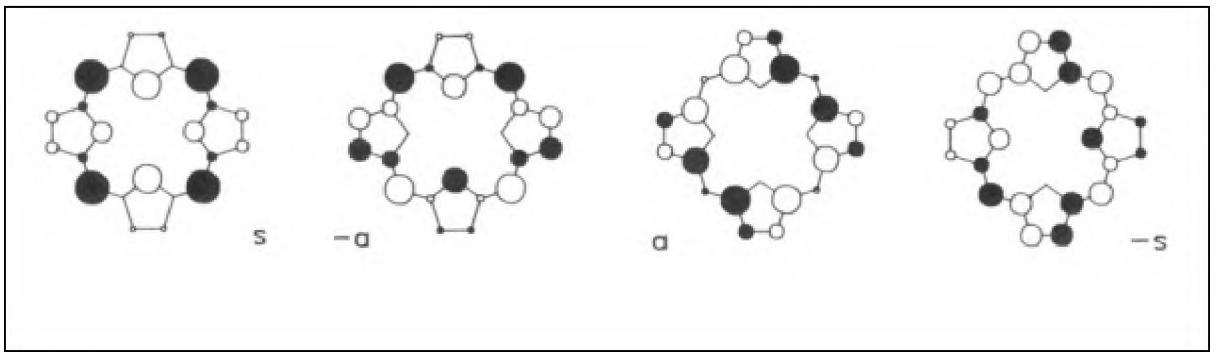

Figure 1.12 : Michl's four ourbitals, with a and –a having anti-nodes on the zy plane and s and –s having nodes on the zy plane [81]**.**

Computational analysis of the octupolar tensorial components can also be used to calculate the polar components of the molecule; these allow us to calculate the second order coefficient of the second order polarisation (β). This value, like the third order term, can be measured experimentally (normally via the Hyper Ryleigh Scattering technique[44]), giving the measurement of β_{HRS}. However direct theoretical calculations can be done for this value as well. These calculations have been shown to have relatively high accuracy if the correct methods are used[82–84]. These calculations are dependent on higher order terms, like other calculations for excited states, and so tend to be more accurate if done with far more HF components to the functionals as well as any functional that accounts for the perturbation effects of excitation. As such the calculations for these values would be done with either the Møller–Plesset (MP) set of functionals or the connected triple approximation of the single and double couple cluster (CCSD(T)) calculations. Problems arise, however, due to the high computational cost of these functionals which can increase further if a dynamic system model is used[83]. Thus CPDFT is used as a tradeoff, allowing the measurement of the

β_{HRS} to some degree of accuracy, but not to the degree of accuracy that is possible as a full calculation using the relevant functionals would prove computationally prohibitive for a molecule the size of a Pc[85].

The calculations of the β_{HRS} are done by an analysis of the tensorial components of the molecule and then computing the theoretical β_{HRS} with the equations:

$$\beta_{zzz}^2 = \frac{1}{7}\sum_{\varsigma}^{x,y,z}\beta_{\varsigma\varsigma\varsigma}^2 + \frac{9}{35}\sum_{\varsigma\neq\eta}^{x,y,z}\beta_{\eta\varsigma\varsigma}^2 + \frac{2}{35}\sum_{\varsigma\neq\eta\neq\xi}^{x,y,z}\beta_{\eta\varsigma\xi}^2 + \frac{6}{35}\sum_{\varsigma\neq\eta}^{x,y,z}\beta_{\varsigma\varsigma\varsigma}\beta_{\varsigma\eta\eta} + \frac{3}{35}\sum_{\varsigma\neq\eta\neq\xi}^{x,y,z}\beta_{\eta\varsigma\varsigma}\beta_{\eta\xi\xi} \tag{1.32}$$

$$\beta_{xzz}^2 = \frac{1}{35}\sum_{\varsigma}^{x,y,z}\beta_{\varsigma\varsigma\varsigma}^2 + \frac{11}{105}\sum_{\varsigma\neq\eta}^{x,y,z}\beta_{\eta\varsigma\varsigma}^2 + \frac{4}{105}\sum_{\varsigma\neq\eta\neq\xi}^{x,y,z}\beta_{\eta\varsigma\xi}^2 + \frac{2}{105}\sum_{\varsigma\neq\eta}^{x,y,z}\beta_{\varsigma\varsigma\varsigma}\beta_{\varsigma\eta\eta} + \frac{1}{105}\sum_{\varsigma\neq\eta\neq\xi}^{x,y,z}\beta_{\eta\varsigma\varsigma}\beta_{\eta\xi\xi} + \frac{1}{105}\sum_{\varsigma\neq\eta\neq\xi}^{x,y,z}\beta_{\eta\varsigma\varsigma}\beta_{\eta\xi\xi} \tag{1.33}$$

$$\beta_{HRS} = \sqrt{\{(\beta_{zzz}^2) + (\beta_{xzz}^2)\}} \tag{1.34}$$

1.6 Aims

The aims of the study is to determine the imaginary third order susceptibility ($Im[\chi^3]$) of a series of similar Pcs using an open aperture Z-Scan in a range of solvents. Simultaneously, computational models of the same Pcs in solvent will be done and the theoretical second order susceptibility in the same solvent range will be determined using methods outlined in literature[86].

Comparisons will be done strictly on similar trends observed in both the experimental third order and the theoretical second order, in order to establish fast rules to determine NLO properties in the future.

Chapter 2. Synthesis and Experimental

2.1 Synthesis of SnPcs

2.1.1 Reagents used

N,N-dimethylformamide (DMF), dichloromethane (DCM),Hexane, Chloroform, Toluene, Tetrahydrofuran (THF), methanol, ethanol, 1-octanol, 1-pentanol and silica gel were purchased from Merck. 4-t-butylphenol, Phthalamide,1,8 diazabicyclo[5.4.0]undec-7-ene (DBU), Tin Chloride ($SnCl_2$), Thionol Chloride and 1-thiol Pentane were purchased from Sigma Aldrich. Chloroform, DCM, THF and Toluene were dried using molecular sieves (0.4 nm, rods).

2.1.2 Synthesis of precursers

Compound (1a) 4- tert-butylphenoxyether phthalonitrile:

0.5 g of 4-nitrophthalonitrile was dissolved in DMF (5ml) under nitrogen gas. To this solution 0.7 g of 4-tert-Butylphenol was added. Reaction was left to react under nitrogen for 50 hours. Product was precipitated out using cold water, and re-crystallised in methanol. Yield: 73.6%, Elemental: expected values (%):(C=78.2), (H=5.8), (N=10.1), (S= -), results (%) (C=77.1), (H=6.3), (N=11.23), (S=2.1) IR: (C≡N =2230.90), (C-H=2930, 3075), (Ph-O=1242)

Compound (1b) 3- tert-butylphenoxyether phthalonitrile:

0.15 g of 3-nitrophthalonitrile was dissolved in DMF (2ml) under nitrogen gas. To this solution 0.2 g of 4-tert-Butylphenol was added. Reaction was left to react under nitrogen for 50 hours. Product was precipitated out using cold water, and re-crystallised in methanol. Yield: 67.7%, Elemental: expected values (%): (C=78.2), (H=5.8), (N=10.1), (S= -), results (%) (C=76.4), (H=7.1), (N=12.34), (S=2.5) IR: (C≡N =2230.89), (C-H =3108, 2928), (Ph-O= 1242)

Compound (1c) 4-Pentanethiolether phthalonitrile:

0.5 g of 4-nitrophthalonitrile was dissolved in DMF (5ml) under Nitrogen gas. To this solution 0.4ml of 1-pentanethiol was added. Reaction was left to react under nitrogen

for 50 hours. Product was precipitated out using cold water, and re-crystallised in methanol. Yield: 70.2%, Elemental: expected values (%): (C=67.8), (H=6.1), (N=12.2), (S=13.9), results (%) (C=67.16), (H=6.8), (N=11.79), (S=13.99) IR: (C≡N =2230.89), (C-H =3108, 2928), (S-C =1188.4), (Ph-S= 1225).

Compound (1d) 3-Pentanethiolether phthalonitrile:

0.2 g of 3-nitrophthalonitrile was dissolved in DMF (2ml) under nitrogen gas. To this solution 0.2ml of 1-pentanethiol was added. Reaction was left to react under nitrogen for 50 hours. Product was precipitated out using cold water, and re-crystallised in methanol. Yield: 71.3%, Elemental: expected values (%): (C=67.8), (H=6.1), (N=12.2), (S=13.9), results (%) (C=67.56), (H=6.5), (N=11.39), (S=14.11) IR: (C≡N =2230.89), (C-H =3108, 2928), (S-C =1188.4), (Ph-S= 1225).

Compound (1e) 4,5-tert-butylphenoxyether phthalonitrile:

0.8 g of 4,5-dichlorophthalonitrile was dissolved in DMF (8ml) under nitrogen gas. To this solution 1.1 g of 4-tert-Butylphenol was added. Reaction was left to react under nitrogen for 50 hours. Product was precipitated out using cold water, and re-crystallised in methanol. Yield: 53.76% Elemental: expected values (%): (C=79.2), (H=6.6), (N=6.6), (S= -), result (%) (C= 75.3), (H= 7.1), (N= 7.2), (S= 4.3). IR: (C≡N =2230.90), (C-H=2930, 3075), (Ph-O=1242).

2.1.3 Synthesis of MPcs

Metal-free tetra 4,4-tert-butylphenoxyether phthalocyanine, β-H_2OtBpPc:

1e (0.25 g, 9.05x10^{-4} mole), was dissolved in 1-octanol in the presence of catalytic amounts of lithium. The mixture was stirred and refluxed at 200° C for 4 hours. Acetic acid was then added to the mixture to remove the lithium metal, after the reaction had cooled down. methanol was added to precipitate the product out of the solution. The

mixture was filtered and the solid green product dried. The product was purified using silica gel column chromatography using chloroform.

Yield: 34.8%, IR: (C-H =3108, 2928), (Ph-O = 1245). UV/vis (DCM): λ max nm (log ε): 711 (4.54), 680(4.53), 339(4.41), 418(4.34), 422(4.33) MS (MALTDI-TOF-dithranol) m/z:Calcd 1102.5, result 1105.1 $[M]^+$.

Metal-free tetra 3,4-tert-butylphenoxyether phthalocyanine, α-H_2OtBpPc:

1b (0.25 g, 9.05×10^{-4} moles), was dissolved in 1-octanol in the presence of catalytic amounts of lithium. The mixture was stirred and refluxed at 200° C for 4 hours. Acetic acid was then added to the mixture to remove the lithium metal, after the reaction had cooled down. methanol was added to precipitate the product out of the solution. The mixture was filtered and the solid green product dried. The product was purified using silica gel column chromatography using chloroform.

Yield: 33.5%, IR: (C-H =3108, 2928), (Ph-O = 1245). UV/vis (DCM): λ max nm (log ε): 718 (4.61), 692(4.60), 335(4.50), 412(4.39), MS (MALTDI-TOF-dithranol) m/z:Calcd 1102.5, result 1104.6 $[M]^+$.

Metal-free tetra 4 –pentanethioletherphthalocyanine, β-H_2SPPc:

1d (0.25 g, 9.99×10^{-4} moles), was dissolved in the mixture of O-dichlorobenzene and 1-octanol (1:3) in the presence of catalytic amounts of lithium. The mixture was stirred and refluxed at 160- 170 C for 4 hours. Acetic acid was then added to the mixture to remove the lithium metal, after the reaction had cooled down. Methanol was added to precipitate the product out of the solution. The mixture was filtered and the solid green product dried. The product was purified using silica gel column chromatography. A mixture of hexane and THF (19:1) was used to purify the product.

Yield: 34.8%, IR: (S-C = 1188.4), (C-H =3108, 2928), (Ph-S = 1225). UV/vis (DCM): λ max nm (log ε): 720 (4.54), 690(4.53), 339(4.41), 418(4.34), 422(4.33) MS (MALTDI-TOF-dithranol) m/z:Calcd 923, result 925 $[M]^+$.

Metal-free tetra 3 –pentanethioletherphthalocyanine, α-H_2SPPc:

1d (0.2 g, 8.70×10^{-4} moles), was dissolved in the mixture of O-dichlorobenzene and 1-octanol (1:3) in the presence of catalytic amounts of lithium. The mixture was stirred and refluxed at 160- 170° C for 4 hours. Acetic acid was then added to the mixture to remove the lithium metal, after the reaction had cooled down. Methanol was added to precipitate the product out of the solution. The mixture was filtered and the solid green product dried. A mixture of hexane and THF (19:1) was used to purify the product.

Yield: 30.2%, IR: (S-C = 1188.4), (C-H =3108, 2928), (Ph-S = 1225). UV/vis (DCM): λ max nm (log ε): 732 (4.62), 701(4.62), 340(4.49), 422(4.41) MS (MALTDI-TOF-dithranol) m/z:Calcd 923, result 926 $[M]^+$.

Metal-free tetra 4,5-tert-butylphenoxyether phthalocyanine, ββ-H_2OtBpPc:

1c (0.2 g, 4.71×10^{-4} mole) was dissolved in 1-octanol in the presence of (0.025 g, 3.60×10^{-3} mole) lithium as catalyst. The mixture was stirred and refluxed at 160- 170 °C for 6 hours. Acetic acid was then added to the mixture to remove the lithium metal, after the reaction had cooled down. Methanol was added to precipitate the product out of the solution. The mixture was filtered and the solid green product dried. The product was purified using silica gel column chromatography. Chloroform was used to elute the first fraction which was found to be the product.

Yield: 43.7%, IR [(KBr) vmax /cm -1)]: ((C-H =3108, 2928), (Ph-O = 1245). UV/vis (DCM): λ max nm (log ε): 708(4.65), 687(4.69), 442(4.23), 360(4.5), 339(4.5). MS (MALTDI-TOF-dithranol) m/z:Calcd 1693.3, result 1698.4 $[M]^+$.

Tin(IV) chloride tetra 4,4-tert-butylphenoxyether phthalocyanine, β-SnOtBpPc:

0.05 g (3.858×10^{-5} moles) of 2a was dissolved in 1-pentanol with excess tin(II) Chloride under Nitrogen. This was heated to 120 °C and stirred for 3 hours. The green product was filtered out using methanol and was purified using column chromatography using a chloroform and methanol mixture (20:1). The first fraction was untreated reagent and the 2nd fraction was retained.

Yield: 79%, IR [(KBr) vmax /cm -1)] (C-H =3108, 2928), (Ph-O = 1245), UV/vis (DCM): λ max nm (log ε): 708(5.03), 642(4.47), 330(4.80). m/z:Calcd 1296.9, result 1292.1 $[M]^+$.

Tin(IV) chloride tetra 3-4-tert-butylphenoxyether phthalocyanine, α-SnOtBpPc:

0.05 g, 3.858×10^{-5} moles, of 2b was dissolved in 1-pentanol with excess tin(II) Chloride under nitrogen. This was heated to 120 °C and stirred for 3 hours. The green product was filtered out using methanol and was purified using column chromatography using a chloroform and methanol mixture (20:1). The first fraction was untreated reagent and the 2nd fraction was retained.

Yield: 73%, IR [(KBr) vmax /cm -1)] (C-H =3108, 2928), (Ph-O = 1245), UV/vis (DCM): λ max nm (log ε): 740(5.17), 659(4.51), 331(4.85). m/z:Calcd 1296.9, result 1298.4 $[M]^+$.

Tin(IV) chloride tetra 4-pentanethiolether phthalocyanine, β-SnSPPc:

0.05 g, 3.900×10^{-5} moles, of 2c was dissolved in 1-pentanol with excess tin(II) Chloride under nitrogen. This was heated to 120 °C and stirred for 3 hours. The green product was filtered out using methanol and was purified using column chromatography using a chloroform and methanol mixture (20:1). The first fraction was untreated reagent and the 2nd fraction was retained.

Yield: 57%, IR [(KBr) vmax /cm -1)] (C-H =3108, 2928), (Ph-O = 1245), UV/vis (DCM): λ max nm (log ε): 721(4.81), 659(4.31), 331(4.75). m/z:Calcd 1110.2, result 1111.3 $[M]^+$.

Tin(IV) chloride tetra 3-pentanethiolether phthalocyanine, α-SnSPPc:

0.05 g, 3.900×10^{-5} moles, of 2d was dissolved in 1-pentanol with excess tin(II) Chloride under nitrogen. This was heated to 120 °C and stirred for 3 hours. The green product was filtered out using methanol and was purified using column chromatography using a chloroform and methanol mixture (20:1). The first fraction was untreated reagent and the 2nd fraction was retained.

Yield: 31%, IR [(KBr) vmax /cm -1)] (C-H =3108, 2928), (Ph-O = 1245), UV/Vis (DCM): λ max nm (log ε): 771(6.02), 687(5.55), 354(5.98). m/z:Calcd 1110.2, result 1109.3 $[M]^+$.

Tin(IV) chloride octa 4,4-tert-butylphenoxyether phthalocyanine, ββ-SnOtBpPc:

0.05 g, 2.648×10^{-5} moles, of 2e was dissolved in 1-pentanol with excess tin(II) Chloride under nitrogen. This was heated to 120 °C and stirred for 3 hours. The green product was filtered out using methanol and was purified using column chromatography using a chloroform and methanol mixture (20:1). The first fraction was untreated reagent and the 2nd fraction was retained.

Yield: 73%, IR [(KBr) vmax /cm -1)] (C-H =3108, 2928), (Ph-O = 1245), UV/Vis UV/vis (DCM): λ max nm (log ε): 709(5.11), 644(4.51), 331(4.78). m/z:Calcd 1888.7, result 1882.9 $[M]^+$.

2.2 Characterisation Techniques

- Ground state electronic absorption spectra were performed on a Shimadzu UV-2550 spectrophotometer between 300 nm and 800 nm.
- Emission and excitation spectra were obtained on a FluoTime 300 'EasyTau' spectrometer.
- Infra-red spectra were collected on a Perkin-Elmer Universal ATR Sampling accessory spectrum 100 FT-IR spectrometer.
- Elemental analyses were done using a Vario-ElementalMicrocube ELIII.
- Mass spectra data were collected on a Bruker AutoFLEX III Smart-beam MALDI-TOF mass spectrometer using various matrices and modes of operation depending on the sample.
- Fluorescence lifetimes and Isometric lifetimes were measured with a FluoTime 300 'EasyTau' spectrometer (PicoQuant GmbH) using a time correlated single photon counting (TCSPC). The samples were excited at 670 nm with a diode laser (LDH-P-670, 20 MHz repetition rate, 44 ps pulse width, PicoQuant GmbH). The detector employed was a Peltier cooled Photomultiplier (PMA-C 192-M, PicoQuant GmbH).
- All Z-scans done in this study were performed with a frequency-doubled Nd:YAG laser (Quanta-Ray, 1.5 J /10 ns FWHM pulse duration) as the excitation source. The laser was operated in a near Gaussian transverse mode at 532 nm (second harmonic), with a pulse repetition rate of 10 Hz and energy range of 8-12 μJ. The beam was spatially filtered to remove the higher order modes and tightly focused with a 15 cm focal length lens. Effects due to damage between runs was mitigated by replacing the sample.

Chapter 3. Results and discussion of Tin(IV) Phthalocyanines and Photophysical Properties

3.1 Synthesis of SnPcs

3.1.1 Phenoxy substituted phthalocyanines

The first class of tin(IV) phthalocyanine (SnPcs) were synthesized as shown in scheme 3.1. They consisted of alkoxy or phenoxy substituents, and were relatively easier to handle, showing good solubility in most non-polar to semi-polar solvents and could easily be purified by silica colums.

3.1.1.1 β-SnOtBpPc(Scheme 3.1)

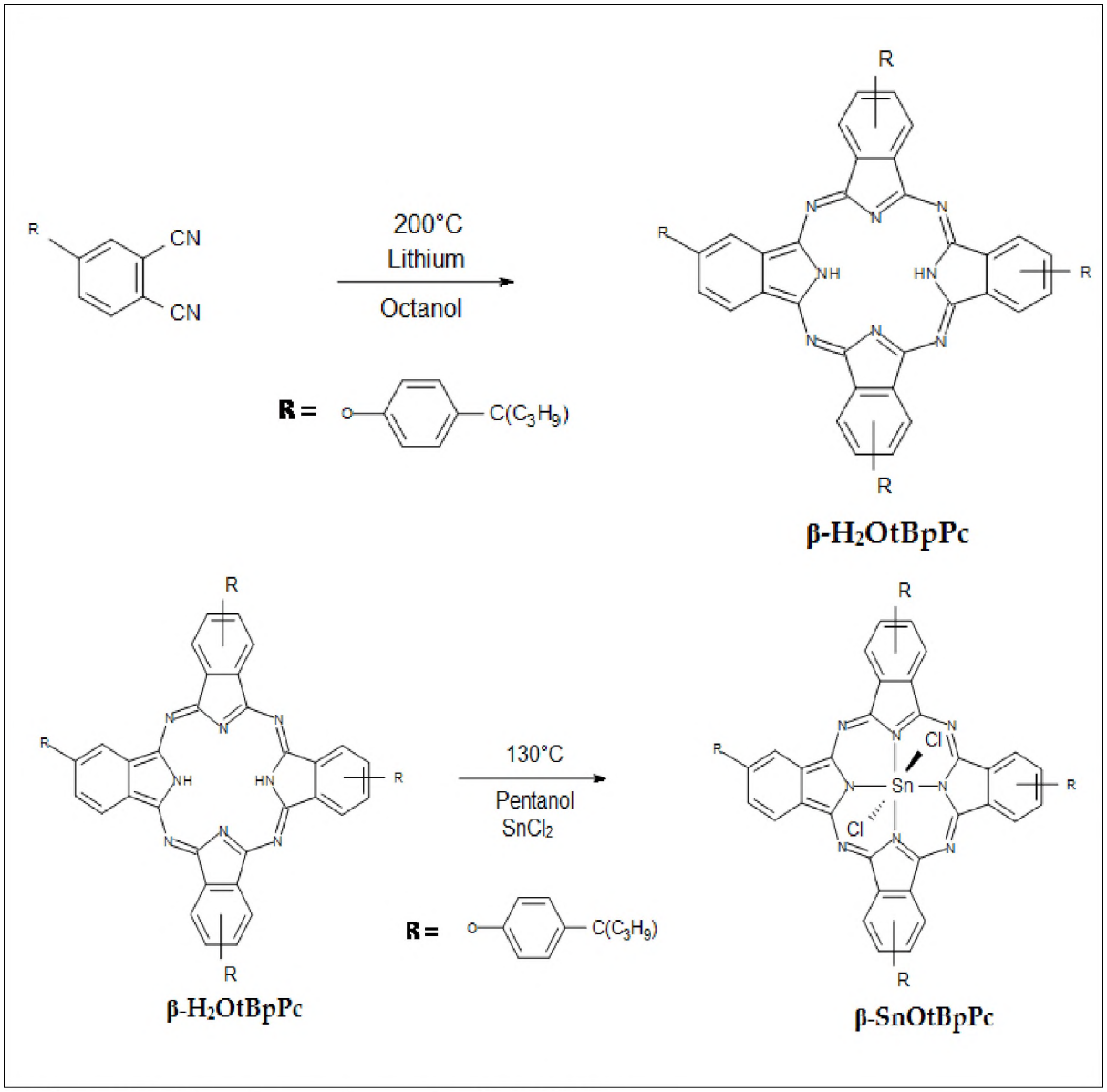

Scheme 3.1: Reaction pathway for β-SnOtBpPc.

β-SnOtBpPc was synthesised by first synthesising **β-H_2OtBpPc**, which was then metalated using the insertion method.

β-H_2OtBpPc was synthesised by cyclising tert-butyl phynoxyphthalonitrile in octanol in the presence of lithium as catalysts. Lithium was the preferred catalyst for the reaction, as it gave slightly higher yields (35% vs 30% of DBU). The reaction was done at 200 °C over 4 hours and under a nitrogen atmosphere. The mixture was then allowed to cool and acetic acid was added to remove the lithium, after which methanol was added to precipitate the Pc out of solution. The resulting blue precipitate was then washed with chilled methanol and filtered. The product was isolated with the use of chromatography (silica gel) using DCM as the eluent.

The synthesis of **β-SnOtBpPc** was done by dissolving **β-H_2OtBpPc** and $SnCl_2$ in pentanol. This mixture was then left to reflux for 12 hours at 130 °C under a nitrogen atmosphere. The metalation reaction progress was followed by UV-vis. During this time the mixture turned from a blue green colour to a green colour, and this was due to the inclusion of the $SnCl_2$ in the Pc macrocycle which providing electrons to lower the energy gap between the relevant orbitals and thus red shifting the absorption spectra. After cooling the reaction, methanol was added to precipitate the SnPc which was washed with chilled methanol. The product was isolated using a silica column with chloroform as the solvent, with the first fraction being the un-reacted **β-H_2OtBpPc** and the second fraction the metalated product **β-SnOtBpPc.**

The isolated products both possessed strong IR bands at 1245, 2928 and 3108 cm^{-1}. The band centred at 1245 cm^{-1} corresponds to an unsymmetrical vibration of ether the bond that was expected to be present due to the substituent, while the bands centred at 2928 and 3108 cm^{-1} were due to the C-H vibrations of the tert-butyl found on the ends of the substituents.

The mass spectral analysis also confirm successful synthesis with the free base Pc shows a peak at 1104 mass units (calculated 1102) while the MPc shows a peak at 1289

(calculated 1282). Both results were at lower masses than calculated masses, though well within acceptable error margins for molecules of this size. Fragmentation was seen in both spectra, with the major fraction attributed to a loss of a substituent.

3.1.1.2 α-SnOtBpPc (Scheme 3.2)

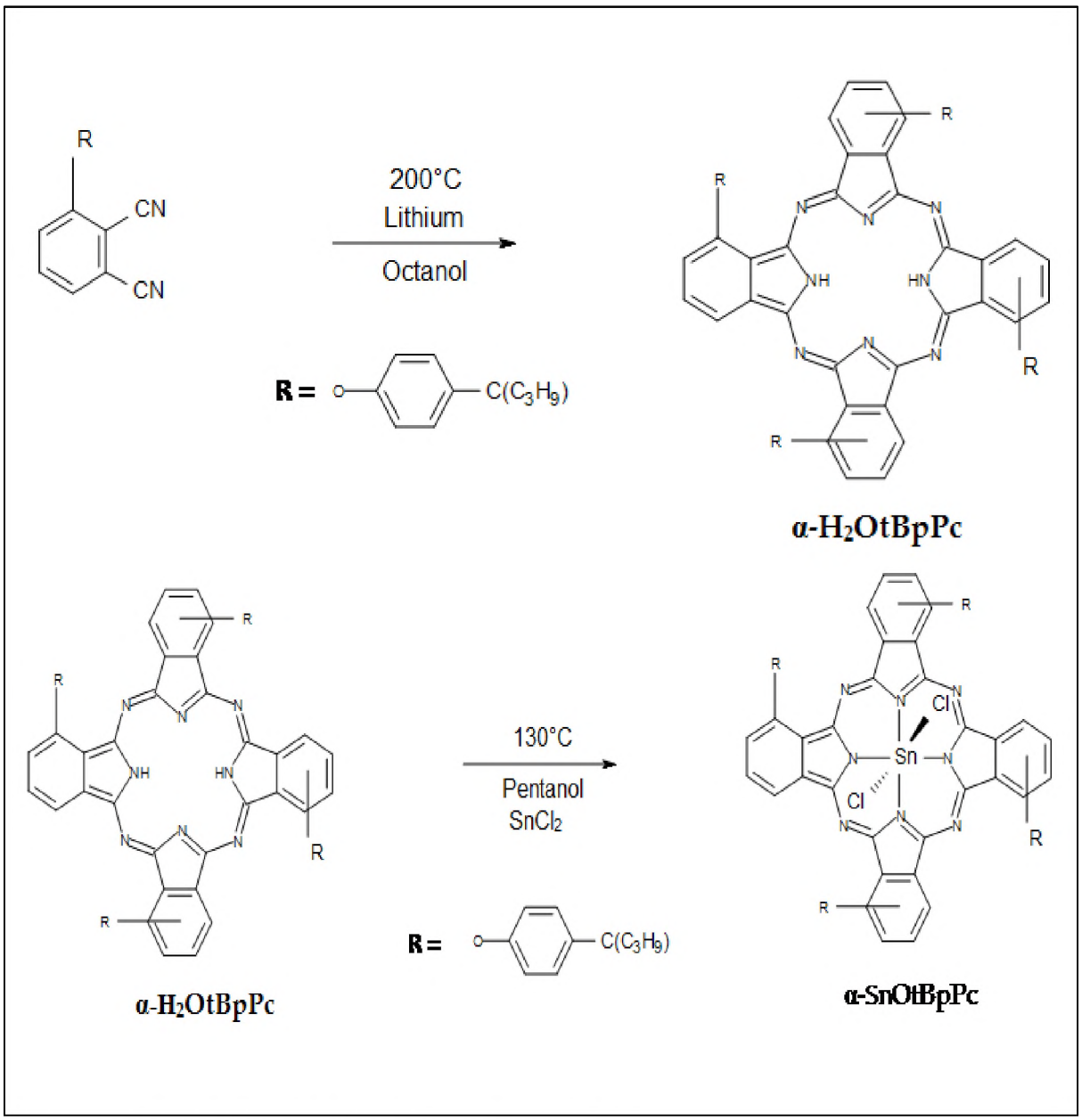

Scheme 3.2: Reaction pathway for α-SnOtBpPc.

The alpha substituted, **α-SnOtBpPc** was synthesised in a very similar manner to the beta substituted **β-SnOtBpPc,** by first synthesising a free-base Pc then metalating it.

α-H_2OtBpPc was synthesised and isolated in a similar manner to **β-H_2OtBpPc**. The synthesis of **α-SnOtBpPc** was also similar to the synthesis of **β-SnOtBpPc.** However the reaction was left to run for only 4 hours, to avoid degrading the MPc**.** Isolation followed the same steps as **β-SnOtBpPc.**

The isolated products both possessed strong IR bands at 1245, 2928 and 3108 cm^{-1}. The band at 1245 cm^{-1} correspond to an unsymmetrical vibrations of the ether bond that was expected to be present due to the substituent, while the bands at 2928 and 3108 cm^{-1}were due to the C-H stretching tert-butyl found on the ends of the substituents. Absent were any vibrations around 2300 cm^{-1}, due to nitrile bonds, confirming the cyclisation to form the Pc.

The mass spectra results showed the free base Pc with 1105 mass units (calculated 1103) and the MPc giving 1292 (calculated 1282). Both results were less than calculated, though well within acceptable error margins for molecules of this size. Fragmentation was seen in both, with the major fraction attributed to a loss of a substituent.

3.1.1.3 ββ-SnOtBpPc (Scheme 3.3)

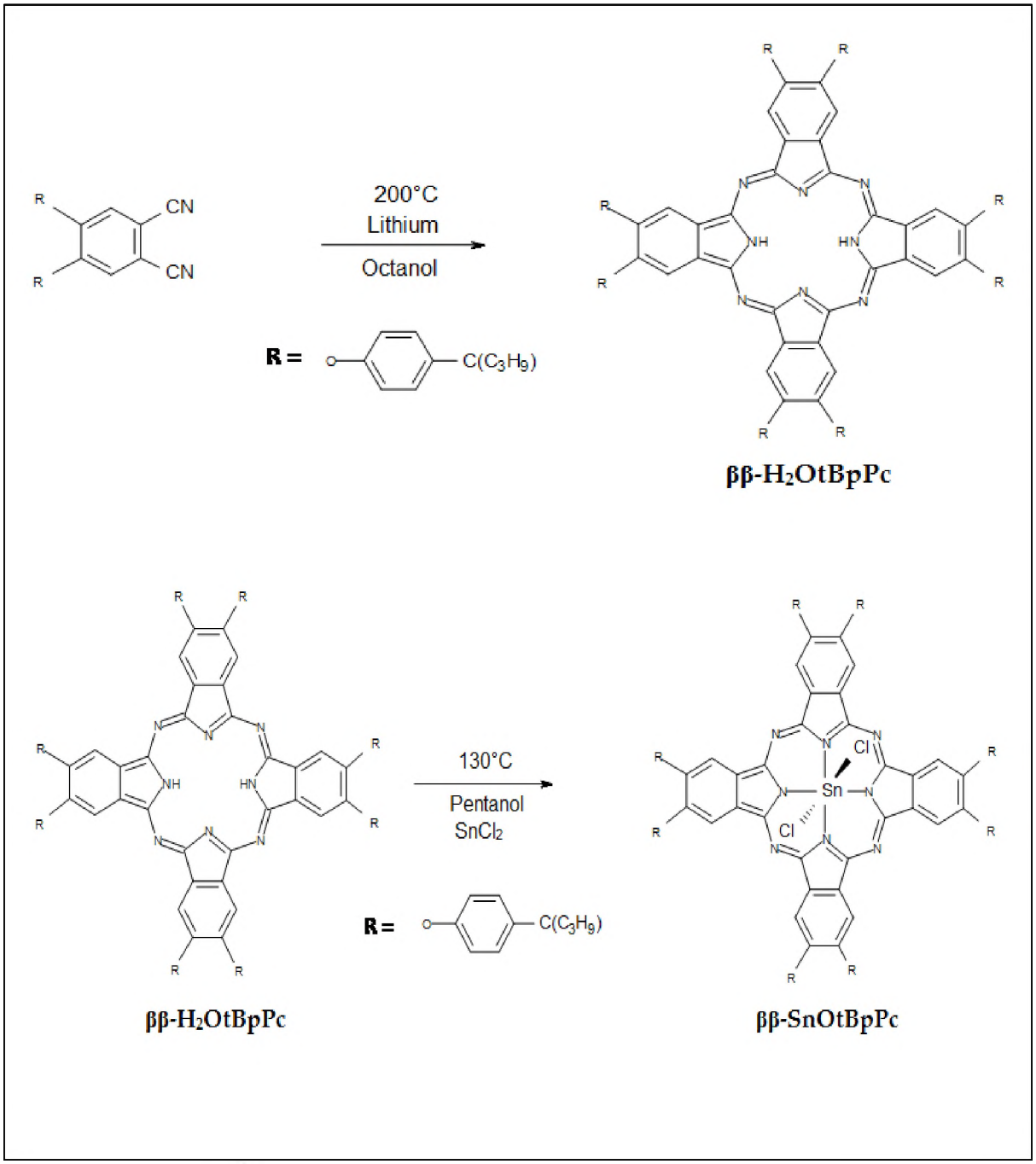

Scheme 3.3: Reaction pathway for ββ-SnOtBpPc.

The octa-substituted **ββ-SnOtBpPc** was synthesised in a very similar manner to the tetra substituted **β-SnOtBpPc,** first creating a free-base Pc then metalating it. **ββ-H_2OtBpPc** was synthesised and purified identically **β-H_2OtBpPc.** The steps taken in

the metaltion of **ββ-H_2OtBpPc** in order the create **ββ-SnOtBpPc** were the same as those used to make **β-SnOtBpPc.**

IR peaks for both Pc are very similar, the most prominent bands at 1245, 2928 and 3108 cm^{-1} being due to the substituents. This is expected as the metal does not change the Pc's substituent structure.

The mass spec. results showed the free base Pc with1698 mass units (calculated 1693) and the MPc giving 1883 (calculated 1875). Both results were less than calculated, though well within acceptable error margins for molecules of this size. Fragmentation was seen in both, with the major fraction attributed to a loss of a substituent.

3.1.2 Thiol substituted phthalocyanines

The thiol substituted SnPcs of **α-SnSPPc** and **β-SnSPPc,** were made in a similar fashion to the phenoxy substituted SnPcs. However, due to the change in the polarity of the end pentane groups, the Pcs had to be handled in solvents with a more non-polar nature.

3.1.2.1 β-SnSPPc (Scheme 3.4)

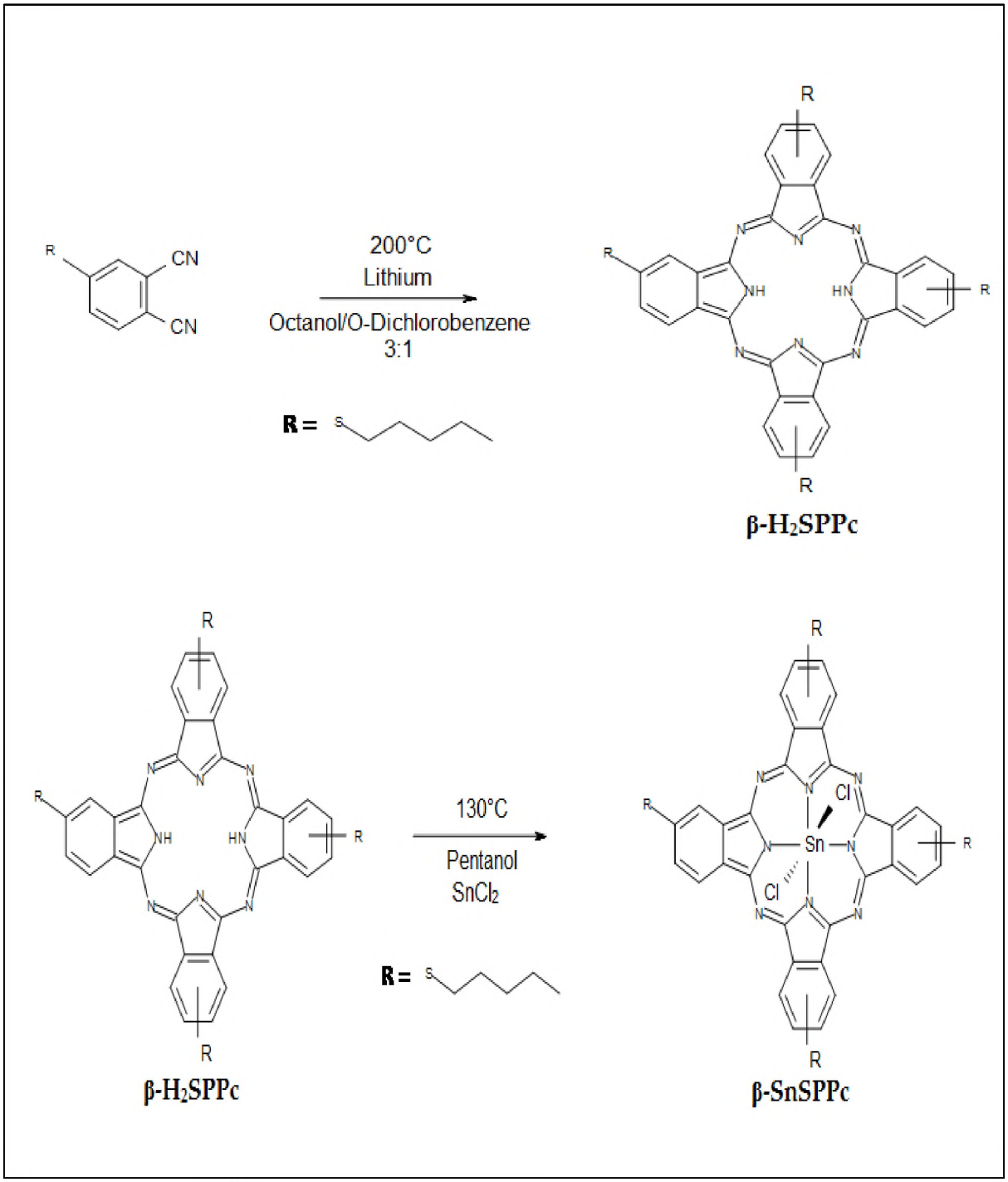

Scheme 3.4: Reaction pathway for β-SnSPPc.

The beta substituted **β-SnSPPc** was synthesised, like all the oxygen SnPcs, by first creating a free-base Pc then metalating it.

β-H_2SPPc was synthesised in a mixture of high boiling solvents, octanol and O-dichlorobenzene in a 3:1 ratio, and catalysed with lithium. The reaction was done at 200 °C over 4 hours and under a nitrogen atmosphere. The mixture was then allowed to cool and acetic anhydride was added to remove the lithium, after which methanol was added to force the Pc out of solution. The resulting green precipitate was then washed with chilled methanol and filtered. The product was isolated with the use of chromatography using a mixture of THF/Hexane at a ratio of 1:19 as the eluent.

The synthesis of **β-SnSPPc** was done by dissolving **β-H_2SPPc** and $SnCl_2$ in pentanol. This mixture was then left to reflux for 2 hours at 130 °C under a nitrogen atmosphere. During the reaction small amounts were taken and run under UV to observe the progress of the metalation. This reaction had to be watched carefully as the yield would decrease if left too long. After allowing the reaction to cool, methanol was added and the precipitate was washed with chilled methanol. The product was isolated using column chromatography with chloroform/methanol (20:1) as the solvent, with the first fraction being the un-reacted **β-H_2SPPc** and the second fraction **β-SnSPPc.**

The isolated products possessed strong IR bands at 1225,1188, 2928 and 3108 cm^{-1}. The band at 1225 cm^{-1} and 1188 cm^{-1} correspond to a thiol-ether-bond substituent, while the bands at 2928 and 3108 cm^{-1}were due to the C-H stretching on the pentane chain.

The mass spectral analysis confirm the successful synthesis free base Pc with 925 mass units (calculated 923) while the MPc giving 1111 (calculated 1105). Fragmentation was seen in both, with the major fraction attributed to a loss of a substituent.

3.1.2.2 α-SnSPPc (Scheme 3.5)

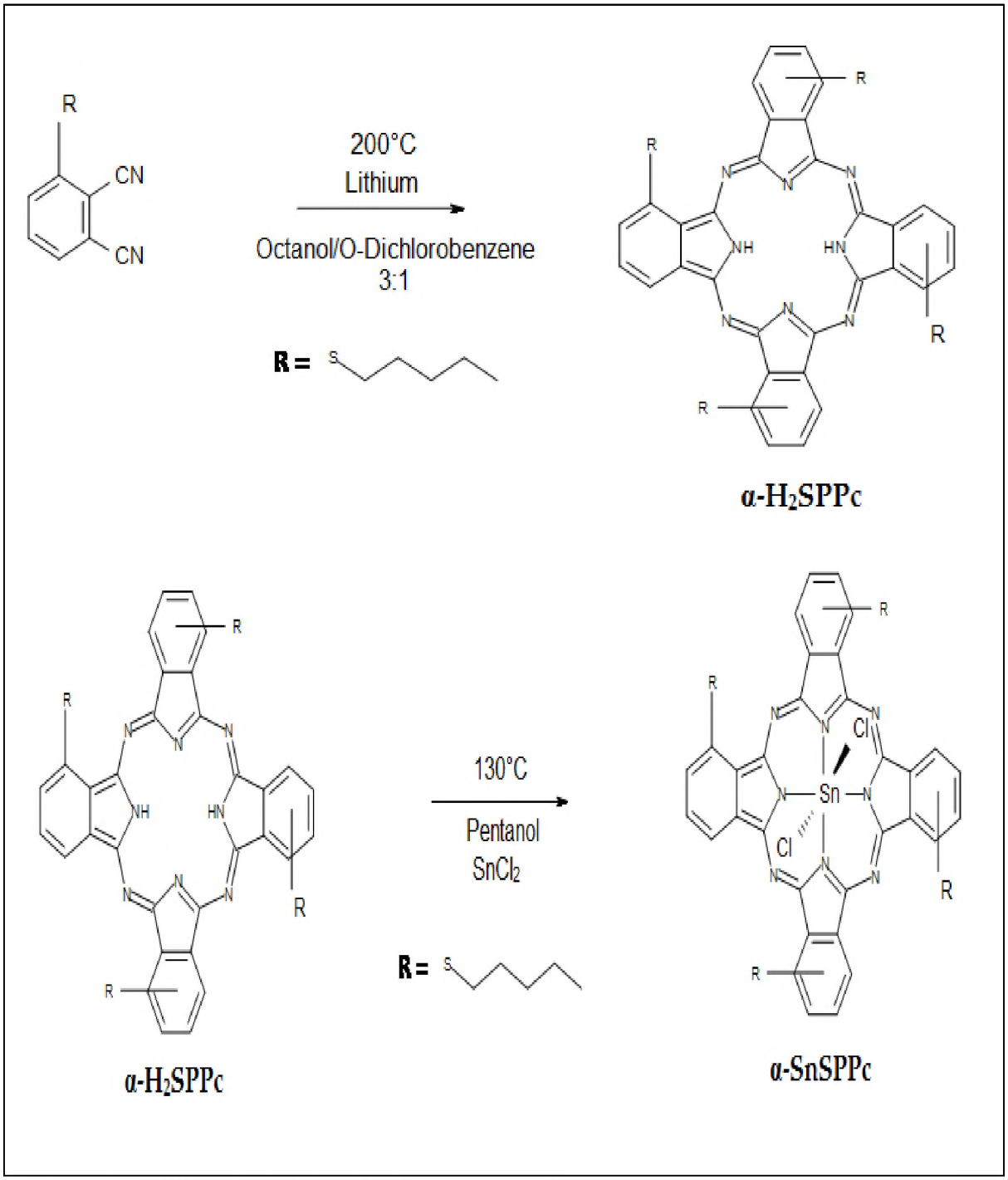

Scheme 3.5: Reaction pathway for α-SnSPPc.

The alpha substituted **α-SnSPPc** was synthesised, like all the oxygen SnPcs, by first creating a free-base Pc then metalating it. **α-H_2SPPc** was synthesised in the same manner as **β-H_2SPPc.**

The metalation of **α-H_2SPPc** was also done in a similar manner to **β-H_2SPPc**, however it was a much shorter reaction. Despite the unmetalated **α-H_2SPPc** showing good thermal stability in the solvent, after adding the $SnCl_2$ to the solution the Pc would degrade after a relatively short time (30-60 min). The best approach was found to only run the reaction for a short time, so that at least some product could be isolated. As such the yields for the metalation of this Pc with $SnCl_2$ are very low.

The purification for **α-SnSPPc** was the same as that for **β-SnSPPc**.The isolated products possessed strong IR bands at 1225,1188, 2928 and 3108 cm^{-1}. The bands at 1225 cm^{-1} and 1188 cm^{-1} correspond to thiol-ether-bonds that were expected due to the substituent, while the bands at 2928 and 3108 cm^{-1}were due to the C-H stretching on the pentane chain.

The mass spec. results showed the free base Pc with 926 mass units (calculated 923) and the MPc giving 1108 (calculated 1105). Fragmentation was seen in both, with the major fraction attributed to a loss of a substituent.

3.1.2.3 ββ-SnSPPc

The octa-substituted **ββ-SnSPPc** was a gift to the study by Dr Khene and its synthesis and characterisation has been reported in literature[87]. **ββ-SnSPPc** possessed strong IR bands at 1225,1188, 2928 and 3108 cm^{-1}. The band at 1225 cm^{-1} and 1188 cm^{-1} correspond to a thiol-ether-bonds that were expected due to the substituent, while the bands at 2928 and 3108 cm^{-1} were due to the hydrogens on the pentane chain.

3.2 Spectral analysis

3.2.1 Alpha Substituted SnPcs

α-SnOtBpPc exhibited a strong Q band near 740 nm, this is shown in Figure 3.2, with a relatively weaker B band in the 350 nm region, typical of most[88]. This absorption is the most red shifted of the oxygen Pcs and can be compared with the alpha substituted **α-SnSPPc**. Like its ether analogue, **α-SnSPPc** exhibited significant red shifting in the primary absorption bands. As sulphur is more electron rich than oxygen, the shifting in this case was more noticeable (from 740 nm for the oxygen to around 770 nm for the sulphur).

The MCD spectra for the Pc was also as expected of a Pc with D_{4h} symmetry, possessing a distinct A_1 Faraday term for the Q band, as opposed to the very closely lying B_0 pair that will be observed in Pcs with D_{2h} symmetry. **α-SnSPPc**'s MCD also showed good correlation with the UV/vis data as well as showing the overlapping Zeeman split transitions that make up the Q band.

The calculated results for the TD-DFT ,as listed in Table 3.1, were as expected, predicting no transition between the Q and B bands and showing good prediction of the two degenerate transitions in both cases. The transitions themselves are to and from the 4 frontier orbitals, shown in Figure 3.1, as described in Chapter 1.

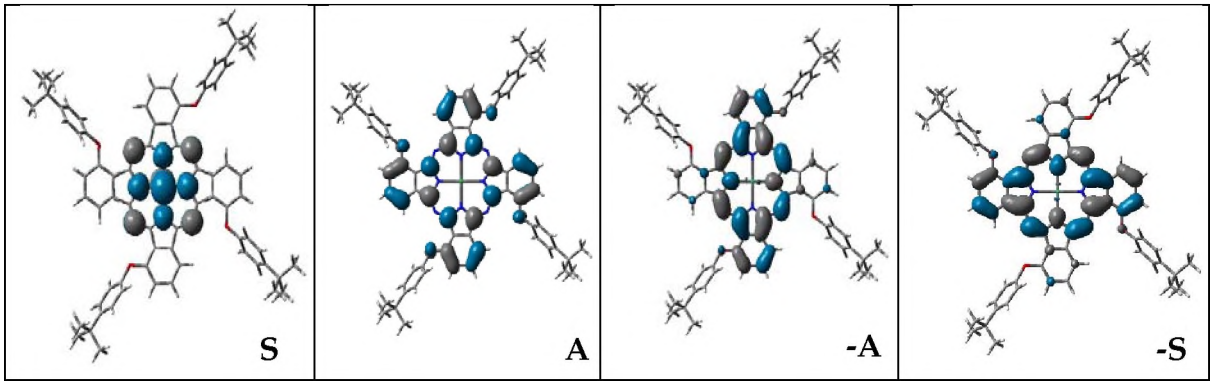

Figure 3.1 : Michl's frontier orbitals of α-SnOtBpPc.

As shown in Figure 3.2 the functional used underestimated the energies of the Q band transitions (for both Pcs). However DFT based functionals and can be remedied by including a functional that incorporates more Hartree-Fock (HF) dependency (typically the coulomb attenuated B3LYP(CAM-B3LYP) would be used[89]) though this increases computational requirements due to the expansive nature of HF. For ***α*-SnSPPc,** the calculations predicted the red shifting between the Pcs, even if the exact degree of red shifting was overestimated.

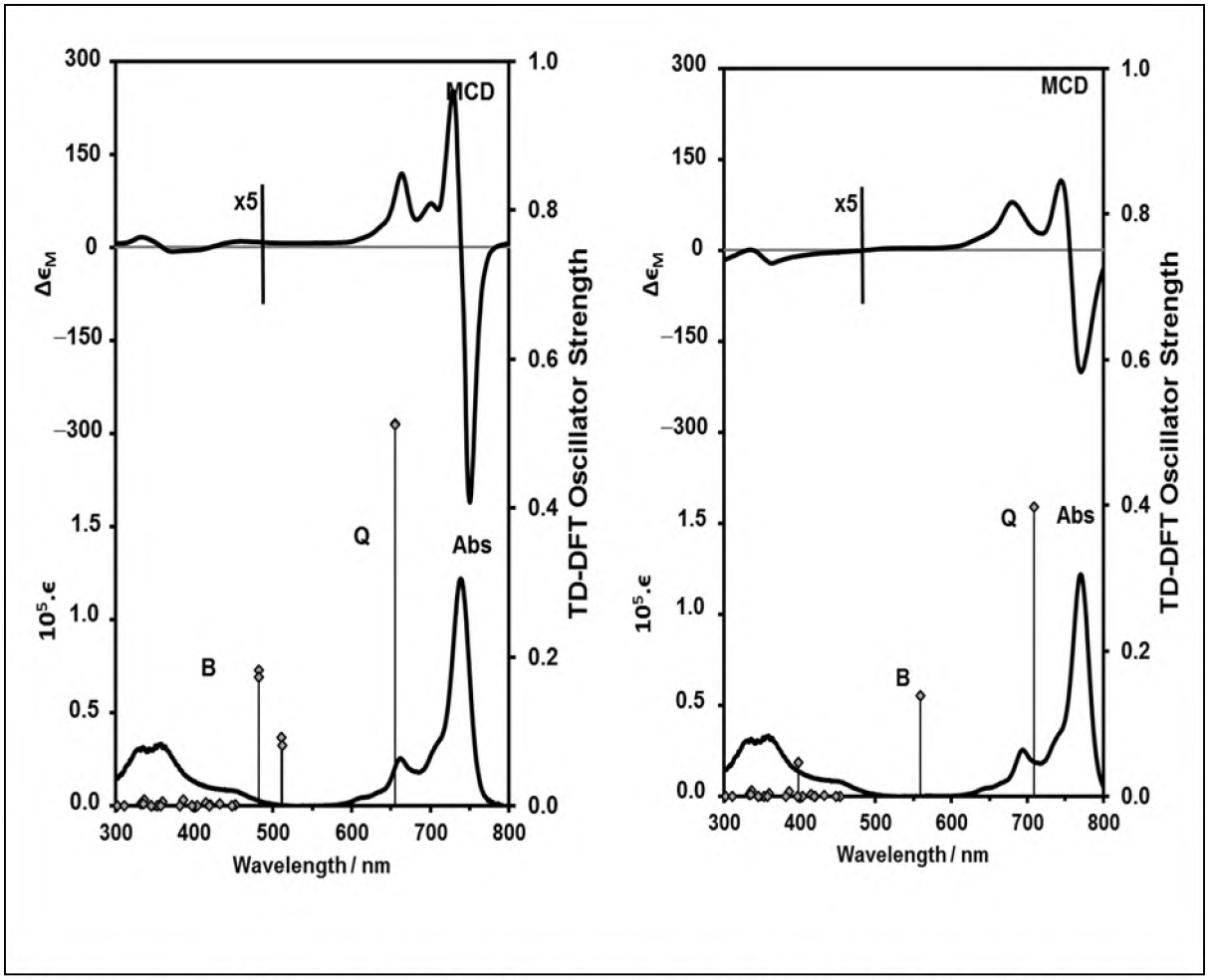

Figure 3.2: TDDFT and MCD/Uv vis spectra of α-SnOtBpPc (left) and α-SnSPPc(right).

3.2.2 Beta Substituted SnPcs

The beta substituted Pcs showed a much higher energy transition for Q bands, when compared to alpha Pcs. This comparison is shown in Figure 3.3, this being due to the destabilising effect of alpha substituents on the **a** MO, which has a node on this carbon. The Beta substitution has no corresponding node as is the case for the α synbstituted carbon MO and as such contributes much less to the relative energy gap between the **a** and **-a/-s** (HOMO-LUMO).

The TD-DFT results, as shown previously in Table 3.1 shows only slight change in energy values that are shown in Figure 3.3 shifting only 3 nm lower in the calculated energy. This is attributed this discrepancy to the DFT functional. It does show the respective red shift for the **β-SnSPPc** but like ***α*-SnSPPc** it overestimates how red shifted the difference will be.

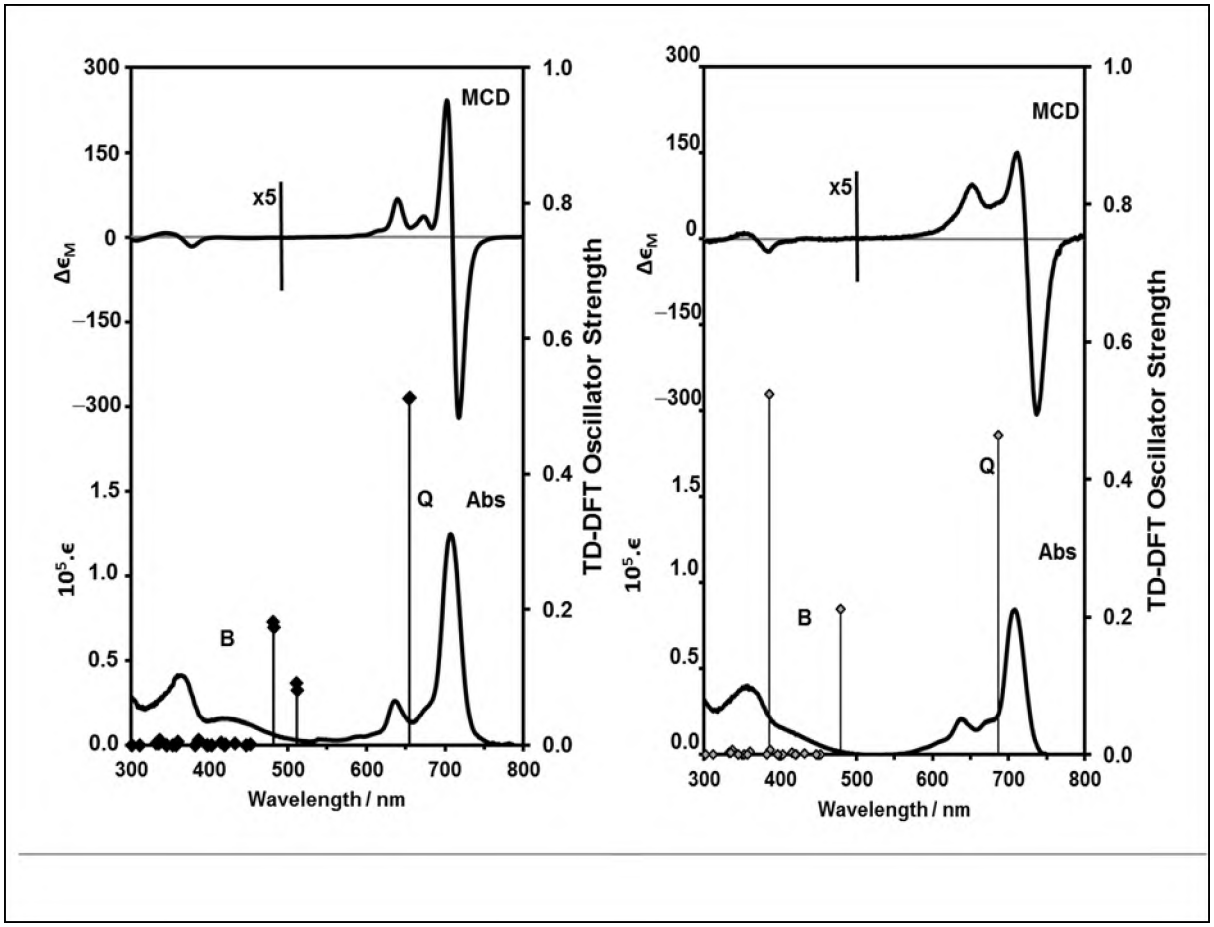

Figure 3.3 : TDDFT and MCD/Uv vis spectra of β-SnOtBpPc (left) and *α*-SnSPPc (right).

3.2.3 Octa-Beta Substituted SnPcs.

Like the tetra substituted beta Pcs, the octa beta Pcs preduced a higher energy transition for Q bands shown in Figure 3.4, when compared to the alpha substituted Pcs. The similarity between octa(beta) and tetra(beta) Pcs can be attributed to the **a** MO having no node on either beta carbon. Thus the combined effect (710 nm for octa vs. 705 nm for tetra) can be interpreted as the addition of very small changes in the

relative energy gap between the **a** and **-a/-s**(HOMO-LUMO). The effect of this small change can be seen when comparing the octa beta to the tetra beta for each type of substituent. In the phenoxy Pc the shift is 5 nm, however, as the thionyl Pcs shown in Figure 3.5 are more redshifted themselves the difference becomes 17 nm (722 nm to 739 nm). This increase is due to the greater electron donating effect of the thio nyl when compared to the phenoxy substituent.

The TD-DFT, shown in Table 3.1, overestimates the transition energies, but does correctly predict the transition being to two degenerate states (the **–a** and **–s**). This calculation also is reflected well in the MCD which shows a well-defined Faraday A_1 term in nature, if not position.

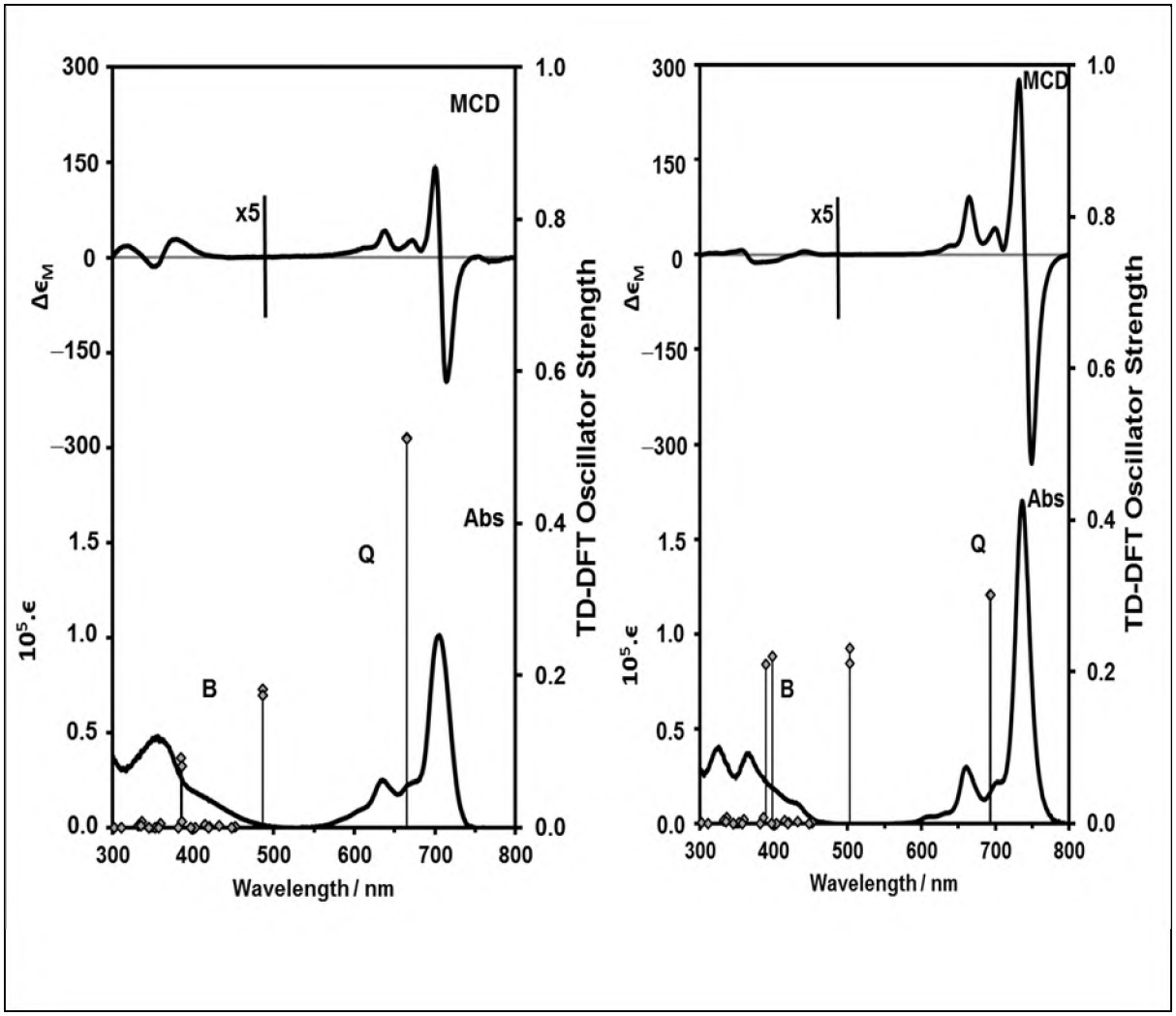

Figure 3.4: TDDFT and MCD/Uv vis spectra of ββ-SnOtBpPc (left) and ββ-SnSPPc(right).

β-SnSPPc

Band[a]	#[b]	Calc[c]			Exp[d]		Wavefunction=[e]
--	**1**	---	---	---	---	---	Ground state
Q	**2**	14.6	686	(0.47)	14.6	719	**75% a → -s; 4% s → -a;** 2% H–6 ($2a_{2u}$) → -s; …
Q	**3**	16.0	686	(0.47)	14.6	719	**75% a → -a;** 2% H–6 ($2a_{2u}$) → -a; **6% s → -a;** …
B1	**9**	20.8	480	(0.21)	25.0	~350	**76% s → -s;** 24% H–3 ($1e_g$) → -a; …
B1	**10**	20.8	480	(0.21)			**76% s → -a;** …
B2	**15**	26.0	385	(0.52)	28.6	~320	70% H–8 ($2a_{1u}$) → -a; 7% H–6 ($2a_{2u}$) → -s; …
B2	**16**	26.0	385	(0.52)			70% H–8 ($2a_{1u}$) → -s; 7% H–6 ($2a_{2u}$) → -s; …

α-SnSPPc

Band[a]	#[b]	Calc[c]			Exp[d]		Wavefunction=[e]
--	**1**	---	---	---	---	---	Ground state
Q	**2**	14.4	693	(0.31)	12.1	742	**71% a → -s; 6% a → -s; 3% s → -s;** …
Q	**3**	14.8	676	(0.23)	12.1	742	**56% a → -a; 24% a → -a;** …
B1	**9**	25.9	452	(0.20)	25.0	~400	**70% s → -s;** 24% H–2 ($1b_{1u}$) → -a; …
B1	**10**	27.5	454	(0.01)			**77% s → -s;** …
B2	**15**	29.0	344	(0.27)	28.6	~350	53% H–7 ($2a_{1u}$) → -a; 41% H–6 ($2a_{2u}$) → -s; …
B2	**16**	29.3	342	(0.11)			56% H–7 ($2a_{1u}$) → -s; 39% H–6 ($2a_{2u}$) → -s; …

β-SnOtBpPc

Band[a]	#[b]	Calc[c]			Exp[d]		Wavefunction=[e]
--	**1**	---	---	---	---	---	Ground state
Q	**2**	15.8	655	(0.51)	14.9	704	**74% a → -s; 4% s → -s;** 7% H–6 ($2a_{2u}$) → -s; …
Q	**3**	16.0	655	(0.51)	14.9	704	**74% a → -a;** 7% H–6 ($2a_{2u}$) → -a; **3% s → -a;** …
B1	**9**	23.2	431	(0.19)	25.0	~400	**72% s → -s;** …
B1	**10**	23.2	430	(0.02)			**72% s → -a;** …
B2	**15**	25.7	388	(0.24)	28.6	~350	53% H–8 ($2a_{1u}$) → -a; 40% H–6 ($2a_{2u}$) → -s; …
B2	**16**	25.9	389	(0.10)			56% H–8 ($2a_{1u}$) → -s; 38% H–6 ($2a_{2u}$) → -s; …

α-SnOtBpPc

Band[a]	#[b]	Calc[c]			Exp[d]		Wavefunction=[e]
--	**1**	---	---	---	---	---	Ground state
Q	**2**	14.8	674	(0.49)	13.6	731	**75% a → -a; 7% a → -s; 4% s → -s;** 2% H–6 ($2a_{2u}$) → -s; …
Q	**3**	14.8	674	(0.49)	13.6	731	**75% a → -s; 7% a → -a; 2% s → -a;** 2% H–6 ($2a_{2u}$) → -a; …
B1	**9**	20.5	486	(0.13)	25.0	~400	**87% s → -s;** 7% H–2 ($1b_{1u}$) → -a; …
B1	**10**	20.5	486	(0.13)			**87% s → -a;** …
B2	**15**	25.0	401	(0.11)	28.6	~350	52% H–7 ($2a_{1u}$) → -a; 37% H–6 ($2a_{2u}$) → -s; …
B2	**16**	25.0	401	(0.11)			52% H–7 ($2a_{1u}$) → -s; 37% H–6 ($2a_{2u}$) → -s; …

ββ-SnOtBpPc

Band[a]	#[b]	Calc[c]			Exp[d]		Wavefunction=[e]
--	**1**	---	---	---	---	---	Ground state
Q	**2**	14.8	693	(0.49)	14.0	708	**71% a → -s; 7% a → -s; 4% s → -s;** 2% H–6 ($2a_{2u}$) → -s; …
Q	**3**	14.8	693	(0.49)	14.0	708	**71% a → -a; 7% a → -a; 2% s → -a;** 2% H–6 ($2a_{2u}$) → -a; …
B1	**9**	20.7	480	(0.13)	25.0	~400	**87% s → -s;** 7% H–2 ($1b_{1u}$) → -a; …
B1	**10**	20.7	480	(0.13)			**87% s → -a;** …
B2	**15**	25.7	389	(0.11)	28.6	~350	52% H–7 ($2a_{1u}$) → -a; 37% H–6 ($2a_{2u}$) → -s; …
B2	**16**	25.7	389	(0.11)			52% H–7 ($2a_{1u}$) → -s; 37% H–6 ($2a_{2u}$) → -s; …

ββ-SnSPPc

Band[a]	#[b]	Calc[c]			Exp[d]		Wavefunction=[e]
--	**1**	---	---	---	---	---	Ground state
Q	**2**	14.8	674	(0.49)	14.5	726	**75% a → -a; 7% a → -s; 4% s → -s;** 2% H–6 ($2a_{2u}$) → -s; …
Q	**3**	14.8	674	(0.49)	14.5	726	**75% a → -s; 7% a → -a; 4% s → -a;** 2% H–6 ($2a_{2u}$) → -a; …
B1	**9**	20.5	486	(0.32)	25.0	~400	**81% s → -s;** 7% H–2 ($1b_{1u}$) → -a; …
B1	**10**	20.5	486	(0.32)			**81% s → -a;** …
B2	**15**	25.0	401	(0.13)	28.6	~350	50% H–7 ($2a_{1u}$) → -a; 37% H–6 ($2a_{2u}$) → -s; …
B2	**16**	25.0	401	(0.13)			50% H–7 ($2a_{1u}$) → -s; 37% H–6 ($2a_{2u}$) → -s; …

a − Band assignment described in the text. b − The number of the state assigned in terms of ascending energy within the TD-DFT calculation. c − Calculated band energies ($10^3.cm^{-1}$), wavelengths (nm) and oscillator strengths in parentheses (f). d − Observed energies ($10^3.cm^{-1}$) and wavelengths (nm) e − The wave functions based on the eigenvectors predicted by TD-DFT One-electron transitions associated with Michl's perimeter model are highlighted in bold. H and L refer to the HOMO and LUMO, respectively. When the H and L nomenclature is used the symmetry label for the corresponding MO in the π-systems of D_{4h}MPc complexes is provided in parentheses where applicable.

Table 3.1 : TD-DFT results for the SnPcs.

3.2.4 Overall comparison of SnPcs

The trends across the two different types of substituents are almost the same. The only notable spectral difference being the octa thiol Pc (ββ-SnSPPc) having a much larger separation from β-SnSPPc than the analogues ββ-SnOtBpPc had from its tetra Pc. This can be seen in the Uv/Vis spectra shown in Figure 3.5 being more red shifted in the thionol substitueted SnPcs than the phenoxy substituted ones. This difference is due to the amount of shifting each substituent created in the absorption spectra, with the greater shift from the thiol substituent giving a larger separation seen in ββ-SnSPPc. In both cases, the furthest redshifted are the alpha Pcs, followed by the octa beta Pcs and lastly the tetra beta Pcs, as expected from theory. The only notable difference between the two types of Pcs is the log(ε) values, with the thiol based Pcs giving slightly larger values than the phenoxy Pcs.

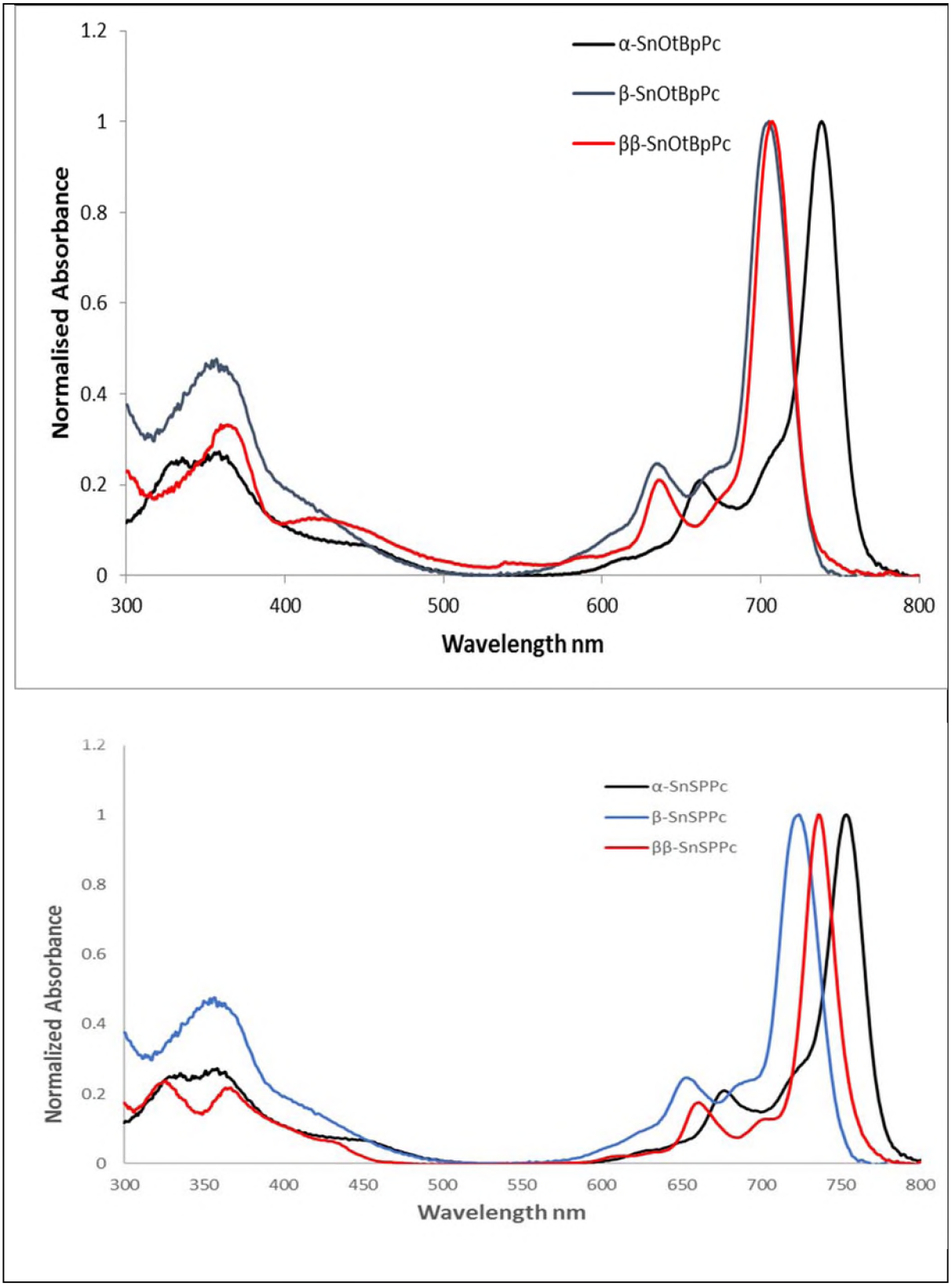

Figure 3.5: Absorption spectra for the thiol SnPcs (bottom) and phenoxy SnPcs (top).

3.3 Photophysical measurements

The photophysical data for the SnPcs was obtained with TCSPC, allowing the study of both the fluorescent decay, an example is shown in Figure 3.6, and the isometric profiles of the tin(IV) phthalocyanines. These studies were done in chloroform, toluene, dichloromethane, and tetrahydrofuran. Although the **α-SnSPPc** did not give sufficient fluorescent yield to acquire the fluorescent decay curve.

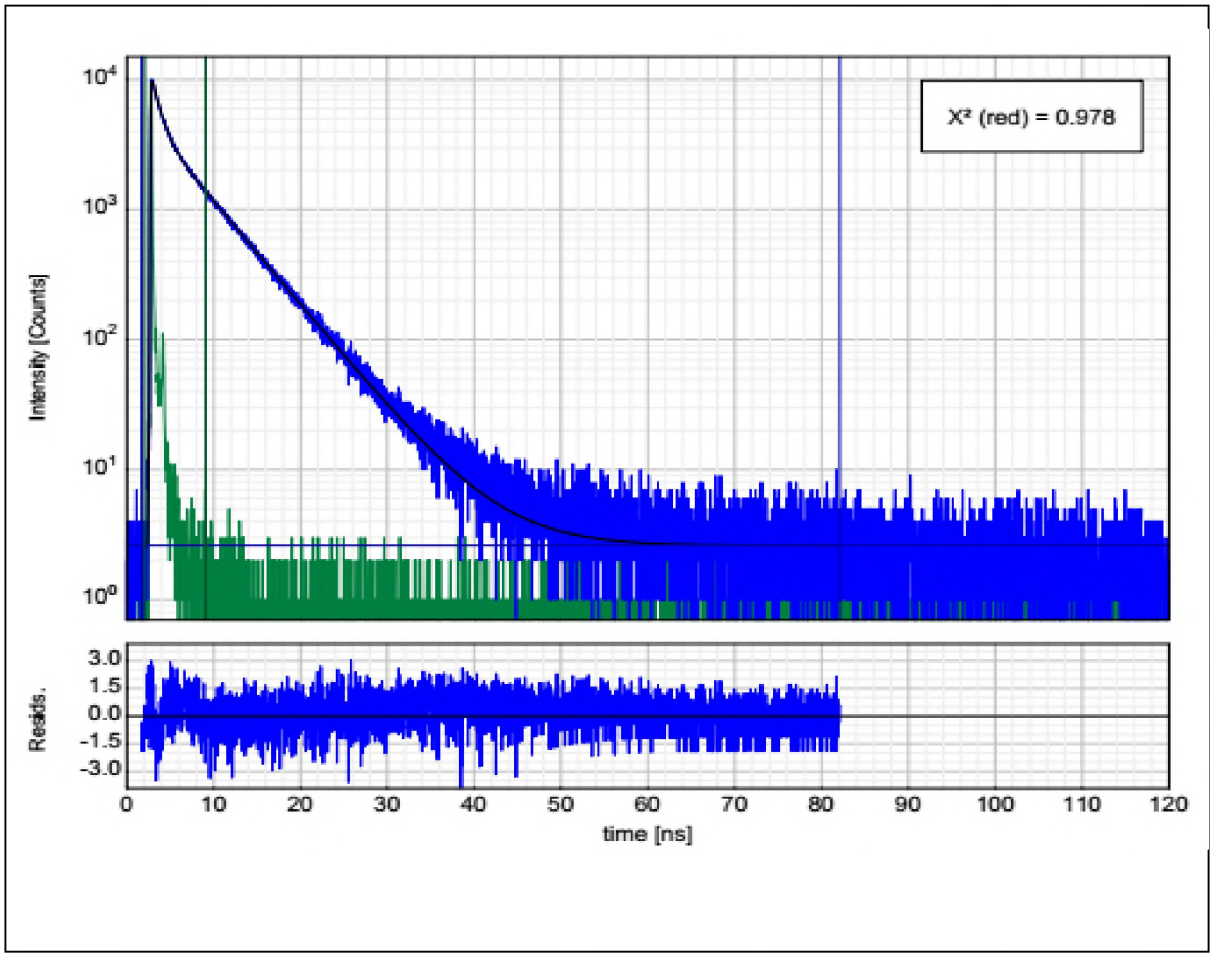

Figure 3.6: Fluorescence decay curve for β-SnOtBpPc

All measurements were taken at very low absorbances, around 0.05 absorbance, to reduce intermolecular interactions. Figure 3.7 illustrates how excitation wavelength was focused on the Q band and varied from Pc to Pc as the absorption shifted

Table 3.2 shows how the solvents did effect the fluorescence life time (τ) of the Pcs, changing it by as much as 20%, and the isometric rotation times saw effects as well, though these were due to the viscosity of the solvents and were expected. Some results gave null values for the rotation times, even after giving normal readings for the τ. The causes for this are unknown.

The Pcs also exhibited rotational times found in similar Pcs[90], which are long owing to the size of the Pc macrocycle.

3.3.1 α-SnOtBpPc

***α*-SnOtBpPc** showed slight changes between solvents (**Table 3.2)**, with DCM giving the lowest τ of the solvents followed by THF, chloroform and toluene which was the longest. The isometric lifetimes were moderately more ordered except for DCM which gave a null reading.

3.3.2 α-SnSPPc

***α*-SnSPPc** gave no fluorescence data, as the emission spectra was far too low for detection, even at higher concentrations of the compound. The cause of this is unknown. However, a single absorption peak was obtained in DCM, though repeats of this step in other solvents resulted in conflicting results with each run.

3.3.3 ββ-SnOtBpPc

For **ββ-SnOtBpPc,** the τ of was the highest on average of all Pcs studied here, with the shortest lifetime at 5.07 ns. Unfortunately, the isometric lifetimes were null figures for all but chloroform. However, this value showed an appropriate value for the slightly heavier Pc when compared to the other Pcs.

3.3.4 ββ-SnSPPc

ββ-SnSPPc had reasonable τ for all but toluene, which only gave a value of 1.4 ns, a value much lower than average for both itself and the other SnPcs. The isometric lifetimes showed DCM having a very long rotation time (0.6 ns, the longest observed in this work) and 0.125 ns for THF. This discrepancy is odd as DCM is slightly less viscous than THF. Both chloroform and toluene gave null results.

3.3.5 β-SnOtBpPc

β-SnOtBpPc τ varied more than other SnPcs observed (excluding outliers) with a minimum of 3.4 ns in toluene and a maximum of 5.6 ns in DCM. Its isometric data showed the lowest rotation times, averaging less than 0.01 ns, and the cause for this is unknown.

3.3.6 β-SnSPPc

β-SnSPPc showed the second longest τ, with very little spread across the four solvents. Its isometric times showed good correlation to the solvents' relative viscosity, with the exception of toluene which had the shortest rotation time.

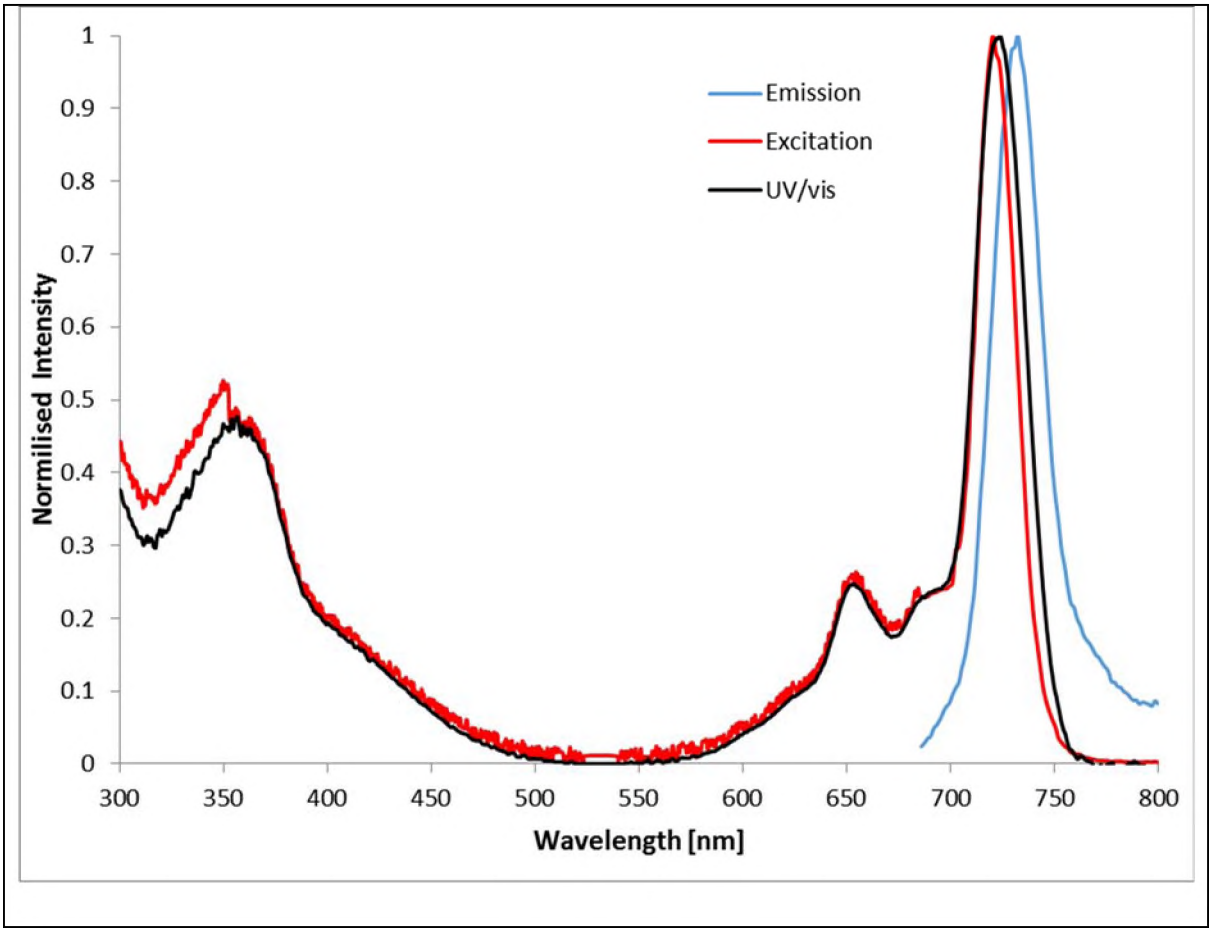

Figure 3.7: Ground state absorption (black), fluorescence emission (blue) and excitation (red) for ββ –SnOtBpPc.

3.3.6 TCSPC overview

No general trend can be extracted from the fluorescent time data, though the rotation times correlate very well with solvent viscosity.

Table 3.2: Table with the fluorescent and isometric data for all 6 SnPcs.

	λ_{max} (nm)								
Pc	Abs	Em	Exc	τ(ns)			ϕ(ns)	V_m	
α-SnOtBpPc									
Chloroform	732	755	733	4.84	±	0.02	0.10	± 0.04	7.64112E-28
Dichloromethane	731	754	731	3.05	±	0.01	0.10	± 0.12	9.56336E-29
Tetrahydrofuran	727	750	727	4.13	±	0.02	0.13	± 0.07	1.14076E-27
Toluene	728	751	729	5.13	±	0.02	0.2	± 0.13	1.65696E-27
α-SnSPPc									
Chloroform	766								-
Dichloromethane	769	780	770	-		-	-		-
Tetrahydrofuran	765								-
Toluene	769								-
ββ-SnOtBpPc									
Chloroform	709	718	710	5.31	±	0.02	0.12	± 0.04	8.98956E-28
Dichloromethane	709	716	710	5.54	±	0.02	0.0	± -	9.56336E-30

Tetrahydrofuran	705	717	706	5.07	±	0.02	0.01	±	0.13	6.89719E-29
Toluene	710	716	711	5.59	±	0.02	0.001	±	-	7.32844E-30
ββ-SnSPPc										
Chloroform	736	760	737	5.51	±	0.02	0.001	±	-	7.4913E-30
Dichloromethane	739	763	740	4.82	±	0.02	0.61	±	0.32	5.73801E-27
Tetrahydrofuran	735	758	736	4.41	±	0.02	0.12	±	0.14	1.09688E-27
Toluene	739	763	740	1.38	±	0.01	0.001	±	-	7.32844E-30
β-SnOtBpPc										
Chloroform	708	726	710	4.52	±	0.02	0.01	±	0.05	5.99304E-29
Dichloromethane	708	725	709	5.55	±	0.02	0.01	±	0.07	9.70968E-29
Tetrahydrofuran	704	721	705	4.37	±	0.02	0.01	±	0.06	6.59884E-29
Toluene	707	722	706	3.43	±	0.01	0.01	±	0.09	5.87228E-29
β-SnSPPc										
Chloroform	725	736	725	5.22	±	0.02	0.32	±	0.15	2.24739E-27
Dichloromethane	723	731	724	5.18	±	0.02	0.25	±	0.12	2.43866E-27
Tetrahydrofuran	721	731	722	5.31	±	0.02	0.11	±	0.12	9.82806E-28
Toluene	722	734	722	5.27	±	0.02	0.07	±	0.11	5.20319E-28

Chapter 4. Z-Scan experiments and NLO properties of SnPcs

4.1 Z-Scan experiment

In this work NLA parameters, (β_I and $\boldsymbol{Im}[\chi^3]$), were measured using Z-Scan and theoretically studied using DFT calculations. The 6 SnPcs were weighed out such that each sample had roughly equivalent moles. These samples were then made into a stock solution, using DCM, Toluene, Chloroform and THF. The solvent choice was made due to their different polarities, with each stock solution creating 16 samples in total, consisting of four samples for each solvent. Z-Scan measurements for each sample were run twice (more if large laser fluctuations were observed) giving 8 data sets for each Pc/solvent combination. Each measurement was done at 3 different powers, 8 $\boldsymbol{\mu J}$, 10 $\boldsymbol{\mu J}$ and 12 $\boldsymbol{\mu J}$. This was repeated for all solvents for all Pcs. These results gave suitable information to account for any accidental variation in concentration or laser strength. The 8 total runs for each solvent/Pc combination made possible the comparison of the rather small changes in $\boldsymbol{Im}[\chi^3]$ that the change in solvent was expected to induce. The first set information extracted from the Z-Scan transmittance plot (see **Figure 4.1** as an example, see appendix A for all plots) was the non-linear absorption coefficient (β_I) which could be converted to the imaginary susceptibility ($\boldsymbol{Im}[\chi^3]$) using **Equation 1.16 .**

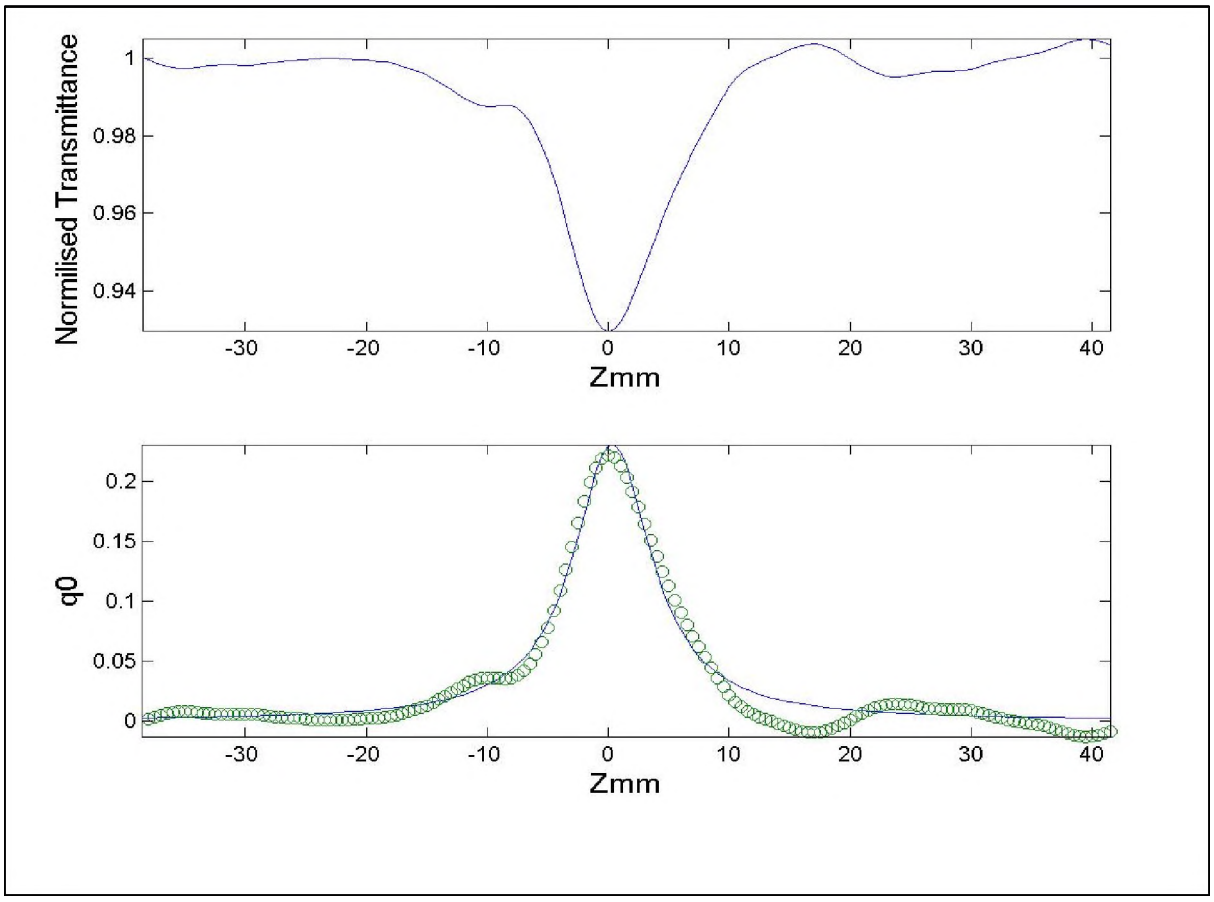

Figure 4.1: Z-scan of α-SnOtBpPc (top) and its fitting (bottom).

The non-linear absorption coefficient (β_I) was extracted using Tsigarida's method[49], as discussed in Chapter 1. The trend in the values were compared with the theoretical calculations for the first order hyperpolarizability (β) that had been done on the SnPcs in different solvent environments. The results were then compared against each other to see if any similar trends arose as solvents where changed. The calculations were entirely theory based and direct comparisons would be impossible as they possess different units C^3 m^3J^{-2} for first hyperpolarizability and $C^4m^4J^{-3}$ for second hyperpolarizability.

Here the second hyperpolarizability will be reported in units e.s.u. to remove any possibility of confusion) and the only values of concern are their responses to change in the solvent field in which the Z-Scan takes place.

The computationally calculated theoretical values of the first hyperpolarizability (β) were also very low (10^{-10} esu); this was expected as the near symmetrical SnPcs should

have samll β due to their center of inversion as shown in Table 4.1. The values that are observed are thus much lower than have been reported for β in other compounds[70] and direct comparison to trends can only be done in a general sense.

4.2 Z-Scan studies in different solvents

4.2.1 α-SnOtBpPc

Figure 4.2 shows the Z-Scan results, these results display an increasing $\boldsymbol{Im}[\chi^3]$ (calculated from β_I values using eqn 1.16, see Table 4.1) with solvent polarity greater than 1, with a relative difference of almost 25% was observed in $\boldsymbol{Im}[\chi^3]$, implying that the solvents had a significant impact on the NLA of the SnPcs analysed. However the least polar solvent (toluene) also showed an increased $\boldsymbol{Im}[\chi^3]$. The error bars in **Figure 4.2** are due to the replicated measurements of $\boldsymbol{Im}[\chi^3]$. The effect of solvents on NLA has been reported before[66]; however here it is significant as the changes in $\boldsymbol{Im}[\chi^3]$is larger than the error margin for each value, giving some confidence on this effect on the effect of the solvent on the NLO properties of the SnPcs.

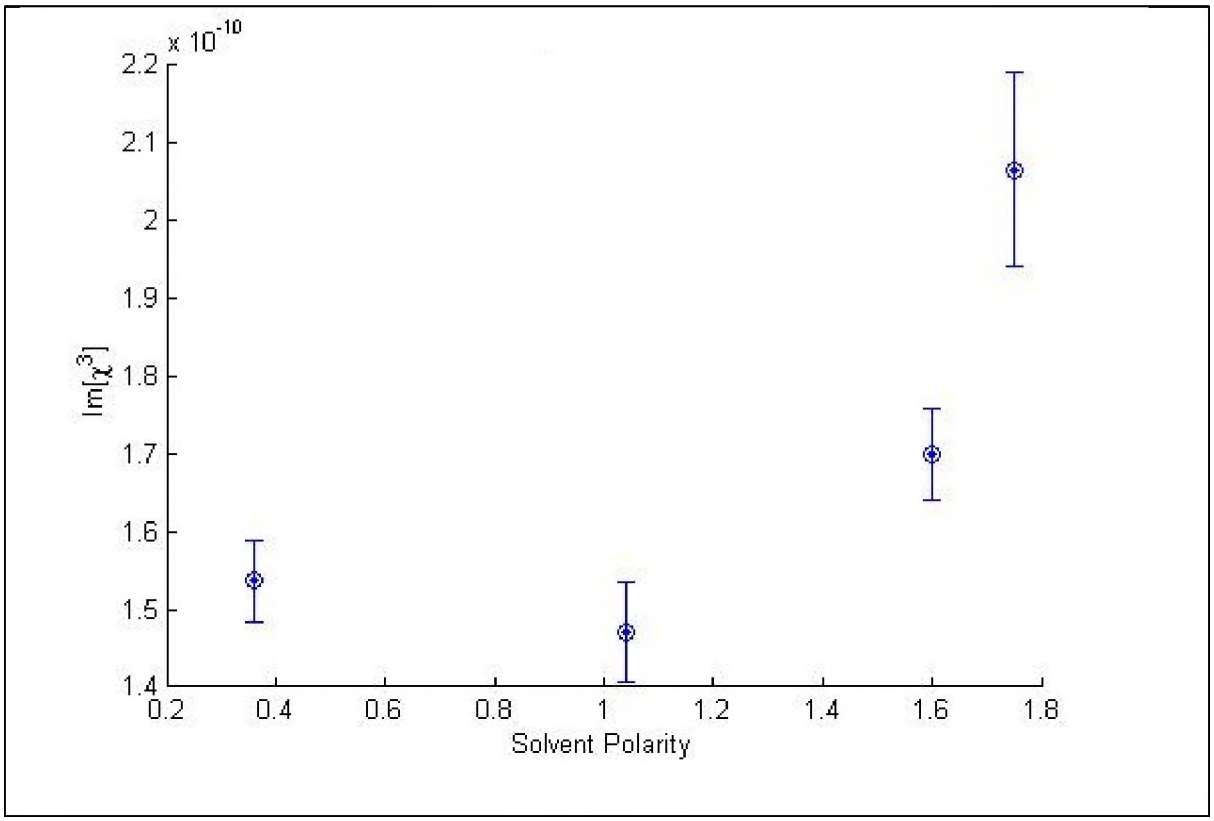

Figure 4.2 : Imaginary susceptibility of α-SnOtBpPcvs solvent polarity.

DFT calculations (based on calculations discussed in Chapter 2) were carried out in different solvents in order to determine if a similar trend can be obtained theoretically. **Figure 4.3** shows a plot of β_{HRS} values versus solvent polarity in the following order: toluene, chloroform, dichloromethane and tetrahydrofuran. The theoretical β_{HRS} response increased with increasing solvent polarity. However, toluene did not correlate with experimental data, in terms of trending.

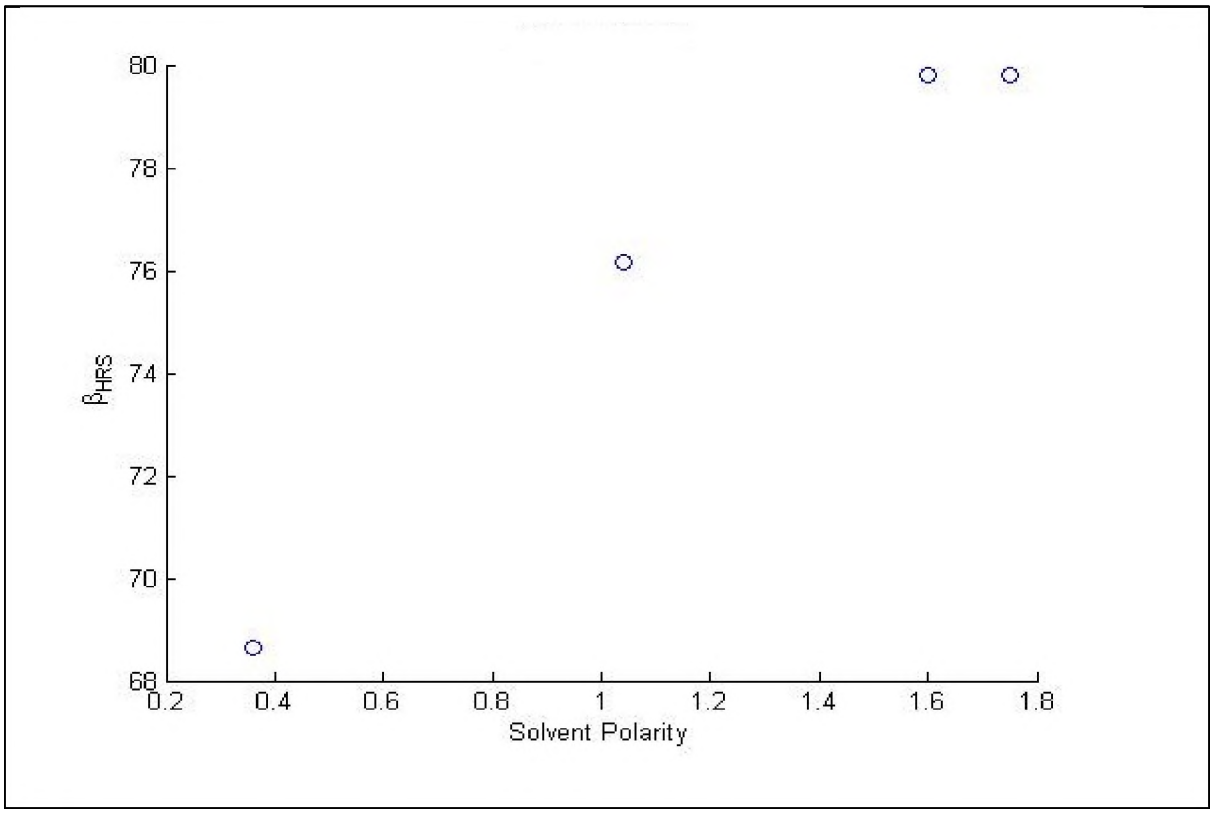

Figure 4.3 : Theoretical first order hyperpolarizability of α-SnOtBpPc vs solvent polarity.

Both values acquired and an overlay of the results made allowed an inspection of their respective trends. Unfortunately, due to the physical limitations on the degree of solubility of all 6 Pcs a larger range of polarity was not possible. However, we do see in **Figure 4.3** that both values favor an increase in environmental polarity. The current experimental data suggests that electron withdrawing substituents, (phenoxy), tend to increase third order imaginary susceptibility of the complex in polar solvents.

4.2.2 β-SnOtBpPc

Figure 4.4 shows the imaginary third order susceptibility ($\boldsymbol{Im}[\chi^3]$) of **β-SnOtBpPc** versus solvent polarity. Similarly to **α-SnOtBpPc,** the multiple measurements were done for each point in order to plot the error bars. **β-SnOtBpPc** $\boldsymbol{Im}[\chi^3]$ values showed

a similar general increasing trend compared to that of **α-SnOtBpPc** with respect to increasing polarity of different solvents. The determined $\boldsymbol{Im}[\chi^3]$ values for **β-SnOtBpPc** were approximately four times higher in magnitude compared to **α-SnOtBpPc**. The above suggest that Sn(IV) phthalocyanine substituted at the beta position with phynoxy substituents will generally have higher beta values compared to alpha substituted Sn(IV) phthalocyanines. The magnitude of the $\boldsymbol{Im}[\chi^3]$ range (an increase of ~1.6 between highest and lowest readings) can be attributed to the wider electron distribution found in the **β-SnOtBpPc,** as the beta position is further from the centre of the Pc macrocycle (**Figure 4.4**). Another explanation could be the different activations at the meta (β) and ortho(α) positions of the benzo rings on the π system of the SnPc.

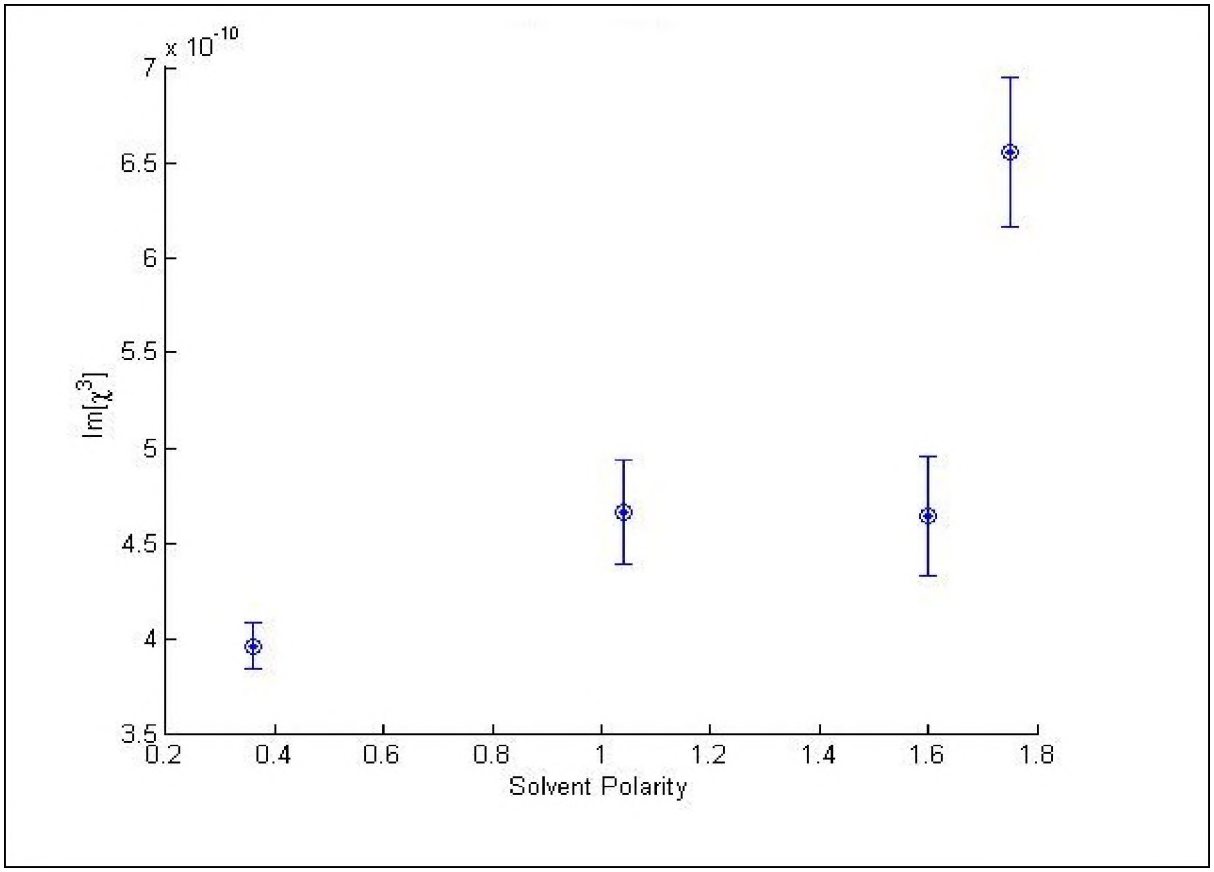

Figure 4.4 : Imaginary susceptibility of β-SnOtBpPc vs solvent polarity.

The theoretical β_{HRS} showed a similar general upward trend seen in Figure 4.5 compared to the experimental $\boldsymbol{Im}[\chi^3]$ values, as solvent polarity was increased. However, there is slight drop in β_{HRS} value for THF in the theoretical trend. This

behavior of the most polar solvent was also observed for **α-SnOtBpPc**. The above behavior of the most polar solvent suggests that DFT calculations inadequate of completely predicting the real solvent–Pc interaction for this THF.

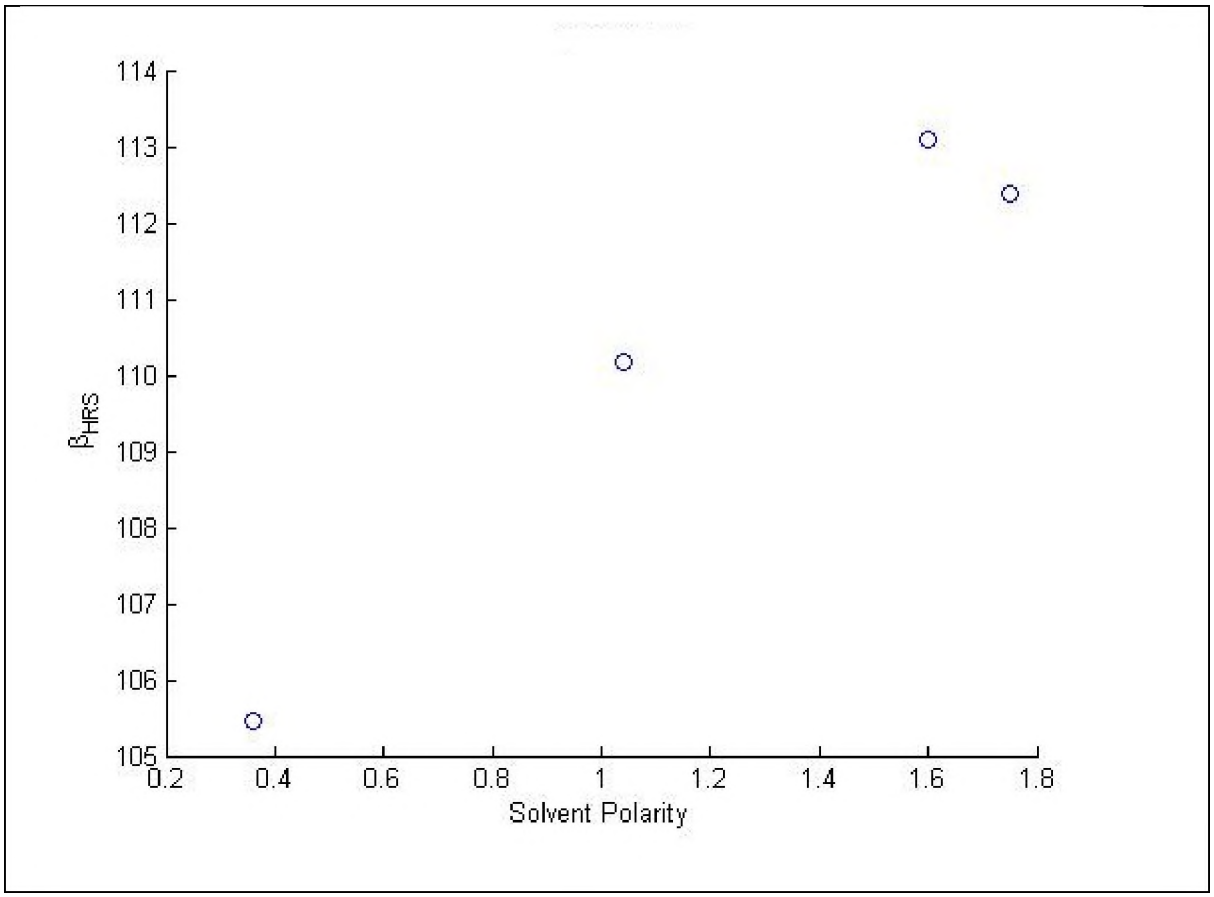

Figure 4.5 : Theoretical first order hyperpolarizability of β-SnOtBpPc vs solvent polarity.

4.2.3 ββ-SnOtBpPc

The $Im[\chi^3]$ values determined for the octa substituted **ββ-SnOtBpPc** closely resembled the tetra substituted **β-SnOtBpPc** in terms of magnitude and trend, except for the most polar solvent (THF), (see **Figure 4.6).** However $Im[\chi^3]$ values in different solvents studied were appreciably lower for **ββ-SnOtBpPc** compared to **β-SnOtBpPc**. The above variation in $Im[\chi^3]$ values between **ββ-SnOtBpPc** and **β-SnOtBpPc** can be attributed to the increased substitution having a greater effect on the electron density of **ββ-SnOtBpPc.**

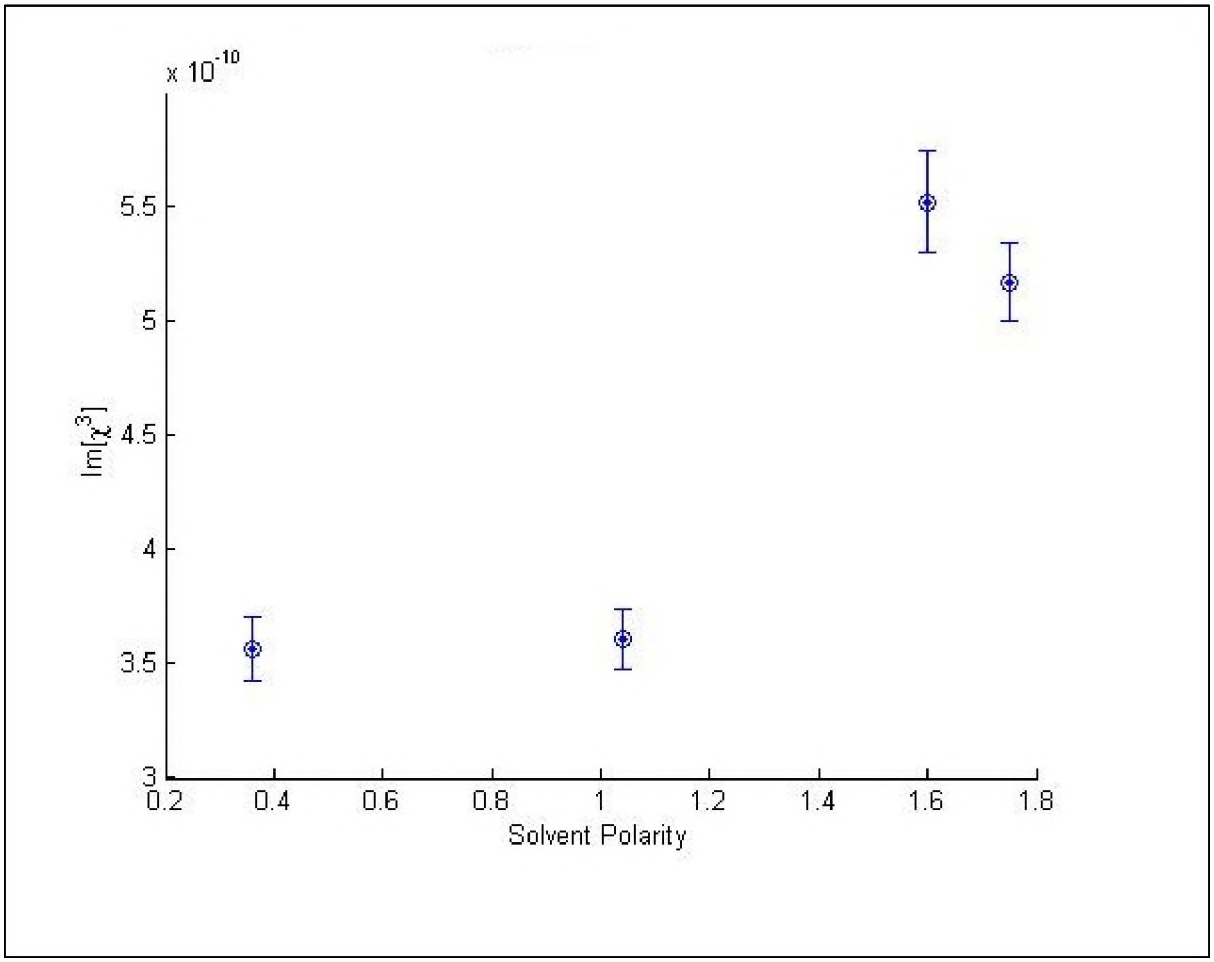

Figure 4.6 : Imaginary susceptibility of ββ-SnOtBpPc vs solvent polarity.

The theoretical β_{HRS} values of **ββ-SnOtBpPc** (shown in **Figure 4.7**) also showed a similar trend to experimental $Im[\chi^3]$ values. In this case the most polar solvent

followed the experimental trend better, compared to **β-SnOtBpPc**. Since **ββ-SnOtBpPc** is more is more symmetrical compared to **β-SnOtBpPc**, it would be expected that the theoretical β_{HRS} values would be lower for **ββ-SnOtBpPc**. However higher β_{HRS} values are observed for **ββ-SnOtBpPc.** This discrepancy could be attributed to the role of solvent-Pc interaction, which is more favourable in **ββ-SnOtBpPc** compared to **β-SnOtBpPc** in terms of β_{HRS} values. However the trend is comparable to the $\boldsymbol{Im}[\chi^3]$ values, with both results showing a maxima in the same solvent.

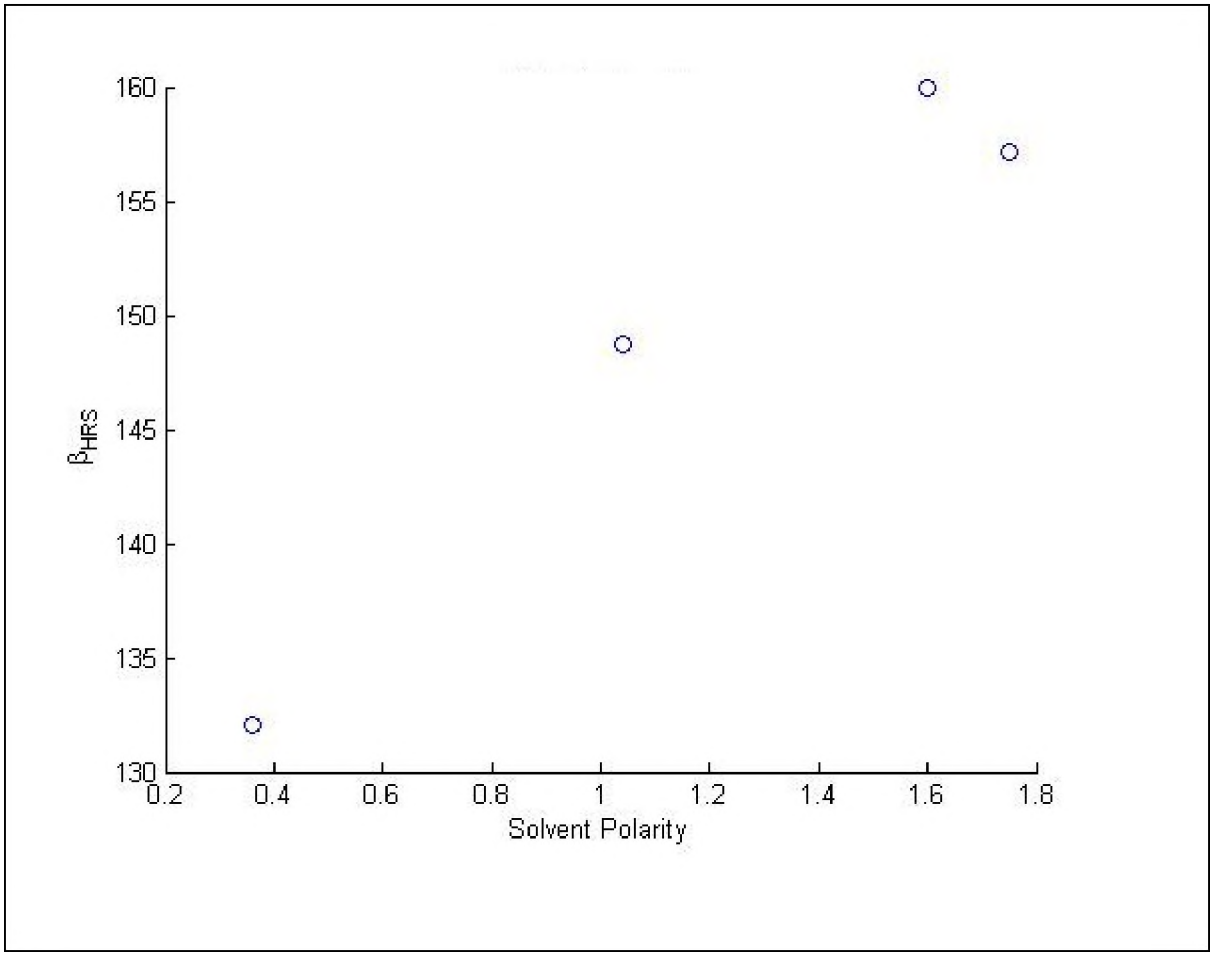

Figure 4.7 : Theoretical first order hyperpolarizability of ββ-SnOtBpPc vs solvent polarity.

4.2.4 α-SnSPPc

Figure 4.8 shows ***α*-SnSPPc** imaginary susceptibility versus solvent polarity. Despite having a higher electron donating substituent the thiol linked ***α*-SnSPPc** showed the reverse trend compared to ***α*-SnOtBpPc** above. This observation suggests that depending on the type of substituents, such as their size and individual polorazability, solvent polarity affects Pcs differently. The trend in the experimental data suggest that more electron donating substituents, like thionyl or alkthiol ether, tend to lower the third order imaginary susceptibility of the α-SnPcs in polar solvents. This is despite the higher magnitude of $\boldsymbol{Im}[\chi^3]$ for the thiol substituted ***α*-SnSPPc** when compared to the nonlinear optical properties of ***α*-SnOtBpPc.**

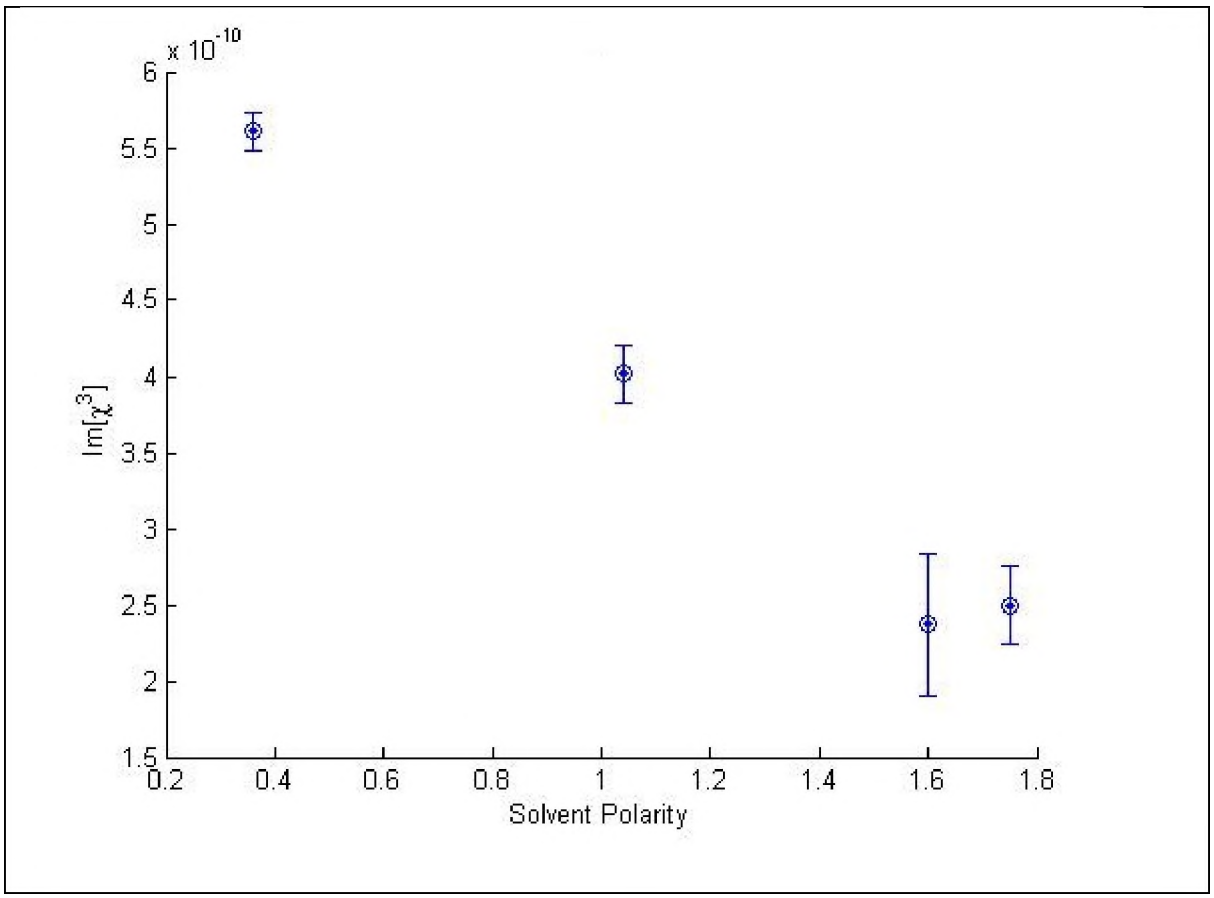

Figure 4.8 : Imaginary susceptibility of *α*-SnSPPc vs solvent polarity.

The trend theoretical β_{HRS} values (see **Figure 4.9**) follows a similar pattern to experimental third order imaginary susceptibility; a decrease in β_{HRS} for **α-SnSPPc** was observed with increasing polarity of the solvent. The difference in trend of the NLO properties of the SnPc compared to its α-phenoxy analogue demonstrate that deferent Pcs behave differently in solvents of different polarity.

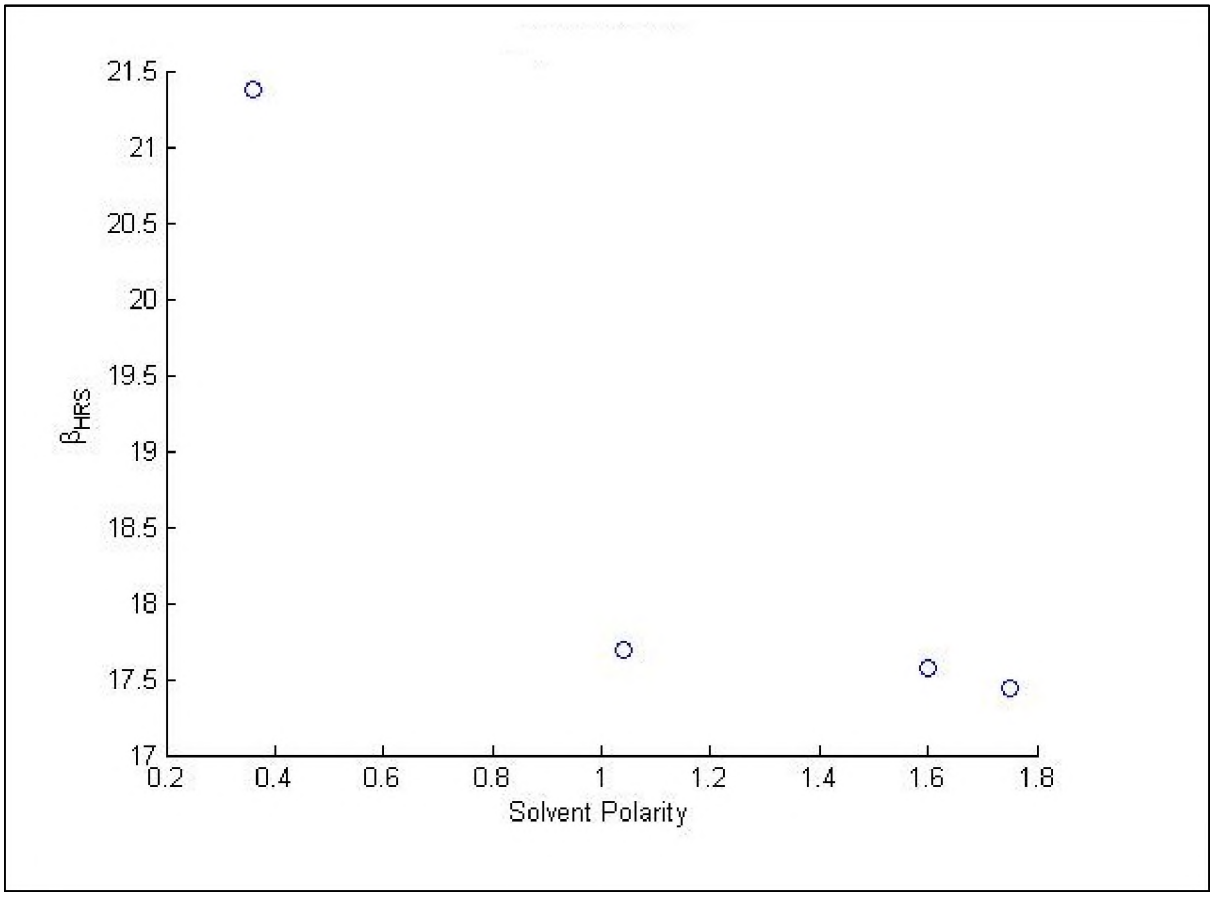

Figure 4.9 : Theoretical first order hyperpolarizability of α-SnSPPc vs solvent polarity.

4.2.5 β-SnSPPc

The $\boldsymbol{Im}[\chi^3]$ values for **β-SnSPPc** in Figure 4.10 showed a generally increasing trend for the first three solvents, except for the last solvent (THF). The trend observed suggests that solvent-Pc interaction is different for **β-SnSPPc** compared to **α-SnSPPc.** The generally increasing $\boldsymbol{Im}[\chi^3]$ trend is similar to the trend observed for **β-SnOtBpPc**

with respect to increasing solvent polarity. The average value for $\boldsymbol{Im}[\chi^3]$ for **β-SnSPPc** is higher compared to ***α*-SnSPPc** values, similar to the differences in **β-SnOtBpPc** and ***α*-SnOtBpPc**. This observation suggests that tetra beta substituted Pcs studied in this work have better nonlinear optical properties compared to tetra alpha substituted Pcs, whether it is a phynoxy or thiol substituent.

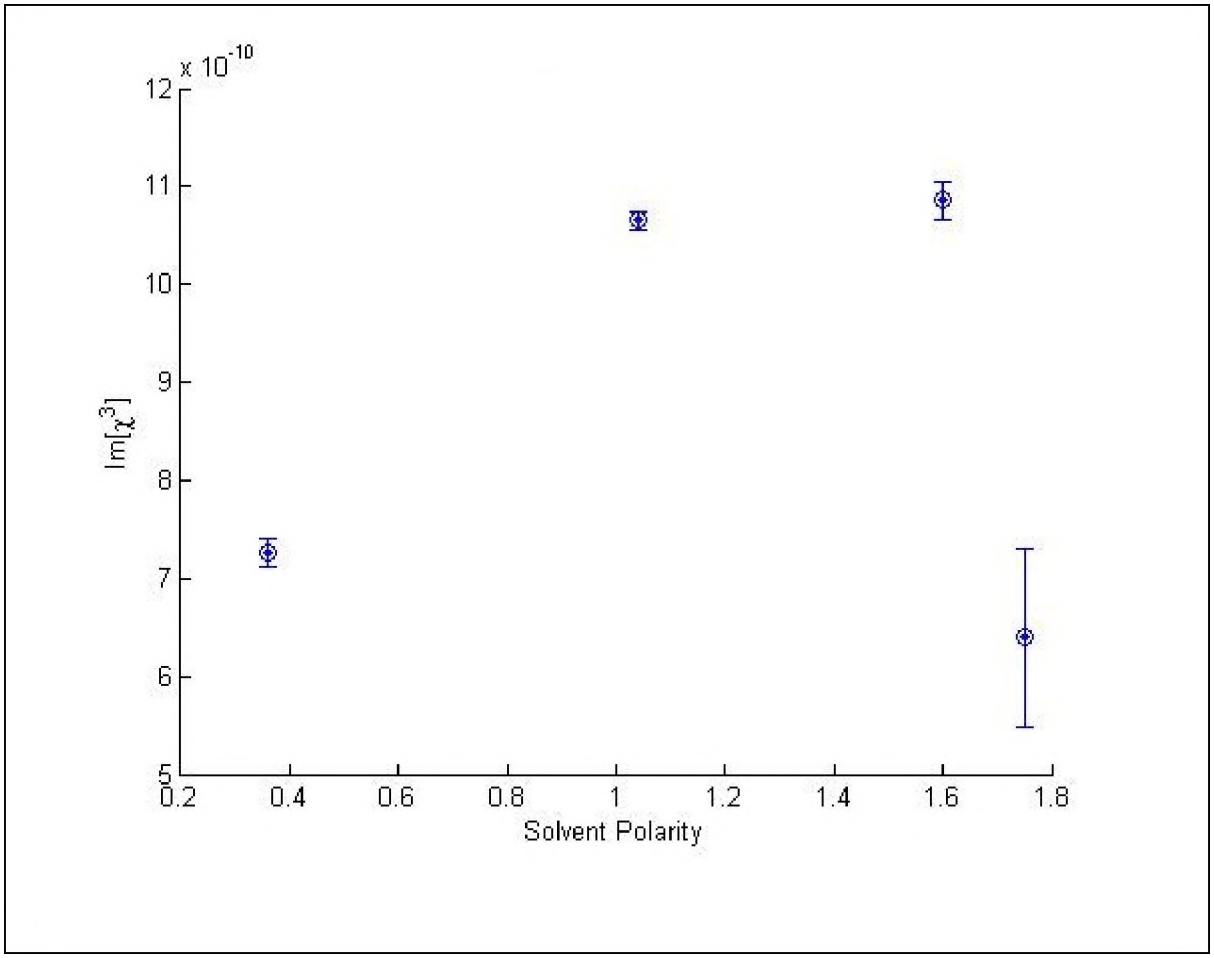

Figure 4.10 : Imaginary susceptibility of β-SnSPPc vs solvent polarity.

Figure 4.11 shows a general decreasing trend of theoretical β_{HRS} values with increasing solvent polarity, similar to ***α*-SnSPPc** β_{HRS} values. The observed trend is a reverse of that observed for the experimental $\boldsymbol{Im}[\chi^3]$ values suggest that in general β_{HRS} values do not follow a similar trend to $\boldsymbol{Im}[\chi^3]$ values. The solvent polarity will have a unique effect depending on the type of molecule.

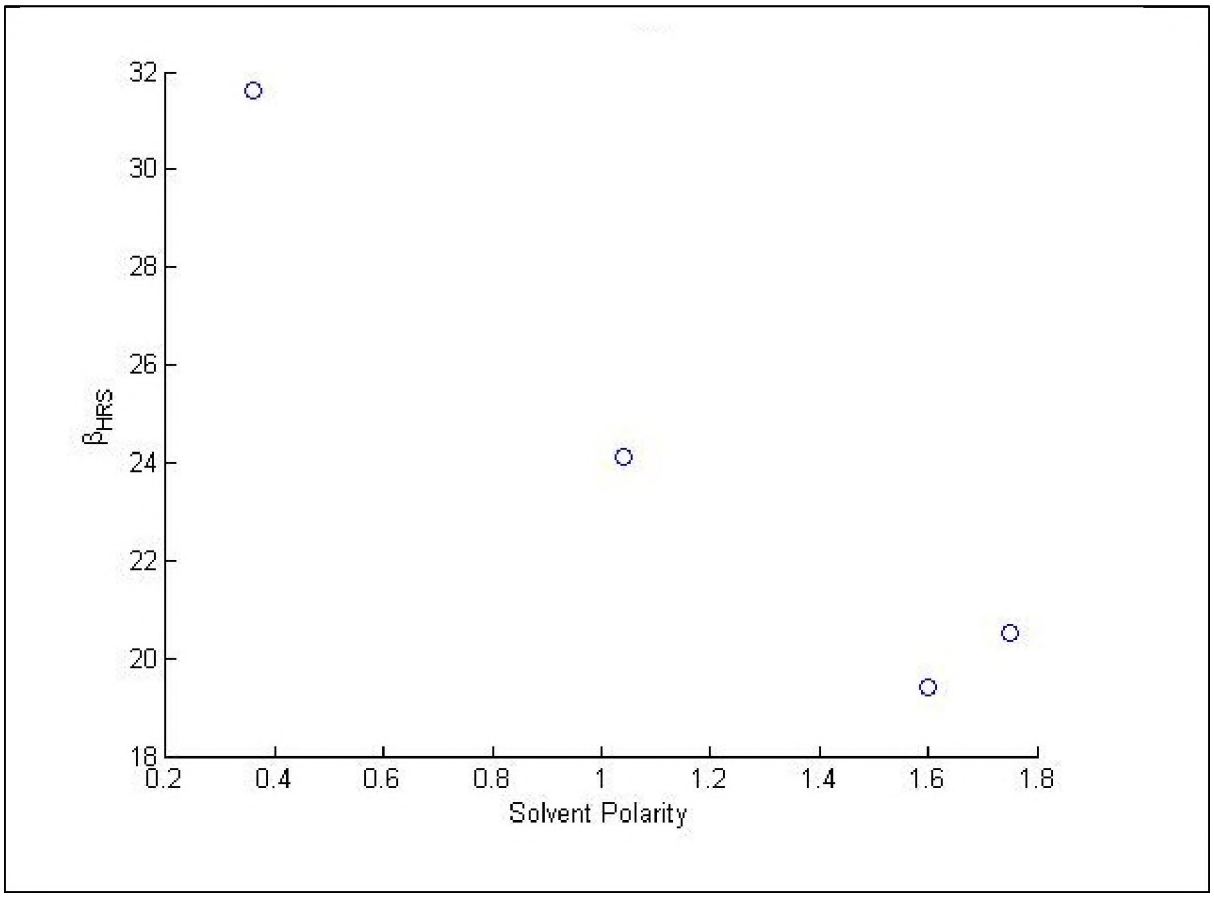

Figure 4.11 : Theoretical first order hyperpolarizability of β-SnSPPc vs solvent polarity.

4.2.6 ββ-SnSPPc

The **SnSPPc** experimental $\boldsymbol{Im}[\chi^3]$ values of the octa-substituted **ββ-** followed a similar trend to **ββ-SnOtBpPc** except for the first measurements in toluene. The maximum $\boldsymbol{Im}[\chi^3]$ value was found to be much lower in **ββ-SnSPPc** compared to **β-SnSPPc** values**.** The lower $\boldsymbol{Im}[\chi^3]$ values for octa-substituted **ββ-SnSPPc** with respect to tetra-substituted **β-SnSPPc** was similarly observed for **ββ-SnOtBpPc** and **β-SnOtBpPc** values. This observation once again suggests that the lower values could be attributed to the increased substitution, having a greater effect on the electron density of **ββ-SnSPPc**.

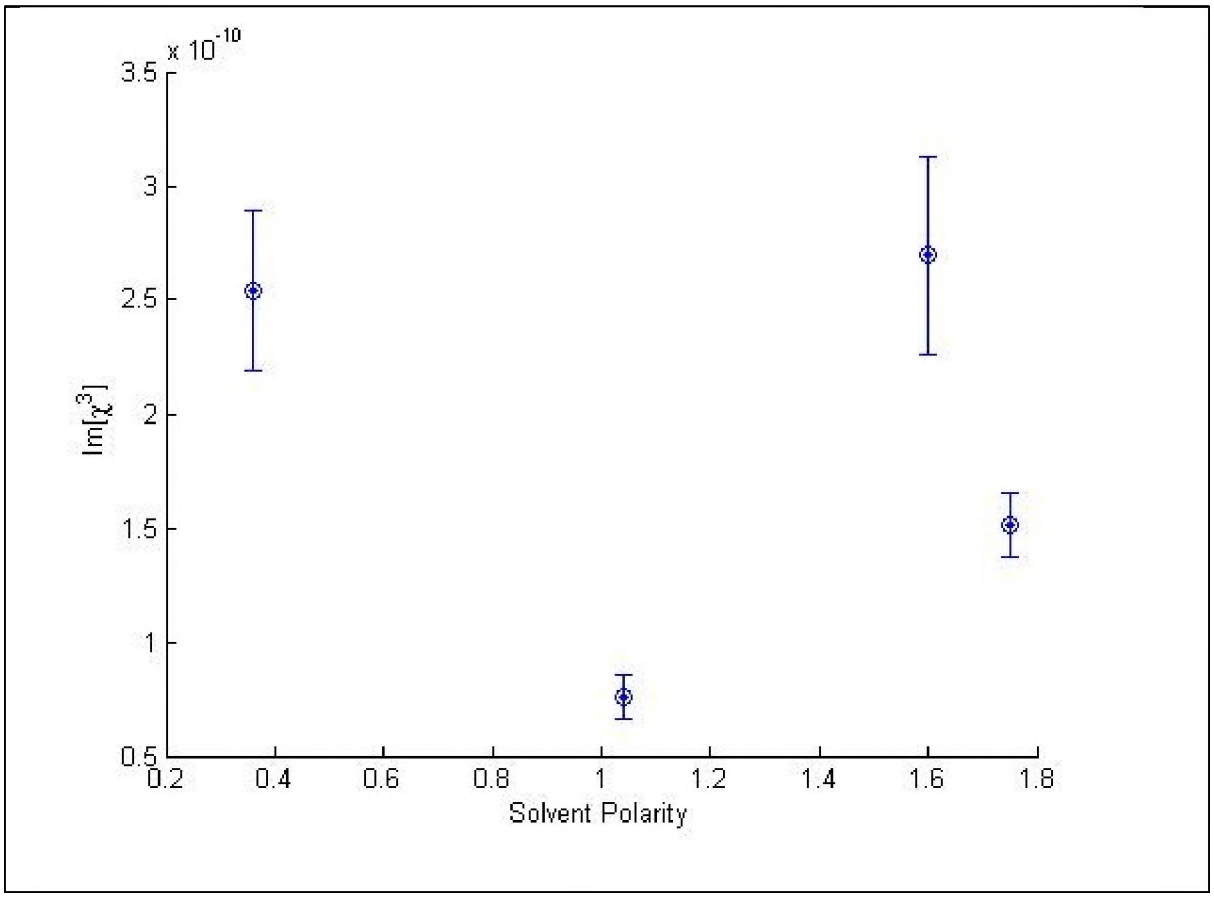

Figure 4.12 : Imaginary susceptibility of ββ-SnSPPc vs solvent polarity.

The theoretical β_{HRS} values shown in Figure 4.13 indicate a strong increase with polarity, with a slight decrease in THF. The β_{HRS} values follow a similar trend to the experimental $\boldsymbol{Im}[\chi^3]$ values for the last three solvents. An explanation for the variation in the first $\boldsymbol{Im}[\chi^3]$ cannot be given by this study. Given that the experimental $\boldsymbol{Im}[\chi^3]$ values were repeated 4 times, there must be a different solvent interaction in real solvent as compared to the theoretical interaction.

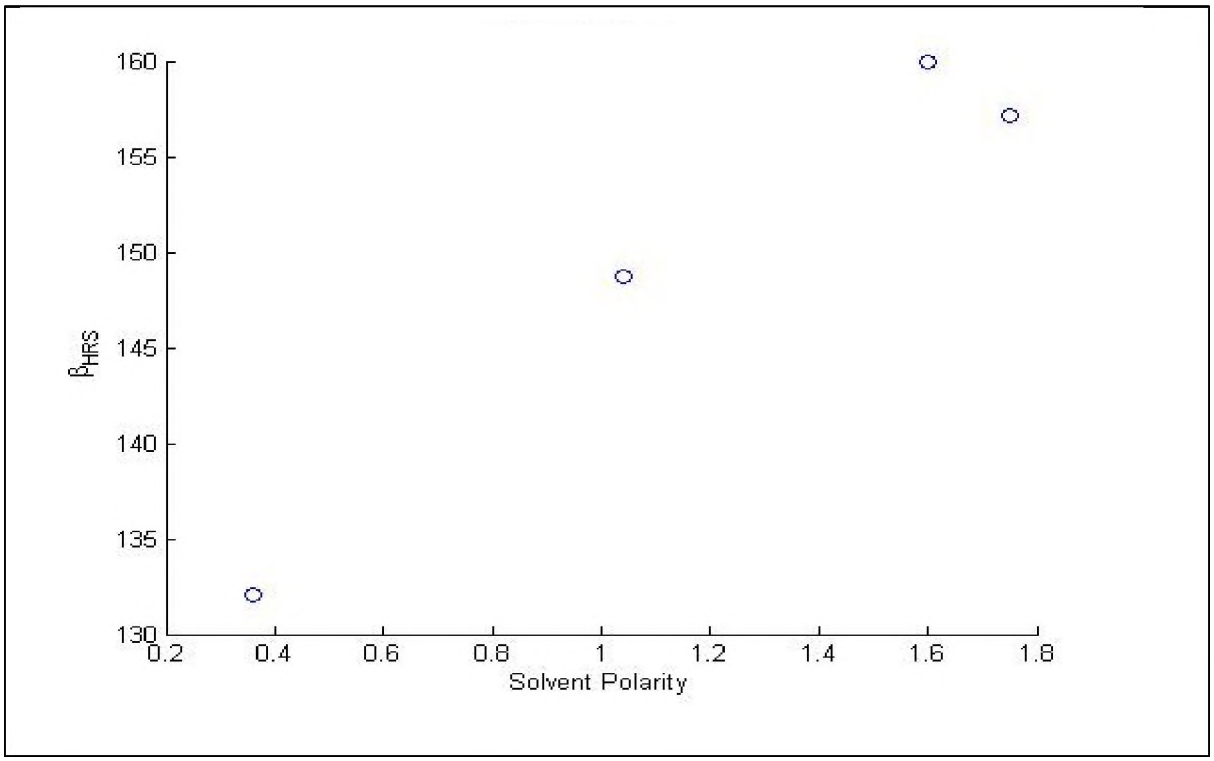

Figure 4.13 : Theoretical first order hyperpolarizability of ββ-SnSPPc vs solvent polarity.

Phthalocyanine/ solvent	$Im(\chi^3)$[esu]x10^{-12}			$Im(\gamma)$[esu]x10^{-31}			$\beta_{HRS}[m^4V^{-1}]$
α-SnOtBpPc							
Chloroform	4.806	±	0.839	2.116	±	0.369	2.76E-40
Dichloromethane	5.464	±	0.916	3.055	±	0.512	2.89E-40
Tetrahydrofuran	6.412	±	1.805	2.603	±	0.733	2.89E-40
Toluene	3.191	±	1.067	1.272	±	0.426	2.49E-40
α-SnSPPc							
Chloroform	13.115	±	2.988	11.187	±	2.548	6.40E-41
Dichloromethane	7.701	±	7.546	6.211	±	0.012	6.36E-41
Tetrahydrofuran	6.706	±	2.608	5.945	±	2.312	6.32E-41
Toluene	18.029	±	1.869	33.238	±	3.446	7.74E-41
ββ-SnOtBpPc							
Chloroform	11.786	±	1.701	7.571	±	1.093	5.38E-40
Dichloromethane	17.806	±	3.508	14.929	±	2.941	5.79E-40
Tetrahydrofuran	15.889	±	1.122	10.802	±	0.763	5.69E-40
Toluene	10.816	±	1.067	7.012	±	0.692	4.78E-40
ββ-SnSPPc							
Chloroform	3.014	±	1.822	2.193	±	1.325	5.29E-40
Dichloromethane	5.225	±	2.421	1.627	±	0.754	5.43E-40
Tetrahydrofuran	4.782	±	2.153	1.167	±	0.525	5.39E-40
Toluene	7.068	±	4.600	4.055	±	2.639	5.05E-40
β-SnOtBpPc							
Chloroform	15.234	±	3.554	2.535	±	0.591	3.99E-40

Dichloromethane	13.327	±	2.139	1.603	±	0.257	4.10E-40
Tetrahydrofuran	20.711	±	6.044	2.939	±	0.858	4.07E-40
Toluene	12.679	±	1.838	1.496	±	0.217	3.82E-40
β-SnSPPc							
Chloroform	34.793	±	1.151	3.981	±	0.132	8.73E-41
Dichloromethane	35.240	±	3.151	7.225	±	0.646	7.03E-41
Tetrahydrofuran	26.677	±	3.429	4.473	±	0.575	7.43E-41
Toluene	24.428	±	1.398	4.272	±	0.245	1.14E-40

Table 4.1: Summery of nonlinear optical properties for the 6 SnPcs.

4.3 Five energy level fitting of Z-scan results

Z-scan results can also be used to obtain the molecules TPA cross-section (σ_{TPA}) , and the excited state (σ_s) triplet state cross-sections (σ_t) . This is done using a much more computationally expensive five orbital fitting (FOL) (see **Chap 1**) and was done on the Pcs in only one solvent. This was due largely to time constraints involved in the calculations. THF was used as the solvent due to the Z-Scan spectra in this solvent being very well behaved. These fittings were done using a method adapted from work by Zhang[60], and were changed to suits the experimental needs, **Scheme 4.1**. Aside from the trivial concentration and laser variable changes to account for the different experimental setup, the most significant modifications were the incorporations of the molecular isometric rotation time into the absorption equations (see **Chap 1).**

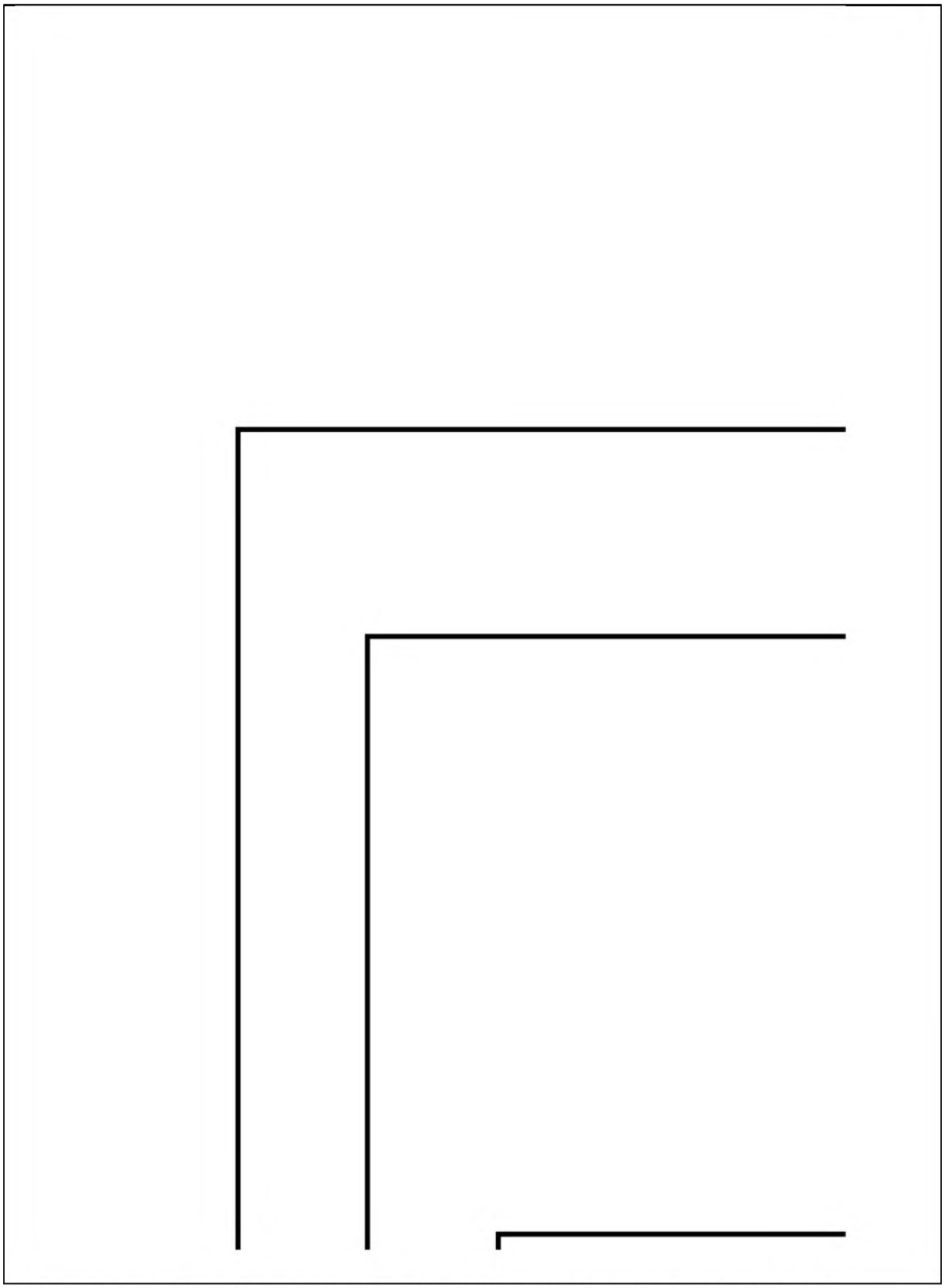

Scheme 4.1 : Flow diagram of the calculations for the five level orbital fit.

Figure 4.14 and **Figure 4.15** show experimental and theoretical z-scan transmittance plot based on the five energy level model for **(A) α-SnOtBpPc, (B) β-SnOtBpPc, (C)ββ- SnOtBpPc, (D) α-SnSPPc, (E) β-SnSPPc** and **(F) ββ-SnSPPc**. A very good fit of the data was obtained for **(A) α-SnOtBpPc** and **(C) α-SnOtBpPc.** The bad theoretical plot obtained for **(C) ββ-SnOtBpPc** suggests that a more complicated nonlinear process is involved and that the five energy level approximation is inadequate for this set of data. From the fitting two photon absorption cross-section (σ_{TPA}), the excited state (σ_s) and triplet state cross-sections (σ_t) for the complexes were obtained, the results are summarised in **Table 4.2**.

Pc	**Im(γ)[esu]$x10^{-31}$**	**σ_{TPA}[GM]**	**$\sigma_s[m^2]x10^{-20}$**	**$\sigma_t[m^2]x10^{-20}$**
ββ-SnSPPc	1.167	126.948	0.00147	0.22635
α-SnOtBpPc	2.603	64.2961	0.00445	0.21999
β-SnOtBpPc	2.939	212.488	4.32E-11	0.32603
β-SnSPPc	4.473	144.296	0.00145	0.40671
α-SnSPPc	5.945	53.1156	0.00413	0.31331
ββ-SnOtBpPc	10.802	122.83	0.00219	0.23248

Table 4.2: FLO fit results sorted by Im(γ).

Grouping the Pcs by substituent, a more discernable trend can be observed.

Pc	$\mathbf{Im(\gamma)[esu]x10^{-31}}$	$\boldsymbol{\sigma_{TPA}}$**[GM]**	$\boldsymbol{\sigma_s[m^2]x10^{-20}}$	$\boldsymbol{\sigma_t[m^2]x10^{-20}}$
ββ-SnSPPc	1.167	126.948	0.00147	0.22635
β-SnSPPc	4.473	144.296	0.00145	0.40671
α-SnSPPc	5.945	53.1156	0.00413	0.31331
α-SnOtBpPc	2.603	64.2961	0.00445	0.21999
β-SnOtBpPc	2.939	212.488	4.32E-11	0.32603
ββ-SnOtBpPc	10.802	122.83	0.00219	0.23248

Table 4.3: FLO fit results grouped by Pc and sorted by Im(γ).

Table 4.3 shows the reversal of the **Im(γ)** trends for the two classes of Pcs, increasing from alpha, tetra beta and octa beta in the oxygen substituents but decreasing in the same order for the sulphur substituents. This trend is best explained with the difference in the electro negativity of the two substituents, with sulphur having a much higher electron donating nature. The more notable trend in the NLO parameters is the variation in the σ_{TPA} across the Pcs. This is correlated very well with the shifting of the Q band, with the most red shifted Pc (**α-SnSPPc**) having the smallest σ_{TPA}, while the largest belongs to the least red shifted (**β-SnOtBpPc**). This is attributed to the separation of the two orbitals responsible for the TPA transition falling further away from twice the energy of the exciting light source. The excited state absorptions (due to either σ_s or σ_t) vary, though a comparison of the ratio of the two gives a direct correlation to **Im(γ) (**the exception is the values for **β-SnOtBpPc** which has a notably smaller σ_s). With both substituents the tetra beta was found to possess the largest σ_t and the tetra alpha was found to possess the largest σ_s. This is surprising as the octa

substituted Pc would be expected to have a larger absorption cross-section for both cases. This implies that there are more favourable transitions available for both the singlet and triplet absorptions in each respective case. This may require some further theoretical modelling to fully understand this result.

The FOL fit for the values mentioned **in Tables 4.2** and **4.3** used a number of photophysical properties (as outlined in **Chapter 1**). As fluorescence was also incorporated into the fitting it was important that the contribution of fluorescence to the **Im(γ)** was measured. The laser used to determine **Im(γ)** had a pulse length of 10 ns, and the fluorescent decay time for the SnPcs was around 5 ns. This meant that the excited state would be populated for the duration of a single pulse and thus that the total absorption would depend on the ESA of the system. Thus any Pc with a slightly longer fluorescence lifetime would exhibit higher values of **Im(γ)** than a Pc with equal cross-sections but a shorter fluorescent lifetime. This can all be said for the phosphorescent nature of the SnPcs as well. These two additional factors are the cause of some Pcs possessing higher **Im(γ)** values than a comparison of cross-sections would indicate.

The values are of the order expected for a non-sandwich Pc complex, which have values typically twice the size of those reported here. However, a more accurate analysis would be a comparison of the ratio of the ground state absorption coefficient (σ_g) with the total excited state cross-section (σ_E). The ratio ($\boldsymbol{\sigma_E/\sigma_g}$) of the cross-sections (**Table 4.4)** shows that the results closely follow what has been reported for similar molecules[36]. As optical limiters these values fall short of having high efficacy (ratios of 20 or greater)[28]. However, the comparison of the difference between the excited and ground state ($\boldsymbol{\sigma_E - \sigma_g}$) show that (for low power levels at least) the primary NLO parameter would be TPA.

Pc	$\sigma_g[m^2]x10^{-22}$	$\sigma_E[m^2]x10^{-20}$	σ_E/σ_g	$\sigma_E-\sigma_g(\mathrm{cm}^2)$
ββ-SnSPPc	4.167	0.32635	7.831773	2.8468E-21
β-SnSPPc	4.473	0.40671	9.092555	3.6198E-21
α-SnSPPc	5.945	0.31331	5.270143	2.5386E-21
α-SnOtBpPc	2.603	0.21999	8.451402	1.9396E-21
β-SnOtBpPc	2.939	0.32603	11.09323	2.9664E-21
ββ-SnOtBpPc	10.802	0.23248	2.152194	1.2446E-21

Table 4.4: Cross-section analysis of the SnPcs.

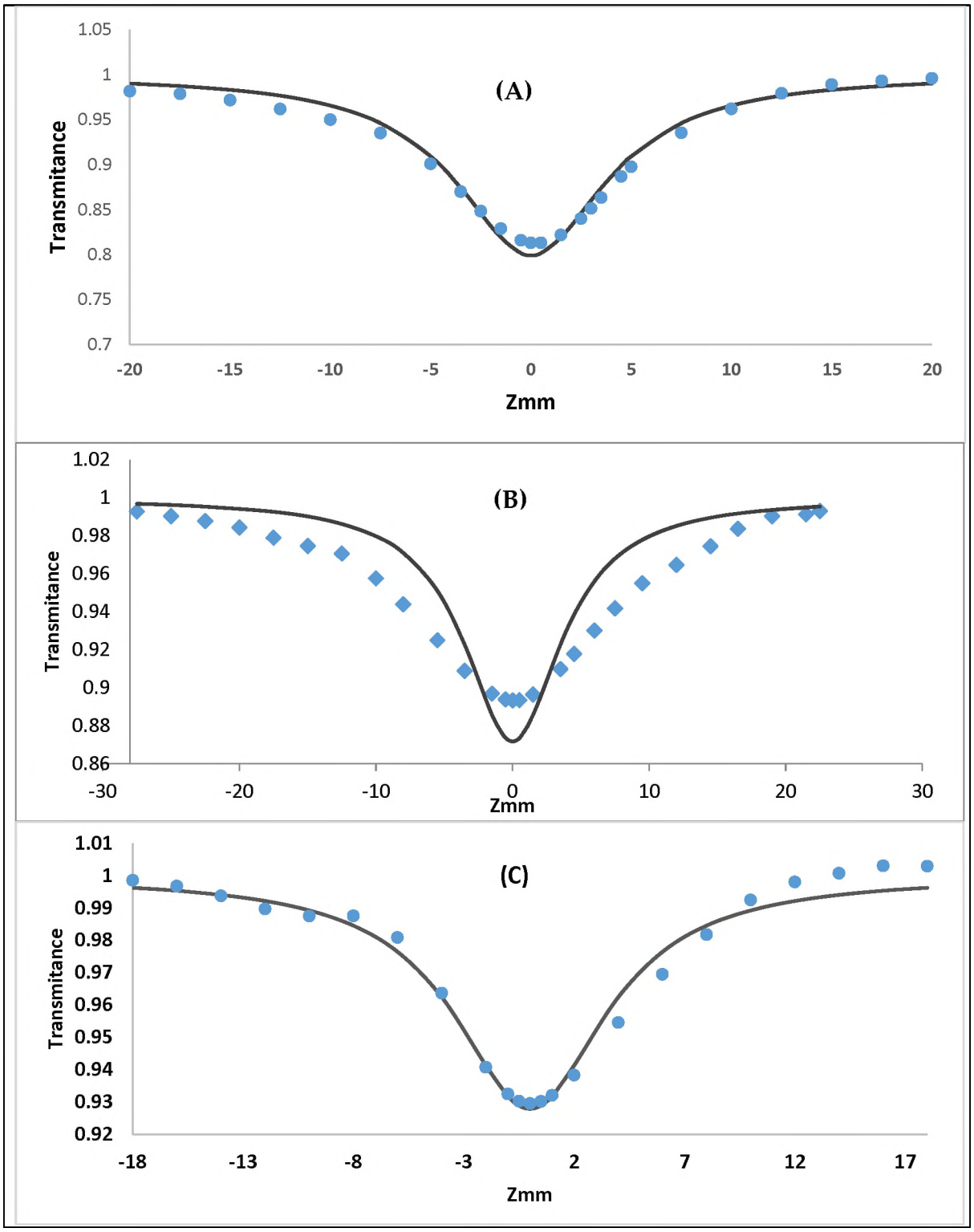

Figure 4.14: Experimental and theoretical z-scan transmittance plot based on the five energy level model for (A)α-SnOtBpPc, (B) β-SnOtBpPc and (C) ββ-SnOtBpPc. The experimental results were obtained in THF.

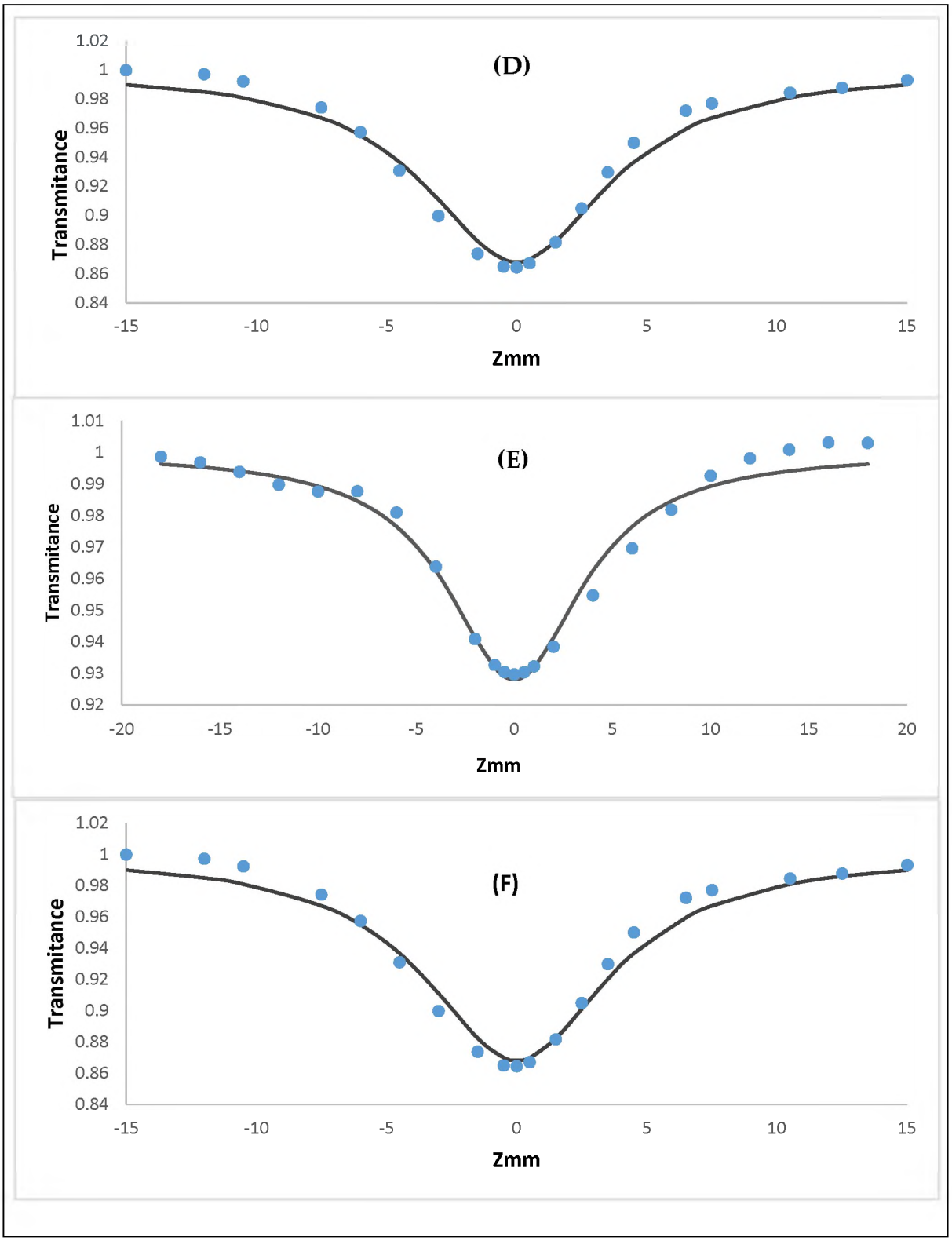

Figure 4.15: Experimental and theoretical z-scan transmittance plot based on the five energy level model for (D)α-SnSPPc, (E) β-SnSPPc and (F) ββ-SnSPPc. The experimental results were obtained in THF.

Chapter 5. Conclusions

A series of 6 Sn(IV) Phthalocyanines were synthesized and characterized with two different classes of substituents. The Pc were then characterized and modeled using various techniques. The modeling done with DFT and TD-DFT as well as CP-DFT in order to calculate the NLO properties. Unfortunately TD-DFT calculations gave deviating results which deviated from the experimentally obtained results in some of the instances measured. These deviations were, however, expected as the accuracy of the methods was dependent on the volume of calculations that were needed and can easily be improved. Though the theoretically calculated wavelengths of absorption were lower than the experimental values, the trends predicted from the TD-DFT corresponded to the shifts in the peaks due to the substituted effect.

Nonlinear optical studies were then done on the Pcs in a series of solvents to determine the second hyperpolarizability as a function of solvent polarity solvents, as well as CP-DFT calculations to determine the first hyperpolarizability (β_{HRS}) in the same solvents. The same parameters where used to calculate the CP-DFT as were used for the TD-DFT calculations and thus a degree of inaccuracy was expected. These were done with the expectation of obtaining similarities in the first and second hyperpolarizabilities of a Pc if there is only a slight change in the environment that it is analyzed in. After comparisons of the 6 SnPc's first and second hyperpolarizabilities, it was found that there was only a partial overlap of the two values. Whether this overlap exists as chance, or the lack of overlap in the other case was due to insufficiently accurate DFT methods, will require more study. An observation can be made however that the Beta substituted Pc in both the thiol and oxy- ether Pcs hade higher values of Im(χ), even when compared to the Octa substituted Pcs, suggesting a degree of fine balancing may be needed in future when designing other NLO materials. Finally, the excited state cross-sections and the ground state cross-sections were compared, and the results showed good correlation with reported values for similar Pcs.

Future work will involve a FLO analysis of theother three solvent results, to better understand the effects of solvation on the MPcs as well as more accurate DFT calculations. Unfortunately, no real discernable best solvent can be shown here for NLO, though these results show how much a simple change in solvation can affect the NLO results of a study. This should be a consideration for any future study as a comparison for NLO properties in different solvents will different far more than the normal spectral results.

References

1. Dahlen MA. The Phthalocyanines. *Ind engernering Chem.* 1939;31(7):839-847.

2. Shirota K, Eida T, Yamamoto T, Yamamoto M. Phthalocyanine dyes. June 1992.

3. Chen R, Li H, Chu D, Wang G. Unraveling oxygen reduction reaction mechanisms on carbon-supported Fe-phthalocyanine and Co-phthalocyanine catalysts in alkaline solutions. *J Phys Chem C.* 2009;113(48):20689-20697.

4. Herron N, Stucky GD, Tolman CA. Shape selectivity in hydrocarbon oxidations using zeolite encapsulated iron phthalocyanine catalysts. *J Chem Soc Chem Commun.* 1986;(20):1521-1522.

5. Mackintosh HJ, Budd PM, McKeown NB. Catalysis by microporous phthalocyanine and porphyrin network polymers. *J Mater Chem.* 2008;18(5):573-578.

6. Fukasawa K, Ishii H. Converts light into soft, intermedicate pastel color using single chip; current efficiency; low cost; small; having multiple different fluorescent particles composed of phthalocyanine, anthraquinone, azo and/or quinophthalone dyes. June 2004.

7. Simon J, Sirlin C. Mesomorphic molecular materials for electronics, opto-electronics, iono-electronics: octaalkyl-phthalocyanine derivatives. *Pure Appl Chem.* 1989;61(9):1625-1629.

8. González-rodríguez D, Torres T, Guldi DM, Rivera J, Ángeles M. Subphthalocyanines : New Tuneable Tectons for Intramolecular Electron and Energy Transfer Processes. 2004;(2):1-36.

9. Vogel M, Doka S, Breyer C, Lux-Steiner MC, Fostiropoulos K. On the function of a bathocuproine buffer layer in organic photovoltaic cells. *Appl Phys Lett.*

2006;89(16):163501.

10. Peumans P, Forrest SR. Very-high-efficiency double-heterostructure copper phthalocyanine/C60 photovoltaic cells. *Appl Phys Lett*. 2001;79(1):126-128.

11. Walter MG, Rudine AB, Wamser CC. Porphyrins and phthalocyanines in solar photovoltaic cells. *J Porphyr Phthalocyanines*. 2010;14(9):759-792.

12. Xue J, Uchida S, Rand BP, Forrest S. High efficiency organic photovoltaic cells employing hybridized mixed-planar heterojunctions. August 2015.

13. Nyokong T. Desired properties of new phthalocyanines for photodynamic therapy. *Pure Appl Chem*. 2011;83(9):1763-1779.

14. Bonnett R. Photosensitizers of the porphyrin and phthalocyanine series for photodynamic therapy. *Chem Soc Rev*. 1995;24(1):19-33.

15. Spikes JD. Phthalocyanines as photosensitizers in biological systems and for the photodynamic therapy of tumors. *Photochem Photobiol*. 1986;43(6):691-699.

16. Chambrier I, Cook MJ, Cracknell SJ, McMurdo J. Synthesis and characterisation of some non-uniformly substituted mesogenic phthalocyanines. *J Mater Chem*. 1993;3(8):841-849.

17. Shishkina O V, Maizlish VE, Shaposhnikov GP. Nucleophilic substitution in 4-bromo-5-nitrophthalodinitrile: IV. 5-nitro-4-(phenylthio) phthalodinitrile and octa-substituted metal phthalocyanines based thereon. *Russ J Gen Chem*. 2001;71(2):243-245.

18. George RD, Snow AW, Shirk JS, Barger WR. The alpha substitution effect on phthalocyanine aggregation. *J Porphyr Phthalocyanines*. 1998;2(1):1-7.

19. Siejak A, Wróbel D, Ion RM. Study of resonance effects in copper phthalocyanines. *J Photochem Photobiol A Chem*. 2006;181(2-3):180-187. doi:10.1016/j.jphotochem.2005.11.022.

20. Balkus KJ, Eissa M, Levado R. Oxidation of alkanes catalyzed by zeolite-

encapsulated perfluorinated ruthenium phthalocyanines. *J Am Chem Soc.* 1995;117(43):10753-10754. doi:10.1021/ja00148a022.

21. Kerber RC. If It's Resonance, What Is Resonating? *J Chem Educ.* 2006;83(2):223. doi:10.1021/ed083p223.

22. Edwards L, Gouterman M. Porphyrins. *J Mol Spectrosc.* 1970;33(2):292-310. doi:10.1016/0022-2852(70)90040-8.

23. Keizer SP, Mack J, Bench BA, Gorun SM, Stillman MJ. Spectroscopy and electronic structure of electron deficient zinc phthalocyanines. *J Am Chem Soc.* 2003;125(23):7067-7085. doi:10.1021/ja0299710.

24. Gouterman M. Spectra of Porphyrins. *J Mol Spectrosc.* 1961;6(1):138-. doi:10.1016/0022-2852(61)90236-3.

25. Liao M, Watts JD, Huang M, Box PO, State J, Uni V. DFT Study of Unligated and Ligated Manganese II Porphyrins and Phthalocyanines. 2005;44(6):1941-1949. doi:10.1021/ic0401039.

26. Shirk JS, Pong RGS, Flom SR, Heckmann H, Hanack M. Effect of Axial Substitution on the Optical Limiting Properties of Indium Phthalocyanines. *J Phys Chem A.* 2000;104(7):1438-1449. doi:10.1021/jp993254j.

27. Doyle JJ, Wang J, Flaherty MO, Chen Y. Nonlinear optical performance of chemically tailored phthalocyanine – polymer films as solid-state optical limiting devices. 2008;10. doi:10.1088/1464-4258/10/7/075101.

28. Hanack M, Schneider T, Barthel M, Shirk JS, Flom SR, Pong RGS. Indium phthalocyanines and naphthalocyanines for optical limiting. *Coord Chem Rev.* 2001;219-221:235-258. doi:10.1016/S0010-8545(01)00327-7.

29. Nalwa HS, Kobayashi S. Large third-order optical non-linearities of spin-cast thin films of novel metallo-naphthalocyanines. *J Porphyr Phthalocyanines.* 1998;2(1):21-30.

30. Hashimoto T, Choe Y, Nakano H, Hirao K. Theoretical Study of the Q and B Bands of Free-Base, Magnesium, and Zinc Porphyrins, and Their Derivatives. *J Phys Chem A*. 1999;103(12):1894-1904. doi:10.1021/jp984807d.

31. Mack J, Stillman MJ. Photochemical Formation of the Anion Radical of Zinc Phthalocyanine and Analysis of the Absorption and Magnetic Circular Dichroism Spectral Data. Assignment of the Optical Spectrum of [ZnPc (-3)]-. *J Am Chem Soc*. 1994;116(4):1292-1304.

32. Rio Y, Salomé Rodríguez-Morgade M, Torres T. Modulating the electronic properties of porphyrinoids: a voyage from the violet to the infrared regions of the electromagnetic spectrum. *Org Biomol Chem*. 2008;6(11):1877-1894. doi:10.1039/b800617b.

33. O'Flaherty SM, Hold S V., Cook MJ, et al. Molecular engineering of peripherally and axially modified phthalocyanines for optical limiting and nonlinear optics. *Adv Mater*. 2003;15(1):19-32. doi:10.1002/adma.200390002.

34. Dini D, Calvete MJF, Hanack M, Pong RGS, Flom SR, Shirk JS. Nonlinear Transmission of a Tetrabrominated Naphthalocyaninato Indium Chloride. 2006:12230-12239.

35. Long NJ. Organometallic Compounds for Nonlinear Optics. *Angew Chemie - Int Ed*. 1995;34:21-38. doi:10.1002/anie.199500211.

36. Slodek A, Wöhrle D, Doyle JJ, Blau W. Metal Complexes of Phthalocyanines in Polymers as Suitable Materials for Optical Limiting. *Macromol Symp*. 2006;235:9-18. doi:10.1002/masy.200650302.

37. Venugopal Rao S, Anusha PT, Prashant TS, Swain D, Tewari SP. Ultrafast nonlinear optical properties and excited state dynamics of phthalocyanine thin films. *Spie Opto*. 2011;7935:793517-793517-11. doi:10.1117/12.874632.

38. Flaherty BSMO, Hold S V, Cook MJ, et al. Molecular Engineering of Peripherally And Axially Modified Phthalocyanines for Optical Limiting and

Nonlinear Optics **. 2003;(1):19-32.

39. Srinivas NKMN, Rao SV, Rao DN. Saturable and reverse saturable absorption of Rhodamine B in methanol and water. *J Opt Soc Am B*. 2003;20(12):2470. doi:10.1364/JOSAB.20.002470.

40. Wei T-H, Huang T-H. Signs of nonlinear refraction in chloroaluminum phthalocyanine solution. *Appl Phys Lett*. 1998;72(20):2505-2508.

41. Dini D, Calvete MJF, Hanack M, Pong RGS, Flom SR, Shirk JS. Nonlinear transmission of a tetrabrominated naphthalocyaninato indium chloride. *J Phys Chem B*. 2006;110(25):12230-12239. doi:10.1021/jp0571776.

42. Verbiest T, Houbrechts S, Kauranen M, Clays K, Persoons a. Second-order nonlinear optical materials: recent advances in chromophore design. *J Mater Chem*. 1997;7(11):2175-2189. doi:10.1039/a703434b.

43. Dalton R, Shi Y, Steier WH. New-polymers-with-large-and-stable-second-order-nonlinear-optical-effects_1991_Macromolecules.pdf. 1991;(1):5421-5428.

44. Clays K, Persoons A. Hyper-Rayleigh scattering in solution. *Phys Rev Lett*. 1991;66(23):2980-2983. doi:10.1103/PhysRevLett.66.2980.

45. Nsley TRRE, Onghua HHU, Eichert MAR, et al. Quasi-three-level model applied to measured spectra of nonlinear absorption and refraction in organic molecules. 2016;33(4):780-796. doi:10.1364/JOSAB.33.000780.

46. Said A, Wamsley C, Hagan D. Third-and fifth-order optical nonlinearities in organic materials. *Chem Phys Lett*. 1994;228(October):646-650. http://www.sciencedirect.com/science/article/pii/0009261494009996.

47. de la Torre G, Vázquez P, Agulló-López F, Torres T. Phthalocyanines and related compounds:organic targets for nonlinear optical applications. *J Mater Chem*. 1998;8(8):1671-1683. doi:10.1039/a803533d.

48. Boyd R. *Nonlinear Optics*. Third Edit. Elsevier; 2008.

49. Tsigaridas G, Polyzos I, Persephonis P, Giannetas V. A novel approach for analyzing open Z-scan experiments. *Opt Commun*. 2006;266(1):284-289. doi:10.1016/j.optcom.2006.04.015.

50. Physics A, Tsigaridas G, Fakis M, Polyzos I, Persephonis P, Giannetas V. Z-scan technique through beam radius measurements. *Appl Phys B Lasers Opt*. 2003;76(1):83-86. doi:10.1007/s00340-002-1067-5.

51. Kogej T, Beljonne D, Meyers F, Perry JW, Marder SR, Brédas JL. Mechanisms for enhancement of two-photon absorption in donor–acceptor conjugated chromophores. *Chem Phys Lett*. 1998;298(1-3):1-6. doi:10.1016/S0009-2614(98)01196-8.

52. Rumi M, Ehrlich JE, Heikal AA, et al. Structure - Property relationships for two-photon absorbing chromophores: Bis-donor diphenylpolyene and bis(styryl)benzene derivatives. *J Am Chem Soc*. 2000;122(39):9500-9510. doi:10.1021/ja994497s.

53. Pawlicki M, Collins HA, Denning RG, Anderson HL. Two-photon absorption and the design of two-photon dyes. *Angew Chemie - Int Ed*. 2009;48(18):3244-3266. doi:10.1002/anie.200805257.

54. Baev A, Gel'mukhanov F, Macák P, Luo Y, Ågren H. General theory for pulse propagation in two-photon active media. *J Chem Phys*. 2002;117(13):6214-6220. doi:10.1063/1.1499719.

55. Raavi SSK, Venugopal Rao S, Giribabu L, Narayana Rao D. Nonlinear optical properties of alkyl phthalocyanines in the femtosecond, nanosecond, and cw excitation regimes. *Proc SPIE*. 2008;6875:68751D. doi:10.1117/12.761815.

56. Van Stryland EW, Sheik-Bahae M. Z-Scan Measurements of Optical Nonlinearities. In: *Characterization Techniques and Tabulations for Organic Nonlinear Materials*. ; 1998:655-692.

57. De Boni L, Piovesan E, Gaffo L, Mendonça CR. Resonant nonlinear absorption

in Zn-phthalocyanines. *J Phys Chem A*. 2008;112(30):6803-6807. doi:10.1021/jp8049735.

58. Kasha BYM. Characterization Of Electronic Transitions In Complex Molecules. *Discuss Faraday Soc*. 1950;9(c):14-19.

59. Dini D, Hanack M. Physical Properties of Phthalocynine-based Materials. In: *The Porphyyrin Handbook*. Vol 17. ; 2003:1-36.

60. Yaunli Zhang. Nonlinear Optical Characterisation of Bithiophenes with Phosphorus containing substituents. *Thesis*. 2013;53(9). doi:10.1017/CBO9781107415324.004.

61. Schroeder R, Ullrich B, Graupner W, Scherf U. Excitation density and photoluminescence studies of polyfluorene excited by two-photon absorption. *J Phys Condens Matter*. 2001;13(16):L313-L318. doi:10.1088/0953-8984/13/16/102.

62. Penzkofer A, Blau W. Theoretical analysis of S1-state lifetime measurements of dyes with picosecond laser pulses. *Opt Quantum Electron*. 1983;15(4):325-347. doi:10.1007/BF00619902.

63. Barker JA, Watts RO. Monte Carlo studies of the dielectric properties of water-like models. *Mol Phys*. 1973;26(3):789-792.

64. Achar BN, Fohlen GM, Parker JA, Keshavayya J. Synthesis and structural studies of metal(II) 4,9,16,23-phthalocyanine tetraamines. *Polyhedron*. 1987;6(6):1463-1467. doi:10.1016/S0277-5387(00)80910-9.

65. Ogunsipe A, Maree D, Nyokong T. Solvent effects on the photochemical and fluorescence properties of zinc phthalocyanine derivatives. *J Mol Struct*. 2003;650(1-3):131-140. doi:10.1016/S0022-2860(03)00155-8.

66. Albert IDL, Marks TJ, Ratner MA. Rational Design of Molecules with Large Hyperpolarizabilities. Electric Field, Solvent Polarity, and Bond Length Alternation Effects on Merocyanine Dye Linear and Nonlinear Optical

Properties. *J Phys Chem*. 1996;100(23):9714-9725. doi:10.1021/jp960860v.

67. Jasinski R. Cobalt phthalocyanine as a fuel cell cathode. *J Electrochem Soc*. 1965;112(5):526-528.

68. Van Dyke TG. Perfluoroalkylated phthalic anhydride, copper phthalocyanine and their preparation. October 1966.

69. Champagne B, Spassova MI. Assessing long-range corrected functionals with physically-adjusted range-separated parameters for calculating the polarizability and the second hyperpolarizability of polydiacetyl ... 2014;(April 2016). doi:10.1039/c4cp00105b.

70. Geskin VM, Lambert C, Br??das JL. Origin of High Second- and Third-Order Nonlinear Optical Response in Ammonio/Borato Diphenylpolyene Zwitterions: The Remarkable Role of Polarized Aromatic Groups. *J Am Chem Soc*. 2003;125(50):15651-15658. doi:10.1021/ja035862p.

71. Lam YC. Synthesis , Oxidation and Photophysics of Perfluoroborated Tetrakis (pyrophosphito) diplatinate (II) and Density Functional Theory (DFT) Study of Electrochemical CO 2 Reduction by Mn Catalysts. *Thesis*. 2015;2015(March).

72. Maker PD, Terhune RW. Study of optical effects due to an induced polarization third order in the electric field strength. *Phys Rev*. 1965;137(3A):A801.

73. McDonagh AM, Humphrey MG, Samoc M, et al. Organometallic Complexes for Nonlinear Optics. 16.1 Second and Third Order Optical Nonlinearities of Octopolar Alkynylruthenium Complexes. *J Am Chem Soc*. 1999;121(6):1405-1406.

74. Mohammed Ali Q, Palanisamy PK. Investigation of nonlinear optical properties of organic dye by Z-scan technique using He–Ne laser. *Opt - Int J Light Electron Opt*. 2005;116(11):515-520. doi:10.1016/j.ijleo.2005.05.001.

75. Mason W. A practical guide to magnetic circular dichroism spectroscopy. 2008:322.

76. Kobayashi N, Muranaka A. A mutually perpendicular phthalocyanine pentamer obtained by a one-step reaction. *Chem Commun*. 2000;(19):1855-1856. doi:10.1039/b005969m.

77. M.J. Frisch, G.W. Trucks, H.B. Schlegel, G.E. Scuseria, M.A. Robb, J.R. Cheeseman, G. Scalmani, V. Barone, B. Mennucci, G.A. Petersson, H. Nakatsuji, M. Caricato, X. Li, H.P. Hratchian, A.F. Izmaylov, J. Bloino, G. Zheng, J.L. Sonnenberg, M. Hada, M. Ehar DJF. Guassian09. 2009.

78. Nemykin VN, Hadt RG, Belosludov R V, Mizuseki H, Kawazoe Y. Influence of Molecular Geometry, Exchange-Correlation Functional, and Solvent Effects in the Modeling of Vertical Excitation Energies in Phthalocyanines Using Time-Dependent Density Functional Theory (TDDFT) and Polarized Continuum Model TDDFT Methods:&n. 2007;111(50):12901-12913. http://pubs.acs.org/doi/abs/10.1021/jp0759731.

79. Grimme S, Antony J, Ehrlich S, Krieg H. A consistent and accurate ab initio parametrization of density functional dispersion correction (DFT-D) for the 94 elements H-Pu. *J Chem Phys*. 2010;132(15):1-20. doi:10.1063/1.3382344.

80. Yang Y, Weaver MN, Merz KM. Assessment of the '6–31+G** + LANL2DZ Mixed Basis Set Coupled with Density Functional Theory Methods and Effective Core Potential: Prediction of Heats of Formation and Ionization Potentials for First Row Transition Metal Complexes. *J Phys Chem A*. 2009;113(36):9843-9851. doi:10.1021/jp807643p.

81. Waluk J, Michl J. The Perimeter Model and Magnetic Circular Dichroism of Porphyrin Analogues. *J Org Chem*. 1991;56(8):2729-2735.

82. Seidler T, Champagne B. Second-Order Nonlinear Optical Susceptibilities of Metal–Organic Frameworks Using a Combined Local Field Theory/Charge

Embedding Electrostatic Scheme. *J Phys Chem C*. 2016;120(12):6741-6749. doi:10.1021/acs.jpcc.6b00217.

83. Nénon S, Champagne B, Spassova MI. Assessing long-range corrected functionals with physically-adjusted range-separated parameters for calculating the polarizability and the second hyperpolarizability of polydiacetylene and polybutatriene chains. *Phys Chem Chem Phys*. 2014;16(April 2016):7083-7088. doi:10.1039/c4cp00105b.

84. Champagne B, Plaquet A, Guillaume M, et al. In silico optimization of merocyanine-spiropyran compounds as second-order nonlinear optical molecular switches. *Phys Chem Chem Phys*. 2008;10(41):6223-6232. doi:10.1039/b806561f.

85. Li A, Muddana HS, Gilson MK. Quantum Mechanical Calculation of Noncovalent Interactions: A Large-Scale Evaluation of PMx, DFT, and SAPT Approaches. *J Chem Theory Comput*. 2014;10(4):1563-1575. doi:10.1021/ct401111c.

86. Chen C, Zhang L, Zhao L, Qi D, Jiang J. Density functional theory prediction for the second-order nonlinear optical responses of phenanthroline-fused phthalocyanine derivatives. *J Porphyrins Phthalocyanines*. 2014;18(01n02):58-66. doi:10.1142/S1088424613500855.

87. Khene S, Geraldo DA, Togo CA, Limson J, Nyokong T. Synthesis, electrochemical characterization of tetra- and octa-substituted dodecyl-mercapto tin phthalocyanines in solution and as self-assembled monolayers. *Electrochim Acta*. 2008;54(2):183-191. doi:10.1016/j.electacta.2008.08.018.

88. Young JG, Onyebuagu W. Synthesis and characterization of di-disubstituted phthalocyanines. *J Org Chem*. 1990;55(6):2155-2159. doi:10.1021/jo00294a032.

89. Yanai T, Tew DP, Handy NC. A new hybrid exchange-correlation functional using the Coulomb-attenuating method (CAM-B3LYP). *Chem Phys Lett*.

2004;393(1-3):51-57. doi:10.1016/j.cplett.2004.06.011.

90. Ngubeni GN, Britton J, Mack J, et al. Spectroscopic and nonlinear optical properties of the four positional isomers of 4α-(4-tert-butylphenoxy)phthalocyanine. *J Mater Chem C*. 2015;3:10705-10714. doi:10.1039/C5TC01601K.